THE UNIVERSITY OF
WARWICK

AUTHOR: **Brenda Quinn** DEGREE: **Ph.D.**

TITLE: **Rossby Wave, Drift Wave and Zonal Flow Turbulence**

DATE OF DEPOSIT: .....

I agree that this thesis shall be available in accordance with the regulations governing the University of Warwick theses.

I agree that the summary of this thesis may be submitted for publication.

I **agree** that the thesis may be photocopied (single copies for study purposes only).

Theses with no restriction on photocopying will also be made available to the British Library for microfilming. The British Library may supply copies to individuals or libraries. subject to a statement from them that the copy is supplied for non-publishing purposes. All copies supplied by the British Library will carry the following statement:

> "Attention is drawn to the fact that the copyright of this thesis rests with its author. This copy of the thesis has been supplied on the condition that anyone who consults it is understood to recognise that its copyright rests with its author and that no quotation from the thesis and no information derived from it may be published without the author's written consent."

AUTHOR'S SIGNATURE: .....

USER'S DECLARATION

1. I undertake not to quote or make use of any information from this thesis without making acknowledgement to the author.
2. I further undertake to allow no-one else to use this thesis while it is in my care.

DATE SIGNATURE ADDRESS

.....

.....

.....

.....

.....

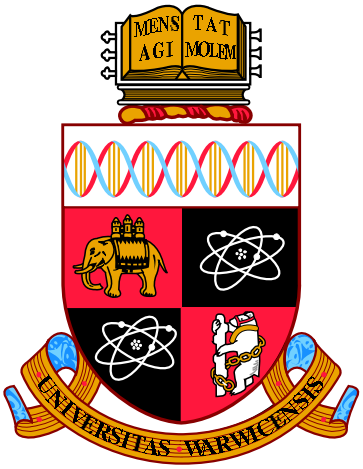

Rossby Wave, Drift Wave and Zonal Flow Turbulence

by

Brenda Quinn

Thesis

Submitted to the University of Warwick

for the degree of

Doctor of Philosophy

Mathematics Institute

June 2011

THE UNIVERSITY OF WARWICK

Contents

List of Tables

List of Figures

Acknowledgments

For their immeasurable patience and unrelenting support over these past few years, I cannot thank enough my PhD supervisor, Professor Sergey Nazarenko whose academic experience and enthusiasm never ceases to amaze me. Equally so, Dr. Colm Connaughton, without whom, I am under no illusions that, I would never have reached this far.

I have been blessed with the constant help, encouragement, coffee-break chats and entertainment of great friends Jason, Chris and Thorwald at Warwick university which I have missed over the past year.

I shall be eternally indebted to my mother, Ann and sisters, Shelly and Zenia for their many hours of babysitting and entertaining Domenico.

I would also like to express my sincere gratitude to Carole Fisher and all the staff in the Mathematics Institute at Warwick who have helped me in any way during my time there.

Above all, thanks to Domenico, for teaching me the important things in life.

Declarations

I declare that the work contained in this thesis is my own except where otherwise stated. Chapters 1 and 2 contain no original work but provide a general understanding and theoretical background to the subject of drift wave and Rossby wave turbulence with zonal flows. Chapter 3 derives the Charney-Hasegawa-Mima equation which provides the basis of this thesis based on classical sources [1; 2; 3; 4]. Chapters 4, 5 and 6 each contain original work. All of the numerical results presented are original work, carried out with a numerical code written by the author. Results presented in Chapters 4 and 5 have been submitted for publication as separate journal articles [5; 6; 7]. The mathematical analysis of Chapter 4 is based on the work of Gill [8]. To my knowledge, neither the numerical verification of the conservation of the extra invariant in the CHM equation nor the methods used to track the centroids of the invariants in Chapter 5 have been used before. The mathematical derivations in Chapter 6 are detailed derivations carried out with collaborators, which fill between the lines of the original theory [9; 10; 11]. The work presented in Chapter 6 has been submitted to two journals for review. This thesis has not been submitted for a degree at another university.

Abstract

An extensive qualitative and quantitative study of Rossby wave, drift wave and zonal flow turbulence in the Charney-Hasegawa-Mima model is presented. This includes details of two generation mechanisms of the zonal flows, evidence of the nonlocal nature of this turbulence and of the energy exchange between the small and large scales.

The modulational instability study shows that for strong primary waves the most unstable modes are perpendicular to the primary wave, which corresponds to the generation of a zonal flow if the primary wave is purely meridional. For weak waves, the maximum growth occurs for off-zonal modulations that are close to being in three-wave resonance with the primary wave. Nonlinear jet pinching is observed for all nonlinearity levels but the subsequent dynamics differ between strong and weak primary waves. The jets of the former further roll up into Kármán-like vortex streets and saturate, while for the latter, the growth of the unstable mode reverses and the system oscillates between a dominant jet and a dominant primary wave. A critical level of nonlinearity is defined which separates the two regimes. Some of these characteristics are captured by truncated models.

Numerical proof of the extra invariant in Rossby and drift wave turbulence is presented. While the theoretical derivations of this invariant stem from the wave kinetic equation which assumes weak wave amplitudes, it is shown to be relatively-well conserved for higher nonlinearities also. Together with the energy and enstrophy, these three invariants cascade into anisotropic sectors in the k-space as predicted by the Fjørtoft argument. The cascades are characterised by the *zonostrophy* pushing the energy to the zonal scales.

A small scale instability forcing applied to the model has demonstrated the well-known drift wave - zonal flow feedback loop. The drift wave turbulence is generated from this primary instability. The zonal flows are then excited by either one of the generation mechanisms, extracting energy from the drift waves as they grow. Eventually the turbulence is completely suppressed and the zonal flows saturate. The turbulence spectrum is shown to diffuse in a manner which has been mathematically predicted.

The insights gained from this simple model could provide a basis for equivalent studies in more sophisticated plasma and geophysical fluid dynamics models in an effort to fully understand the zonal flow generation, the turbulent transport suppression and the zonal flow saturation processes in both the plasma and geophysical contexts.

Chapter 1

Introduction

A zonal flow is a prominent band-like structure with a dominant jet velocity profile in an otherwise general flow domain. Some well-known examples in geophysical fluid dynamics (GFD) include the rings or equatorial jets around Saturn and the belts and zones of the Jovian atmosphere [12; 13; 14]. The latitudinaly-aligned bands observed on the giant planets are zonal flows, visible due to the ammonia cloud formations. Far from being extra-terrestrial phenomena however, zonal flows also exist near the tropopause in the earth's atmosphere such as the polar and subtropical jet streams [15] which eastward-bound aircraft take advantage of and in the earth's oceans [16] such as the Antarctic circumpolar current.

Zonal flows are also striking features of plasma turbulence in fusion devices. They are observed as radially localised, toroidally symmetric, strongly sheared flows in the poloidal direction. They are created exclusively by the nonlinear energy transfer from drift wave turbulence in the core of the plasma, sucking the energy from the drift wave packet as they grow. In this respect, zonal flows reduce the level of drift wave turbulence.

It is generally accepted that zonal flows in a tokamak grow from drift wave turbulence and from Rossby wave turbulence in GFD [17] and are the result of self-organisation of a turbulent state to a coherent flow. Their generation and maintenance is a topic of much research because they play a major part in the dynamics of both the atmospheres and of magnetically-confined plasmas.

The understanding of Rossby wave - zonal flow turbulence is deemed crucial to

fully comprehend the bigger picture of the overall atmosphere-ocean dynamics and those of the planets such as Jupiter and Saturn [18]. A clear and concise understanding of the atmosphere-ocean dynamics is highly desirable, more so now with the surge in global interest in issues such as climate change and the rise in sea-levels which threaten to submerge low-lying islands. Developments of geophysical models since the mid-twentieth century have led to advances such as being able to predict the general path of hurricanes and tropical cyclones, such as that of cyclone Yasi just this year in February as it approached the east coast of Australia, ultimately saving lives. Being able to predict the occurance of El Niño due to improved knowledge of long oceanic waves and air-sea interactions has meant early warnings can be given to communities along the west coast of South America to help prevent or lessen ecological damage [19] when it arrives. Furthermore, it is believed that the cyclones and anticyclones inherent of the weather in midlatitudes are due to the baroclinic instability of the atmospheric jet stream indicating that a greater understanding of such features would improve parametrisation of weather forecast models.

Another global issue, the depletion of commonly-used fuel resources is one that could be resolved by the use of fusion energy, a clean and sustainable energy source. Although construction of the International Thermonuclear Experimental Reactor (ITER) in France is already under way, there are still some underlying fundamental issues which need to be resolved for successful ignition to occur. One of those issues is related to plasma turbulence. The reduction in anomalous transport, observed when a discharge undergoes Low-to-High (LH) transition in fusion devices, is generally believed to be due to zonal flows [17]. These zonal flows represent transport barriers and their existence is in fact crucial in regulating the turbulence from the small scale instabilities from which they stem [20], further strengthening the necessity to fully understand drift wave - zonal flow turbulence.

A similar feedback mechanism exists for Rossby waves in the atmosphere and is sometimes referred to as the *barotropic governor* in that the barotropic flow controls the level of turbulent behaviour [21]. Barriers to mixing and transport are evident in the atmosphere at the edge of the Arctic and Antarctic winter polar vortices. The

concentration of certain gases, which are otherwise evenly distributed over the poles, can have large gradients at the edge of the polar vortex, which creates a barrier to mixing towards the equator [22; 23]. Likewise, the equatorial jet in the stratosphere acts as a barrier, reducing polewards transport of volcanic aerosols. By comparison, in the troposphere where the equatorial jet does not reach, the volcanic aerosol is more evenly distributed rather more concentrated in equatorial latitudes [24; 23].

With the mention of turbulence the usual thought is of hydrodynamic turbulence as described by the Navier-Stokes (NS) equations. The typical picture of turbulence is of large vortices which transfer their energy to subsequently smaller scales, one painted by Richardson [25] in 1926. Progress in turbulence theory came with its statistical description developed by Taylor [26; 27] with the realisation that the correlation between the velocities at two points was a significant quantity in describing turbulence. Kolmogorov's contribution in 1941 [28; 29] is based on fully-developed, locally isotropic and homogeneous turbulence and is the origin of the famous *two-thirds law*. Together with further developments by Obukhov [30], this turbulence theory is characterised by cascades of energy and enstrophy within the inertial range where neither forcing nor dissipation exist.

Turbulent motions are not restricted to vortices nor indeed to hydrodynamics. Turbulence is the chaotic motion of a physical system which is out of equilibrium accompanied by an energy cascade [31]. A system of weakly nonlinear waves, described only by its dispersion law and interaction coefficient, can also be described as being in a turbulent state.

Based on the kinetic theory of gases, wave turbulence theory was originally used by Peierls to describe the kinetic theory of thermal conduction in crystals [32] when it was recognised that it was necessary to consider higher-order terms than linear in the expansion of the energy, which would have lead to time-varying wave amplitudes and ultimately, a statistical equilibrium between waves. Wave turbulence theory describes a random field of weakly nonlinear dispersive waves and it is now a well-established theory for waves in an extensive range of physical systems [31; 33] such as planetary atmospheres and oceans [34], plasmas of fusion devices [35] and in superfluid helium [36] to name but a few.

While wave turbulence deals with the spectrum of weakly nonlinear waves, there is a general consensus that the theory must be further developed to include the co-existence of coherent structures such as zonal flows and vortices with the weak waves [33]. The main objective is to understand the role that the turbulence, generated by these fast small scale waves, plays in the slower large-scale dynamics. Furthermore, the systems of Rossby wave and drift wave - zonal flow turbulence are typical of the coexistence of two distinctly different spatial and time scales. The drift waves are generated at the scale of the ion Larmor radius and have very high frequency compared to that of the zonal flows. Likewise, Rossby waves have a higher frequency than the zonal flows in the atmosphere.

Geophysical quasi-geostrophic (QG) flows and plasma drift turbulence are frequently discussed together [37; 4; 17], in particular when discussing zonal flow formation, because some basic linear and nonlinear properties of these two systems can be described by the same partial differential equation (PDE).It is known collectively as the Charney-Hasegawa-Mima (CHM) equation [1; 2], the origin and derivation of which is detailed in Chapter 3 and provides the basic model for the present study.

Two of the main candidates for the mechanism of zonal flow generation, applicable to both Rossby wave and drift wave turbulence are; the modulational instability of a single drift or Rossby wave, also referred to as a parametric instability and the inverse cascade mechanism or resonant instability, supported by wave kinetic theory.

The modulational instability of a primary Rossby wave to a weak large scale perturbation is well-studied [38; 8; 39] as is that of the drift wave [40; 41; 20]. It leads to a resonant interaction between the zonal mode and the wave, with the result that energy is transferred *directly* to the large zonal scales [38; 8; 40; 41; 39], bypassing the intermediate scales. This instability is analysed in great detail in Chapter 4 where it is shown that for high nonlinearity of a primary drift or Rossby wave, narrow zonal jets are formed which represent transport barriers, which exist in the atmosphere and in a magnetically-confined plasma.

The second generation mechanism, the inverse cascade [42], transports the energy from the small scale turbulence to large scale zonal flows in a step-by-step process, similar to the inverse cascade in two-dimensional (2D) NS turbulence [43; 44]. In contrast, the

energy cascade in the CHM model could be local or nonlocal [45; 46; 47] and is anisotropic due to the beta-effect with the result that the flow self-organises to large scale zonal flows, rather than round vortices [48; 49; 50].

In reality, it is unlikely that the two mechanisms mentioned are exclusive and can co-exist although it is believed that the relevant mechanism depends on the specific parameter regime. A narrow initial spectrum of the waves with large initial amplitude favours the modulational instability leading to fast zonal flow generation while bypassing the turbulent cascade stages and intermediate scales. Conversely, for broad initial spectra the cascade scenario is likely to be more relevant [41; 42; 20]. A similar competition between the modulational instability and the inverse energy cascade mechanisms is known to exist in the turbulence of surface gravity waves on water. In this medium, the instability is also known as the Benjamin-Feir [51] instability and depends on the width of the initial wave spectrum [52].

Pioneering work [46; 45] found that drift and Rossby wave turbulence conserves not only energy and enstrophy but also a third invariant in Fourier space. Until then, it was assumed that all wave systems conserve only the energy and enstrophy or that they conserve an infinite number of extra invariants. This discovery was the first example of a wave system with a finite number of additional invariants [45]. Chapter 5 presents numerical proof of this conserved quantity, now referred to as *zonostrophy* as well as its effect on the cascades of energy and enstrophy.

Richardson's notable hypothesis on the local nature of turbulence cascades suggests that energy is transferred through the scales from large vortices down to smaller vortices in three-dimensional (3D) turbulence or from small scales to larger scales in the case of 2D turbulence [25] such that turbulent structures interact only with other structures of similar size, that is, it is local in physical space. With this idea in mind and working from dimensional considerations, Kolmogorov and Obukhov derived the famous $k^{-5/3}$ energy spectrum of turbulence [28; 29; 30] in an incompressible fluid which then led to Kraichnan's derivation of the k^{-3} enstrophy spectrum for 2D turbulence [44].

Equivalent spectra can be derived from the equations of the medium for many weak turbulence situations. Using these *Kolmogorov-Zakharov (KZ)* spectra, Zakharov

deduced that the hypothesis of locality can be tested explicitly by determining whether the collision integral of the given kinetic equation converges or diverges. Based on such an analysis of the KZ spectra, it has been suggested that drift wave and Rossby wave turbulence are nonlocal [9; 10; 11]. If there is no dissipation at large scales, energy accumulates at the largest available scale, generally the size of the physical system and further turbulence evolution is mainly determined by a nonlocal interaction between the small scale waves and the 'condensate'-scale structures. Assuming nonlocality, the theory suggests that the turbulence spectrum in k-space splits into two unconnected components with intermediate scales dying out. One component is the high-frequency short-wavelength drift turbulence which defines the level at which the second component, the low-frequency turbulence of the zonal flow saturates. Numerical work presented in Chapter 6 confirm the theoretical predictions.

Chapter 2

Theoretical background

When the electrostatic forces of the particles of a gas are overcome, the gas is said to be a plasma. A plasma is in a fully ionised state so that the dynamics of the ions and electrons can be treated separately. Plasma constitutes the sun, stars and solar wind as well as interstellar and interplanetary media. Closer to Earth, lightening and the aurorae are examples of plasma. Common man-made plasma include plasma lamps and televisions and of course, magnetically-confined plasmas which are used for fusion research.

The field of fusion research is of great interest today as a possible sustainable energy resource as a response to recent global warnings on the use of non-renewable energy resources. In contrast to nuclear fission which splits high-atomic number nuclei, nuclear fusion fuses together the nuclei of two low atomic number elements. The tokamak is the main fusion device today [53], utilised in fusion research with the aim of efficient production of fusion energy, the ultimate goal being commercial use of fusion energy.

Traditionally tokamaks used deuterium and hydrogen but the output power from the fusion reactor was quite low until the early 1990s, tritium atoms were injected with a deuterium plasma at the Joint European Torus (JET) tokamak outside Oxford in the UK, yielding a greater power output. Although the JT-60 tokamak in Naka in Japan is roughly the same size as JET, with a plasma volume of approximately $90m^3$, JET is currently the only one capable of using tritium.

When the deuterium plasma is heated and tritium atoms injected, their nuclei

fuse together according to the reaction

$$ {}^{2}_{1}\mathrm{D} + {}^{3}_{1}\mathrm{T} = {}^{4}_{2}\mathrm{He} + {}^{1}_{0}\mathrm{n}\,, \tag{2.1} $$

where the subscript is the atomic number and the superscript is the atomic weight, resulting with a helium nucleus and a neutron, both with extremely high kinetic energy [54; 53]. Both deuterium and tritium are hydrogen isotopes and therefore abundantly available on earth, either naturally from sea water or via a side reaction between lithium and a neutron. Furthermore, it is currently under consideration that the neutron by-product could be recycled by reacting with lithium walls to create more tritium [55]. The plasma temperature in JET can reach up to 2×10^8K and by comparison the temperature of the nuclear core of the sun, a natural fusion reactor which generates thermal energy when hydrogen is converted to helium, is 2×10^7K [53].

The next step in fusion research is the current construction of ITER in the south of France. Achieving plasma ignition requires a sufficiently high plasma density, temperature and confinement time being achieved simultaneously before the plasma loses its energy. The minimum value of the product of these three quantities provides a revised version of the Lawson criterion [56], which must be met for sustained confinement [53]. If this experiment is successful, fusion energy could then be commercially available towards the middle of this century.

However, plasma instabilities tend to generate turbulence in the form of weakly interacting waves with the result that transport of the plasma from the core to the edge is greatly enhanced and the plasma confinement in the hot core subsequently reduced. This anomalous transport had baffled engineers and scientists for many years as it was too great to be explained by classical collisional or neoclassical trapped particle theory [53]. Fresh hope was given to fusion research when it was discovered experimentally [57] in the Axially Symmetric Divertor EXperiment (ASDEX) divertor tokamak near Munich in Germany, that this anomalous transport was not always observed in the discharges. Two separate regimes were defined as L-type and H-type referring to low and high values respectively of the plasma β_p which measures the ratio of the plasma pressure to the magnetic pressure. Under certain conditions, the plasma discharge would undergo an LH transition, with enhanced plasma confinement times and reduced anomalous transport.

It is generally accepted that this reduced transport is due to the transport barriers that zonal flows represent, stemming from the drift wave turbulence [17; 23; 58]. One of the major outstanding issues to be resolved in the field of fusion energy is believed to be related to this feedback loop mechanism. As the Chief Executive Officer of United Kingdom Atomic Energy Authority (UKAEA) and Head of EURATOM/CCFE Fusion Association, Steve Cowley once posed the multi-billion dollar question in a lecture, "Can turbulence be switched off?" - a question to which many hope the answer is yes.

Drift waves are so-called as they are the low frequency small oscillations which result from the balancing of the parallel and drift dynamics in a neutral magnetically-confined plasma [59]. The electrons with higher energy and velocity contribute most to the dynamics parallel to the magnetic field. The magnetic force is always perpendicular to the dynamics in a plane at right-angles. In this perpendicular plane, as they orbit, the ions and electrons are accelerated then decelerated in the direction of the electric field so that there is a slight velocity imbalance between opposite sides of the orbit path, resulting in the particle drifting perpendicular to the electric field. Drift wave turbulence arises when the drift waves are unstable to steep temperature gradients.

Rossby waves, otherwise known as planetary waves exist due to the planet's rotation. Following the observation of large recurring eddies in the atmosphere over the USA, analysis of data for the earth's northern hemisphere in 1939 by Carl Gustaf Rossby [60; 61] determined the velocity of these large scale flow patterns in the zonal direction which propagate westward in the atmosphere with very low frequency. They are characterised by a very long wavelength of the order 10^5m, an amplitude of 10^1m and modenumber of order 5 in the earth's atmosphere and their velocity is proportional to the gradient of the Coriolos force. However they are more difficult to observe in the oceans since they exist in the thermocline where they are characterised by a very long wavelength of the order 5×10^5m, amplitude 5×10^1m. These waves and their stability properties are largely responsible for the unpredictable mid-latitude weather systems experienced on earth due to the creation of cyclones and anticyclones.

All types of waves, including Rossby and drift waves, can be considered weakly nonlinear if they have sufficiently small amplitudes such that for short times they evolve as

independent linear waves. This suggests that in the small time limit the wave amplitudes are time-independent. For longer times the wave amplitudes do vary but at a rate much slower than the linear wave period. Wave turbulence theory therefore, passes from the dynamic description of a wave system to a kinetic or statistical description in order to eliminate the slow evolution of approximately constant wave amplitudes in the linear approximation and the rapid phase dynamics which neither have a great effect on the amplitude evolution.

By the superposition principle, any linear combination of two or more waves of different wavenumber is simply linear solution also and there is no energy exchange between the modes in the linear approximation. Energy exchange only occurs in higher energy approximations and while the nonlinear interactions can be non-resonant where the waves will simply generate other waves of very low amplitude, the energy exchanged between modes is maximised when the modes are in resonance. It is resonant interactions which are therefore important and of more interest. The nature of the nonlinear interaction depends on the medium and in the case of Rossby and drift waves described by the CHM equation, these interactions are resonant triad interactions [34; 3] since the nonlinearity is quadratic. Resonant interactions transfer energy between modes whose wavenumbers and dispersion relations both sum to zero. The nonlinear dynamics of a triad of Rossby waves is constrained by the imposition of energy and enstrophy conservation.

Lorenz was the first to analyse the stability of Rossby's solution to a small perturbation, concluding that Rossby waves may in fact be unstable and are therefore not regularly observed in the atmosphere since they give rise to other structures [38]. A couple of years later, Gill took up the stability problem and deduced that Rossby waves of all wavenumbers can in fact be unstable [8] but that the nature of the instability depends on a parameter related to the velocity and wavenumber of the initial primary wave.

More recent work has taken an alternative view of the instability of quasigeostrophic Rossby waves as growth of a phase perturbation to the base wave and extended it to a baroclinic situation [62] to account for stratification although the growth rate in this is not as accurately predicted as the traditional linear stability analysis.

Work presented here extends the theory of Gill [8] to show that for strong primary

waves the most unstable modes are perpendicular to the primary wave, which correspond to generation of a zonal flow if the primary wave is purely meridional. For weak waves, the maximum growth occurs for off-zonal inclined modulations which are close to being in three-wave resonance with the primary wave. Numerical simulations confirm the theoretical predictions of the linear theory [8] as well as showing nonlinear jet pinching [63]. For strong primary waves, these narrow zonal jets further roll up into Karman-like vortex streets while for weak primary waves, the growth of the unstable mode reverses and the system oscillates between a dominant jet and a dominant primary wave.

The Rossby and drift wave system is a special case of wave turbulence in that the wave kinetic equation exactly conserves an extra quadratic invariant that is not a linear combination of the other two. Actually, the invariant also contains a cubic term whose form depends on the nonlinear action between the waves but it was shown that for long times, the cubic term can be neglected [64]. Recently the physical space representation of this invariant was determined, a step towards deducing its actual physical meaning [65] since it is always referred to in Fourier space. Furthermore, it was shown that the zonostrophy could be more significant than the enstrophy since it is less sensitive to dissipation than enstrophy is, thought to be due to the fact it is based on large scale modes, as is the energy while the enstrophy integral is based mainly on small scale modes [64; 65].

When the turbulence is dominated by waves which are involved in triad interactions, it conserves the energy, potential enstrophy and zonostrophy. For the particular case of small scale turbulence, the zonostrophy is a positive quantity so that an argument similar to the standard Fjørtoft argument, originally developed for the 2D NS turbulence [43], is used to examine the triple cascade process of the invariants. It was found that each of the invariants is forced by the other two to cascade into its own anisotropic sector of scales and in particular, the energy is forced to cascade to long zonal scales.

The original theory [66; 45] was limited to considering either very large scales, longer than the Rossby deformation radius or the Larmor radius, or to the scales which are already anisotropic and are close to zonal. Besides, the conservation of the extra

invariant is based on the weakness of nonlinearity and on the randomness of phases, conditions too of the validity of the wave kinetic equation, which even if present initially, can break down later during the zonation process. Thus, numerical checks of robustness of the zonostrophy conservation were required.

Soon after the original theory was presented [66; 45], the zonostrophy invariant was generalised to the whole of the k-space in [46]. This was a significant achievement because the extra invariant of such a kind appeared to be unique for Rossby and drift systems and is not observed in any other known nonlinear wave model. However the general expression for zonostrophy appeared to have a form for which the Fjørtoft argument cannot be used since it is neither scale invariant nor sign-definite.

Some of the main features of hydrodynamic turbulence, the most-recognised form of turbulence, are those previously mentioned, namely, Richardson's cascade [25] and the Kolmogorov-Obukhov spectra [28; 29; 30] and much research on turbulence, numerical and experimental, aim to prove or disprove the universality of this spectrum. More than two decades after Kolmogorov's work, Zakharov derived similar spectra for wave turbulence theory from the medium of the waves from which the hypothesis of locality can be tested explicitly [67; 68]. He deduced that a necessary condition for turbulence to be local is that the collision integral of the kinetic equation converges so that the KZ spectra is a solution of the kinetic equation. These spectra can be derived for both isotropic and anisotropic media.

Assuming nonlocality, Chapter 6 presents an extended derivation of the nonlocal kinetic equation first presented in [10; 11] which simplifies to an anisotropic diffusion equation showing the diffusion of the turbulence spectrum in k-space. As predicted, numerical simulations show that this spectrum breaks into two unconnected parts.

Chapter 3

The Charney-Hasegawa-Mima Equation

The work presented in this thesis is based on the CHM equation so a full derivation of both the Charney equation and the Hasegawa-Mima (HM) equation are now detailed.

3.1 Dynamic equation

3.1.1 The Charney equation

Until the late 1940s numerical calculations of the atmospheric equations of motion remained unduly complicated since they required integrating over the whole range of scales. It had been pointed out by meteorologists that the motions which contribute to the large scale weather patterns could be classified as quasi-hydrostatic, quasi-adiabatic, quasi-horizontal and quasi-geostrophic [1] so using this as a basis, Charney filtered out the noise from the governing fluid equations to leave only the important long wavelength waves that contribute to the large scale weather phenomena in the midlatitudes. The derivation of the Charney equation [1; 3] from first principles is presented.

The x-axis is in the zonal direction, directed west to east, the y-axis is the meridional axis, from south to north and z is in the vertical direction. Derived from Newton's law in a rotating framework, the equations which govern geophysical flows for

u, the velocity in the x-direction, v, the velocity in the y-direction, w, the velocity in the z-direction, the pressure p and density ϱ are:
the x-momentum

$$\frac{\partial u}{\partial t} + u\frac{\partial u}{\partial x} + v\frac{\partial u}{\partial y} + w\frac{\partial u}{\partial z} - fv = -\frac{1}{\varrho}\frac{\partial p}{\partial x} + \nu\frac{\partial^2 u}{\partial z^2}, \tag{3.1}$$

the y-momentum

$$\frac{\partial v}{\partial t} + u\frac{\partial v}{\partial x} + v\frac{\partial v}{\partial y} + w\frac{\partial v}{\partial z} + fu = -\frac{1}{\varrho}\frac{\partial p}{\partial y} + \nu\frac{\partial^2 v}{\partial z^2}, \tag{3.2}$$

the z-momentum

$$0 = -\frac{\partial p}{\partial z} - \varrho g, \tag{3.3}$$

the incompressibility condition

$$\frac{\partial u}{\partial x} + \frac{\partial v}{\partial y} + \frac{\partial w}{\partial z} = 0, \tag{3.4}$$

and the continuity equation

$$\frac{\partial \varrho}{\partial t} + u\frac{\partial \varrho}{\partial x} + v\frac{\partial \varrho}{\partial y} + w\frac{\partial \varrho}{\partial z} = \kappa\frac{\partial^2 \varrho}{\partial z^2}\,. \tag{3.5}$$

The forces due to the Coriolis parameter $f = 2|\Omega_e|sin\varphi$, arise due to the rotating framework of reference, where Ω_e is the dynamically important normal component of the earth's rotation rate, parallel to the vertical axis through the centre of the earth and φ is latitude. g is the gravitational force, ν and κ are constant kinematic viscosity and diffusivity coefficient respectively.

The incompressibility condition given by equation (Eq.) 3.4 derives from the conservation of mass otherwise known as the continuity equation given by Eq. 3.5. For an incompressible fluid, the density variation is negligible so that the density can be considered constant and the continuity equation is reduced to the incompressibily condition.

These nonlinear equations can be simplified under various different assumptions and scaling arguments. The introduction of the β-plane, as sketched in figure 3.1, a plane tangent to the earth's surface at the latitude φ_0, where a spatially local approximation is taken of the Coriolis parameter is one such simplification. The β-plane is finite in size

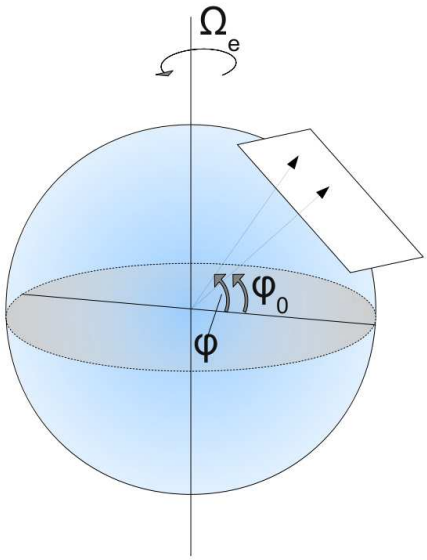

Figure 3.1: Sketch of a β-plane

such that $\varphi - \varphi_0 \ll 1$ and then f can be Taylor expanded as

$$\begin{aligned} f(\varphi) &\approx 2|\Omega_e| \left(\sin\varphi_0 + \cos\varphi_0(\varphi - \varphi_0)\right) + \mathrm{O}((\varphi - \varphi_0)^2) \\ &= f_0 + \beta(y - y_0) \end{aligned} \tag{3.6}$$

where $f_0 = 2|\Omega_e| \sin\varphi_0$ and $\beta = 2|\Omega_e| \cos\varphi_0$ and $y \equiv \varphi$.

Observational data revealed that the large scale motions in the atmosphere occur approximately in a barotropic atmosphere, i.e. on surfaces of constant density. Thus, consider a shallow layer of inviscid fluid with constant density ϱ_0, at a height $z = h(x, y, t)$ above the reference level $z = 0$ as shown in figure 3.2. Then Eq. 3.3 which describes hydrostatic balance, can immediately be integrated over the layer depth with the boundary condition $p(x, y, h) = p_0$, to give

$$p = -\varrho_0 g h + p_0 \,. \tag{3.7}$$

It follows that the horizontal pressure gradient is independent of z,

$$\begin{aligned} \frac{\partial p}{\partial x} &= \varrho_0 g \frac{\partial h}{\partial x} \\ \frac{\partial p}{\partial y} &= \varrho_0 g \frac{\partial h}{\partial y} \end{aligned} \tag{3.8}$$

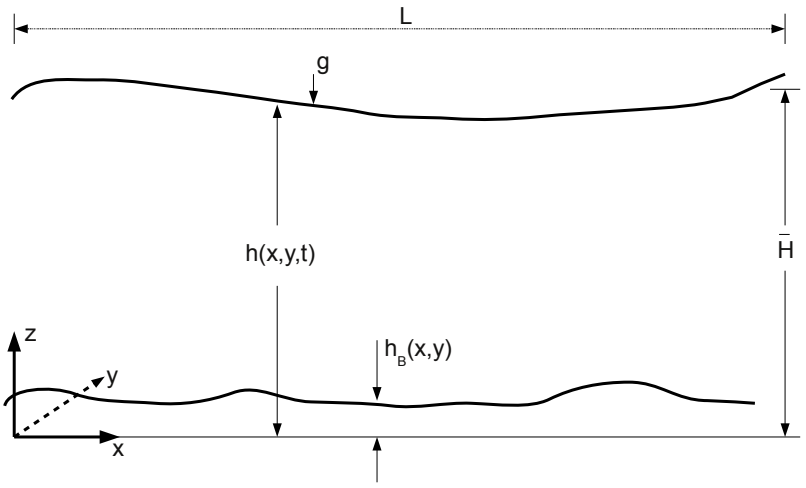

Figure 3.2: Idealisation of the shallow water model

so that the horizontal accelerations must also be independent of z and it can be assumed too that the horizontal velocities u and v are independent of z if they are so initially. Substituting these gradients into Eqs 3.1 and 3.2 respectively, while neglecting vertical acceleration terms since they are small in comparison to those in the horizontal, the horizontal momentum equations then become

$$\begin{aligned} \frac{\partial u}{\partial t} + u\frac{\partial u}{\partial x} + v\frac{\partial u}{\partial y} - fv &= -g\frac{\partial h}{\partial x} \\ \frac{\partial v}{\partial t} + u\frac{\partial v}{\partial x} + v\frac{\partial v}{\partial y} + fu &= -g\frac{\partial h}{\partial y}\,. \end{aligned} \tag{3.9}$$

The vertical velocity at $z = h$ is given by

$$w(x, y, z, t) = \frac{dh}{dt} = \frac{\partial h}{\partial t} + u\frac{\partial h}{\partial x} + v\frac{\partial h}{\partial y} \tag{3.10}$$

Integrating the continuity Eq. 3.4 with the condition of no normal flow at the rigid surface, $z = h_B$

$$w(x, y, h_B, t) = u\frac{\partial h_B}{\partial x} + v\frac{\partial h_B}{\partial y}$$

and combining the result with Eq. 3.10 yields

$$\frac{dH}{dt} + H\left(\frac{\partial u}{\partial x} + \frac{\partial v}{\partial y}\right) = 0\,. \tag{3.11}$$

Eqs 3.9 and 3.11 have reduced the variables in the dynamical equations to u, v and h, thereby eliminating w from the dynamics and z from the governing equations. These equations constitute the shallow water model in geophysical fluid dynamics.

From figure 3.2 the fluid height can also be expressed as

$$H = \bar{H}(x, y) + \eta - h_B \tag{3.12}$$

where the free-surface displacement η from the undisturbed, constant height $\bar{H}$, can directly replace the dynamical variable h in Eqs 3.9 and 3.11. As Charney was interested in the large scale motions in the atmosphere, with time scales longer than the rotation period of the earth, he imposed scales, T, L, U and N_0 on the time, length, velocity and height respectively, which would characterise the dynamics with non-dimensional variables of order unity. These scales can be used to non-dimensionalise the foregoing dynamical equations as

$$\begin{aligned} (x, y) &= L(\hat{x}, \hat{y}) \\ t &= T\hat{t} \\ (u, v) &= U(\hat{u}, \hat{v}) \\ \eta &= N_0\hat{\eta} \end{aligned} \tag{3.13}$$

Inserting Eqs 3.13 into Eqs 3.9 and 3.11, remembering that $\bar{H}$ is constant gives

$$\begin{aligned} \frac{U}{T}\frac{\partial \hat{u}}{\partial \hat{t}} + \frac{U^2}{L}\left[\hat{u}\frac{\partial \hat{u}}{\partial \hat{x}} + v\frac{\partial \hat{u}}{\partial \hat{y}}\right] - fU\hat{v} &= -g\frac{N_0}{L}\frac{\partial \hat{\eta}}{\partial \hat{x}} \\ \frac{U}{T}\frac{\partial \hat{v}}{\partial \hat{t}} + \frac{U^2}{L}\left[\hat{u}\frac{\partial \hat{v}}{\partial \hat{x}} + v\frac{\partial \hat{v}}{\partial \hat{y}}\right] + fU\hat{u} &= -g\frac{N_0}{L}\frac{\partial \hat{\eta}}{\partial \hat{y}} \end{aligned} \tag{3.14}$$

$$\frac{N_0}{T}\frac{\partial \hat{\eta}}{\partial \hat{t}} + \frac{U}{L}\left[\hat{u}\frac{\partial}{\partial \hat{x}}(N_0\hat{\eta} - h_B) + \hat{v}\frac{\partial}{\partial \hat{y}}(N_0\hat{\eta} - h_B)\right] + \frac{U}{L}(\bar{H} + N_0\hat{\eta} - h_B)\left[\frac{\partial \hat{u}}{\partial \hat{x}} + \frac{\partial \hat{u}}{\partial \hat{y}}\right] = 0$$

In these equations, there exists the dimensionless Rossby and temporal Rossby numbers, two very important ratios in GFD defined here respectively as

$$R_o = \frac{U}{fL} \tag{3.15}$$

$$R_T = \frac{1}{fT}\,. \tag{3.16}$$

They both measure ratio of the advection terms to the Coriolis term. If $R_o \ll 1$ and $R_T \ll 1$ then the acceleration terms in Eqs 3.14 will be small and the term on the right-hand side (RHS) must then be large enough to balance the Coriolis terms. To ensure this, choose

$$N_0 = \frac{fUL}{g} \tag{3.17}$$

which can be rearranged to

$$N_0 = R_o \frac{L^2}{R^2} \tag{3.18}$$

where

$$R = \frac{\sqrt{g\bar{H}}}{f} \tag{3.19}$$

is known as the Rossby radius of deformation. Then Eq. 3.12 can be rewritten as

$$H = \bar{H}\left(1 + R_o \frac{L^2}{R^2}\hat{\eta} - \frac{h_B}{\bar{H}}\right) \tag{3.20}$$

and Eqs 3.14 can be expressed wholly in terms of non-dimensional variables and parameters as

$$\begin{aligned} R_T \frac{\partial \hat{u}}{\partial \hat{t}} + R_o \left[\hat{u}\frac{\partial \hat{u}}{\partial \hat{x}} + v\frac{\partial \hat{u}}{\partial \hat{y}}\right] - \hat{v} &= -\frac{\partial \hat{\eta}}{\partial \hat{x}} \\ R_T \frac{\partial \hat{v}}{\partial \hat{t}} + R_o \left[\hat{u}\frac{\partial \hat{v}}{\partial \hat{x}} + v\frac{\partial \hat{v}}{\partial \hat{y}}\right] + \hat{u} &= -\frac{\partial \hat{\eta}}{\partial \hat{y}} \end{aligned} \tag{3.21}$$

$$R_T F \frac{\partial \hat{\eta}}{\partial \hat{t}} + R_o F \left(\hat{u}\frac{\partial \hat{\eta}}{\partial \hat{x}} + \hat{v}\frac{\partial \hat{\eta}}{\partial \hat{y}}\right) - \left(\hat{u}\frac{\partial}{\partial \hat{x}} + \hat{v}\frac{\partial}{\partial \hat{y}}\right)\left(\frac{h_B}{\bar{H}}\right) \tag{3.22}$$

$$+ \left[1 + R_o F\bar{\eta} - \frac{h_B}{\bar{H}}\right]\left(\frac{\partial \hat{u}}{\partial \hat{x}} + \frac{\partial \hat{u}}{\partial \hat{y}}\right) = 0 \tag{3.23}$$

where

$$F = \left(\frac{L}{R}\right)^2 \tag{3.24}$$

Since the flows of interest are for small R_o and small R_T, assume $R_o = R_T$, expand each variable, $\hat{u}$, $\hat{v}$ and $\hat{\eta}$ in orders of R_o i.e.

$$\hat{u}(x, y, t, R_o) = u_0(x, y, t) + R_o\, u_1(x, y, t) + R_o^2\, u_2(x, y, t) + \ldots\ldots, \tag{3.25}$$

etc. Inserting these into Eqs 3.21, equating powers of R_o and dropping the non-dimensional hat symbol for brevity, gives in order $\mathrm{O}(1)$

$$\begin{aligned} u_0 &= -\frac{\partial \eta_0}{\partial y} \\ v_0 &= \frac{\partial \eta_0}{\partial x}\,. \end{aligned} \tag{3.26}$$

Assuming that $\frac{h_B}{\bar{H}}$ is of the same order as the R_o, define

$$\frac{h_B}{\bar{H}} = R_o\,\eta_B \tag{3.27}$$

then the next approximation, $\mathrm{O}(R_o)$ gives

$$\begin{aligned} \frac{\partial u_0}{\partial t} + u_0\frac{\partial u_0}{\partial x} + v_0\frac{\partial u_0}{\partial y} - v_1 &= -\frac{\partial \eta_1}{\partial x} \\ \frac{\partial v_0}{\partial t} + u_0\frac{\partial v_0}{\partial x} + v_0\frac{\partial v_0}{\partial y} + u_1 &= -\frac{\partial \eta_1}{\partial y} \end{aligned} \tag{3.28}$$

$$F\left[\frac{\partial \eta_0}{\partial t} + u_0\frac{\partial \eta_0}{\partial x} + v_0\frac{\partial \eta_0}{\partial y}\right] - u_0\frac{\partial \eta_B}{\partial x} - v_0\frac{\partial \eta_B}{\partial y} + \left(\frac{\partial u_1}{\partial x} + \frac{\partial v_1}{\partial y}\right) = 0\,. \tag{3.29}$$

To obtain a closed dynamical system in the $\mathrm{O}(1)$ fields only, cross-multiplying Eqs 3.29 gives

$$\frac{\partial \varsigma}{\partial t} + u_0\frac{\partial \varsigma}{\partial x} + v_0\frac{\partial \varsigma}{\partial y} = -\left(\frac{\partial u_1}{\partial x} + \frac{\partial v_1}{\partial y}\right) \tag{3.30}$$

where

$$\varsigma = \frac{\partial v_0}{\partial x} - \frac{\partial u_0}{\partial y}\,, \tag{3.31}$$

is the total vorticity. From 3.26, it follows that

$$\varsigma = \nabla^2\eta_0\,, \tag{3.32}$$

which is equivalent to the definition of the vorticity in terms of the stream function ψ and thus, $\eta_0 \equiv \psi(x, y, t)$ in the $\mathrm{O}(1)$ velocity field defined as

$$\begin{aligned} u_0 &= -\frac{\partial \psi}{\partial y} \\ v_0 &= \frac{\partial \psi}{\partial x}\,. \end{aligned} \tag{3.33}$$

The LHS of Eq. 3.30 can be used to eliminate the $\mathrm{O}(1)$ velocity and using the identities in Eq. 3.33, the result is,

$$\frac{\partial}{\partial t}(\nabla^2\psi - F\psi) + \frac{\partial \psi}{\partial x}\frac{\partial \nabla^2\psi}{\partial y} - \frac{\partial \psi}{\partial y}\frac{\partial \nabla^2\psi}{\partial x} + \frac{\partial \psi}{\partial x}\frac{\partial \eta_B}{\partial y} - \frac{\partial \psi}{\partial y}\frac{\partial \eta}{\partial x} = 0 \tag{3.34}$$

The variation in bottom topography η_B in the presence of constant f, plays an equivalent role to the variation of the Coriolis parameter with latitude which from Eq. 3.6 is βy [3] so that replacing η_B with βy in Eq. 3.34, results in the QG PV equation, otherwise known as the Charney equation [1],

$$\frac{\partial}{\partial t}(\nabla^2\psi - F\psi) + \beta\frac{\partial\psi}{\partial x} + \frac{\partial\psi}{\partial x}\frac{\partial\nabla^2\psi}{\partial y} - \frac{\partial\psi}{\partial y}\frac{\partial\nabla^2\psi}{\partial x} = 0\,. \tag{3.35}$$

The QG model is a simplified geophysical fluid model at asymptotically high rotation rate or at small Rossby number, a condition imposed in the derivation, for which the variables are evaluated through their geostrophic values [3]. It assumes a hydrostatic balance between the vertical pressure gradient and gravity and geostrophic balance between the horizontal pressure gradient and Coriolis pressure.

3.1.2 Hasegawa-Mima equation

The HM equation [2] is the simplest single-fluid description of a strongly magnetised plasma. Here, it is derived from first principles, beginning with the continuity of ions.

Assume an inhomogeneous plasma such that the density at any given point depends on the position of that point i.e. $n_0 = n_0(\mathbf{x})$ in an homogeneous background magnetic field $\mathbf{B} = B_0\hat{e_z}$ and subjected to a conservative electric field $\mathbf{E} = -\nabla\phi$, where ϕ is the electric potential. When a plasma is produced by a gas discharge, the electrons are accelerated more efficiently by $\mathbf{E}$ than the heavier ions. As a result, the kinetic energy and thus the temperature of the electrons, T_e, is much greater than that of the ions, T_i so that a non-isothermal plasma is assumed, the so-called *cold ion approximation* in which $T_e \gg T_i$. Neglecting the parallel (to the magnetic field) inertia of the ions, their continuity equation is given by

$$\frac{\partial n}{\partial t} + \nabla_\perp \cdot (n_0\mathbf{v}) = 0. \tag{3.36}$$

The drift velocity $\mathbf{v}$ has components $\mathbf{v}_E + \mathbf{v}_p$ where $\mathbf{v}_E$ is due to the $\mathbf{E}\times\mathbf{B}$ field and $\mathbf{v}_p$ arises from the polarisation. While $\mathbf{v}_E \gg \mathbf{v}_p$, both terms remain in the approximation since it is the polarisation drift that allows for compression of the ions.

Now employing the basic laws of inertia, with respect to a fixed frame of reference, the rate of change of linear momentum of the ions equals the force applied to them.

Assuming that frictional forces are negligible here, the external forces applied to the ions of mass m_i and charge e_i, are that due to the magnetic field, $e_i\mathbf{v}\times\mathbf{B}$, that due to the electric field, $e_i\mathbf{E}$ and the traction force is ∇p_i where p_i is the ion pressure. This gives,

$$n_i m_i\left(\frac{\partial \mathbf{v}_i}{\partial t}+(\mathbf{v}\cdot\nabla)\mathbf{v}_i)\right)=\nabla p_i-n_i(e_i\mathbf{E}+e_i\mathbf{v}\times\mathbf{B}). \tag{3.37}$$

For cold ions, $\nabla p_i=0$ so the balance of ion momentum becomes

$$\frac{\partial \mathbf{v}_i}{\partial t}+(\mathbf{v}\cdot\nabla)\mathbf{v}_i=\frac{e_i}{m_i}(-\nabla\phi+\mathbf{v}\times\mathbf{B}). \tag{3.38}$$

To a first approximation for $\mathbf{v}\sim\mathbf{v}_E$ and assuming the rate of change of linear momentum is zero, $\nabla\phi=\mathbf{v}_E\times\mathbf{B}$. Rearranging this using the triple vector product identity gives an expression for the $\mathbf{E}\times\mathbf{B}$ drift velocity

$$\mathbf{v}_E=\frac{\mathbf{B}\times\nabla\phi}{|B|^2}. \tag{3.39}$$

In the second approximation for $\mathbf{v}\sim\mathbf{v}_p$, following the same procedure, an expression is obtained for the polarisation drift velocity

$$\mathbf{v}_p=\frac{1}{\omega_{ci}B_0}\left[\frac{\partial}{\partial t}\nabla\phi+(\mathbf{v}_E\cdot\nabla_\perp)\nabla_\perp\phi\right] \tag{3.40}$$

where

$$\omega_{ci}=\frac{e_iB_0}{m_i} \tag{3.41}$$

is the ion cyclotron frequency or gyrofrequency which defines the frequency of the circular motion of the ion with Larmor radius

$$\rho_i=\frac{m_iv_\perp}{e_iB_0} \tag{3.42}$$

in the presence of a magnetic field, $v_\perp$ being the velocity component perpendicular to the magnetic field.

The densities of the ions and electrons have a Boltzmann distribution and are adiabatic due to a slow variation of ϕ in the parallel direction,

$$n=n_0\exp\left(\frac{e\phi}{T_e}\right), \tag{3.43}$$

where n and n_0 are the perturbed and unperturbed densities respectively. Taking logarithms and expanding this distribution,

$$\ln n = \ln n_0 + \frac{e\phi}{T_e}. \tag{3.44}$$

Substituting this into Eq. 3.36, the continuity for ions now becomes

$$\frac{\partial}{\partial t}\frac{e\phi}{T_e} + \mathbf{v}_E \cdot \nabla_\perp(\ln n_0 + \frac{e\phi}{T_e}) + \nabla_\perp \cdot \mathbf{v}_p = 0. \tag{3.45}$$

Now introducing the drift velocities Eqs 3.39 and 3.40 into Eq. 3.45,

$$\frac{\partial}{\partial t}\frac{e\phi}{T_e} - [(\nabla\phi \times \hat{z}) \cdot \nabla_\perp]\left(\ln n_0 + \frac{e\phi}{T_e}\right) - \nabla_\perp\left(\frac{1}{\omega_{ci}B_0}\frac{d}{dt}\nabla\phi\right) = 0. \tag{3.46}$$

Use the normalisations $\omega_{ci}t \to t$, $\frac{x,y}{\rho_i} \to x, y$ and $\frac{e\phi}{T_e} \to \phi$ where $\rho_i = \frac{1}{\omega_{ci}}\sqrt{\frac{T_e}{m_i}}$ is the ion gyroradius and with the use of Eq. 3.41, rearrange to give the Hasegawa-Mima equation

$$\frac{\partial}{\partial t}\left(\nabla^2\phi - \phi\right) - \left[(\nabla\phi \times \hat{z}) \cdot \nabla\right]\left[\nabla^2\phi - \ln n_0\right] = 0. \tag{3.47}$$

This is equivalent to

$$\frac{\partial}{\partial t}(\nabla^2\phi - \frac{1}{\rho_i^2}\phi) + \nabla \ln n_0 \frac{\partial\phi}{\partial x} + \frac{\partial\phi}{\partial x}\frac{\partial\nabla^2\phi}{\partial y} - \frac{\partial\phi}{\partial y}\frac{\partial\nabla^2\phi}{\partial x} = 0\,. \tag{3.48}$$

3.1.3 Analogy between Rossby waves and drift waves

The similarities between Eqs 3.35 and 3.48 are evident, as was first pointed out by Hasegawa and Maclennan [37; 4]. It is often referred to as the collective Charney-Hasegawa-Mima equation even though the time and physical scales associated with each of the waves differ by many orders of magnitude. Typical time and space parameters for the drift wave are a wavelength of the order of the ion Larmor radius, typically 1-10mm with a characteristic timescale period of the order 1×10^{-3} s. For the Rossby wave in the atmosphere the wavelength is typically of the order 2×10^6m [1] with a period of approximately 5 days. The linear wave frequency of the Rossby wave is much smaller than the Coriolis frequency just as the drift wave frequency is much smaller than the ion cyclotron frequency. A more detailed analogy between drift and Rossby waves is given in table 3.1 [4] with some typical orders of magnitudes of the variables. Evidently, there are some extreme assumptions made during the derivation of the Charney and HM

Table 3.1: Analogy between the drift wave and the Rossby wave

Drift wave	Rossby wave
Electrostatic potential ϕ	Variable fluid depth η
Background density n_0	Average depth $\bar{H}$
$\mathbf{E} \times \mathbf{B}$ drift	Geostrophic flow
Wavelength $\approx 1 \times 10^{-3}$m	Wavelength $\approx 2 \times 10^{6}$m
Period $\approx 1 \times 10^{-3}$s	Period ≈ 5 days
Ion cyclotron frequency $\omega_{ci} \approx 10^{8} s^{-1}$	Coriolis parameter $f \approx 10^{-4} s^{-1}$
$\beta = \frac{\partial}{\partial y} \ln n_0$	$\beta = \frac{\partial f}{\partial y}$
Larmor radius $\rho_i = \frac{1}{\omega_{ci}} \sqrt{\frac{T_e}{m_i}} \approx 10^{-3}$m	Rossby radius $R = \frac{\sqrt{g\bar{H}}}{f} \approx 2 \times 10^{6}$m
Drift velocity	Rossby velocity
Dispersion relation $\omega_{\mathbf{k}} = -\frac{\beta k_x \rho^2}{1+\rho_i^2 k^2}$	Dispersion relation $\omega_{\mathbf{k}} = -\frac{\beta k_x}{k^2+F}$

equations. Nonetheless, they provide a very simple and useful model for both GFD and plasma theory since the nonlinear dynamics can replicate turbulent, coherent and wave behaviour [4]. While the true dynamics are 3D, they can be approximated as horizontal in GFD or poloidal dynamics in plasma theory because the vertical/toroidal coordinate becomes a dependent variable. Hereafter, the basic dynamic equation will be referred to in the form of Eq. 3.35.

Hereafter, the following expressions are deemed equivalent for the purposes of the CHM equation and shall be used interchangeably,

$$F = \frac{1}{R^2} \equiv \frac{1}{\rho_i^2} \equiv \frac{1}{\rho^2} \,. \tag{3.49}$$

3.1.4 Conservation of energy and enstrophy

Around the middle of the last century, the importance of the vorticity and its effect on the energy cascade in 2D turbulence became apparent [69; 70; 43]. As with 2D hydrodynamic turbulence, energy E and enstrophy Q, otherwise referred to as *the mean squared vorticity*, are conserved for Rossby and drift wave turbulence.

Re-writing the nonlinear term in Eq. 3.35 as $(-\nabla\psi \times \hat{z})\nabla \cdot \nabla^2\psi$, multiplying by ψ and integrating over the periodic domain gives

$$\int \left[\frac{\partial}{\partial t} \left[\psi \nabla^2 \psi - f\psi^2 \right] + \psi\beta \frac{\partial \psi}{\partial x} - \psi \left[(\nabla\psi \times \hat{z}) \nabla \cdot \nabla^2 \psi \right] \right] dx\, dy = 0 \,.$$

With a little manipulation and rearranging of terms, the result is

$$\frac{1}{2}\frac{\partial}{\partial t}\int\left[(\nabla\psi)^2+F\psi^2\right]dx\,dy+\int\nabla\cdot\left[-\psi\nabla\frac{\partial\psi}{\partial t}-\frac{1}{2}\beta\hat{x}\psi^2+\psi\nabla^2\psi\nabla\psi\times\hat{z}\right]dx\,dy=0\,. \tag{3.50}$$

The first integral represents the total energy of the system, E, the first term of which is the kinetic energy. In k-space this equals $\frac{1}{2}k^2\hat{\psi}^2=\frac{1}{2}(k_x^2+k_y^2)\hat{\psi}^2$ which in lieu of Eq. 3.33, is equivalent to $\frac{1}{2}v^2$. The second term is equivalent to the potential energy since $\rho g\int_0^{\eta_0}zdz\propto\eta_0^2\equiv\psi^2(x,y,t)$. In the case of a plasma, the total energy density is given by $\frac{n^2T}{n_0}+m_in_0v_E^2$ [2] and by Eqs 3.43 and 3.39 this can also represents the total energy of the system.

Now defining the term within the square brackets of Eq. 3.50 as

$$\mathbf{G}_E=-\psi\nabla\frac{\partial\psi}{\partial t}-\frac{1}{2}\beta\hat{i}\psi^2+\psi\nabla^2\psi\nabla\psi\times\hat{z}\,, \tag{3.51}$$

Eq. 3.50 can be re-written as

$$\frac{\partial E}{\partial t}+\nabla\cdot\mathbf{G}_E=0 \tag{3.52}$$

and by Gauss' divergence theorem this is equivalent to the surface integral

$$\frac{\partial E}{\partial t}=-\int\mathbf{G}_E\cdot\hat{\mathbf{n}}ds \tag{3.53}$$

where $\hat{\mathbf{n}}$ is the outward unit normal of the surface and s the arc length of the curve which encloses that surface. On a bounded region, the no-slip condition $\mathbf{u}\cdot\hat{\mathbf{n}}=0$ is satisfied and the β term sums to zero, from which it follows that $\frac{\partial}{\partial t}\int(\nabla\psi\cdot\hat{\mathbf{n}})ds=0$. This suggests that

$$\frac{\partial E}{\partial t}=0 \tag{3.54}$$

from which it can be deduced that the quantity

$$E=\frac{1}{2}\int_{\mathbf{k}}(\nabla\psi_{\mathbf{k}})^2+F\psi_{\mathbf{k}}^2\,dx\,dy \tag{3.55}$$

is conserved.

Similarly, multiplying Eq. 3.35 by $\nabla^2\psi$ gives conservation of the potential enstrophy, defined as

$$\int\left[\frac{\partial}{\partial t}\left[(\nabla^2\psi)^2-F\psi\nabla^2\psi\right]+\nabla^2\psi\beta\frac{\partial\psi}{\partial x}-\nabla^2\psi\left[(\nabla\psi\times\hat{z})\nabla\cdot\nabla^2\psi\right]\right]dx\,dy=0\,.$$

With a little manipulation and rearranging of terms, the result is

$$\frac{1}{2}\frac{\partial}{\partial t}\int \left[F(\nabla\psi)^2 + (\nabla^2\psi)^2\right] dx\, dy + \int \nabla\cdot\left[-\nabla\psi\frac{\partial\psi}{\partial t} + \beta\nabla\psi\frac{\partial\psi}{\partial x} + (\nabla^2\psi)^2\nabla\psi\times\hat{z}\right] dx\, dy = 0 \tag{3.56}$$

which again can be written in the format

$$\frac{\partial Q}{\partial t} = -\int \mathbf{G}_Q\cdot\hat{\mathbf{n}} ds \tag{3.57}$$

where the enstrophy Q is defined as

$$Q = \frac{1}{2}\int_{\mathbf{k}} F(\nabla\psi)^2 + (\nabla^2\psi)^2\, d\mathbf{k} \tag{3.58}$$

and

$$\mathbf{G}_Q = -\nabla\psi\frac{\partial\psi}{\partial t} - \nabla\psi\frac{\partial\psi}{\partial x} - (\nabla^2\psi)^2\psi\nabla\psi\times\hat{z}\,. \tag{3.59}$$

The RHS of Eq. 3.57 is zero, yielding the conservation of enstrophy as the result.

3.1.5 Fourier representation

It is often convenient to represent the wave modes, $\mathbf{k}, \mathbf{k}_n$ in Fourier or k-space by introducing the Fourier transform of the streamfunction,

$$\hat{\psi}_{\mathbf{k}} = \int \psi(\mathbf{x})\mathrm{e}^{-\mathrm{i}(\mathbf{k}\cdot\mathbf{x})}\, d\mathbf{x}\,, \tag{3.60}$$

The CHM equation in physical space, Eq. 3.35 is then equivalent to

$$\partial_t\hat{\psi}_{\mathbf{k}} = -i\,\omega_{\mathbf{k}}\,\hat{\psi}_{\mathbf{k}} + \frac{1}{2}\sum_{\mathbf{k}_1,\mathbf{k}_2} T(\mathbf{k},\mathbf{k}_1,\mathbf{k}_2)\,\hat{\psi}_{\mathbf{k}_1}\,\hat{\psi}_{\mathbf{k}_2}\,\delta(\mathbf{k}-\mathbf{k}_1-\mathbf{k}_2)\,, \tag{3.61}$$

where

$$\omega_{\mathbf{k}} = -\frac{\beta k_x}{k^2+F} \tag{3.62}$$

is the anisotropic dispersion relation for the linear solutions, $\mathbf{k} = (k_x, k_y)$, $k = |\mathbf{k}|$ and

$$T(\mathbf{k},\mathbf{k}_1,\mathbf{k}_2) = -\frac{(\mathbf{k}_1\times\mathbf{k}_2)_z\,(k_1^2-k_2^2)}{k^2+F} \tag{3.63}$$

is the nonlinear coupling coefficient.

3.2 Wave kinetic equation

It has been mentioned that in the weak nonlinearity limit, the turbulence of Rossby and drift waves can be described by the statistical description of wave turbulence in which the wave amplitudes can be considered to play the part of probability amplitudes [35; 33]. This wave turbulence approach can be justified when the underlying assumptions of wave turbulence theory are met, i.e. the waves are weakly nonlinear or have small amplitudes and are dispersive, they have random initial phases and the domain is infinite. As such, the coherence of interacting waves is much smaller than the domain size so that the domain contains many correlation lengths. A series of steps, to convert the nonlinear dynamic equation, Eq. 3.35 which describes the evolution the wave amplitudes and their phases, to a kinetic description, which will describe the evolution of their probability amplitudes are detailed below. The work presented in Chapters 5 and 6 are based on this kinetic equation so it is important that these wave turbulence assumptions are met when carrying out numerical work.

The wave action spectrum is defined as

$$n_{\mathbf{k}} = \frac{E}{\omega_{\mathbf{k}}}\,. \tag{3.64}$$

Also defined here is the waveaction variable $a_{\mathbf{k}}$ which acts like a probability amplitude in a large ensemble of wavenumbers

$$n_{\mathbf{k}} = |a_{\mathbf{k}}|^2 \tag{3.65}$$

and from Eqs 3.55 and 3.62, $a_{\mathbf{k}}$ can be defined as

$$a_{\mathbf{k}} = \frac{k^2 + F}{\sqrt{\beta k_x}}\hat{\psi}_{\mathbf{k}}\,. \tag{3.66}$$

Taking into account the $\mathbf{k}_1 \leftrightarrow \mathbf{k}_2$ symmetry of the wavenumbers, Eq. 3.61 can be re-written as

$$\partial_t a_{\mathbf{k}} = -\mathrm{i}\,\omega_{\mathbf{k}}\,a_{\mathbf{k}} + \frac{1}{2}\sum_{\mathbf{k}_1,\mathbf{k}_2} V_{12}^{k}\,\delta(\mathbf{k}-\mathbf{k}_1-\mathbf{k}_2)a_{\mathbf{k}_1}\,a_{\mathbf{k}_2}\,d\mathbf{k}_1 d\mathbf{k}_2 \tag{3.67}$$

where

$$V_{12}^{\mathbf{k}} \equiv V_{\mathbf{k}_1,\mathbf{k}_2}^{k} = \frac{\mathrm{i}}{2}\sqrt{\beta k_x k_{1_x} k_{2_x}}\left(\frac{k_{1_y}}{k_1^2+F} + \frac{k_{2_y}}{k_2^2+F} - \frac{k_y}{k^2+F}\right) \tag{3.68}$$

is the nonlinear interaction coefficient [71] for the waveaction variable, which exhibits the symmetries

$$V^{\mathbf{k}}_{\mathbf{k}_1,\mathbf{k}_2} = V^{\mathbf{k}}_{\mathbf{k}_2,\mathbf{k}_1} = -V^{\mathbf{k}_2}_{\mathbf{k},-\mathbf{k}_1} = -V^{-\mathbf{k}}_{-\mathbf{k}_1,-\mathbf{k}_2} \tag{3.69}$$

In order to filter out the fast linear oscillations, a perturbation series of the interaction variable, assuming a weak nonlinearity parameter, $\epsilon \ll 1$

$$b_{\mathbf{k}} = \frac{a_{\mathbf{k}}}{\epsilon} \mathrm{e}^{\mathrm{i}\,\omega_{\mathbf{k}} t} \tag{3.70}$$

is introduced into Eq. 3.67 to give

$$\mathrm{i}\frac{\partial b_{\mathbf{k}}}{\partial t} = \mathrm{sign} k_x \sum_{\mathbf{k}_1,\mathbf{k}_2} V^k_{12}\, \delta(\mathbf{k}-\mathbf{k}_1-\mathbf{k}_2) b_{\mathbf{k}_1}\, b_{\mathbf{k}_2}\, \mathrm{e}^{\mathrm{i}\,\omega^k_{12} t} \tag{3.71}$$

where

$$\omega^k_{12} = \omega_{\mathbf{k}} - \omega_{\mathbf{k}_1} - \omega_{\mathbf{k}_2}\,. \tag{3.72}$$

Introducing an intermediate time, T which lies between the linear and nonlinear time scale, the complex wave amplitude $b_{\mathbf{k}}$ is expanded in a perturbation series in the small nonlinearity parameter ϵ, at time $t = T$ as,

$$b_{\mathbf{k}}(T) = b^{(0)}_{\mathbf{k}} + \epsilon b^{(1)}_{\mathbf{k}} + \epsilon^2 b^{(2)}_{\mathbf{k}} + \ldots\,. \tag{3.73}$$

The aim is now to perform successive iterations in orders of ϵ to define $b^{(0)}_{\mathbf{k}}$ and note that $b_1 \equiv b_{\mathbf{k}_1}$ etc. for brevity

$$\mathrm{O}(1) \quad b^{(0)}_{\mathbf{k}} = b_{\mathbf{k}}|_{t=0} \tag{3.74}$$

$$\mathrm{O}(\epsilon) \quad b^{(1)}_{\mathbf{k}} = -\mathrm{i}\,\mathrm{sign} k_x \sum_{1,2} V^k_{12}\, b^{(0)}_1 b^{(0)}_2 \delta^k_{12} \Delta_T(\omega^k_{12}) \tag{3.75}$$

$$\mathrm{O}(\epsilon^2) \quad b^{(2)}_{\mathbf{k}} = \mathrm{sign} k_x \sum_{1,2} V^k_{12}\, (2 b^{(0)}_1 b^{(1)}_2) \delta^k_{12} \mathrm{e}^{\mathrm{i}\omega^k_{12} t} \tag{3.76}$$

where

$$\Delta_T(\omega^k_{12}) = \int_0^T \mathrm{e}^{\mathrm{i}\omega^k_{12} t} dt\,. \tag{3.77}$$

Substituting for $b^{(1)}_2$ from Eq. 3.75 into Eq. 3.76 gives,

$$b^{(2)}_{\mathbf{k}} = -\sum_{1,2,3,4} \mathrm{sign}(k_x k_{1_x}) V^k_{12}\, V^1_{34}\, b^{(0)}_3 b^{(0)}_4 b^{(0)}_2 \delta^1_{34} \delta^k_{12} \int_0^T \Delta_T(\omega^1_{34}) \mathrm{e}^{\mathrm{i}\omega^k_{12} t}\, dt\,. \tag{3.78}$$

$b_{\mathbf{k}}^{(0)}$ are time-independent and correspond to solutions to the dynamic equation when there are no interactions between modes. It is assumed that the phases of the modes are randomly distributed in k-space when an ensemble of experiments is considered and the change in the waveaction spectrum, $n_{\mathbf{k}}$ can be determined by the change in the probability amplitude, given by,

$$\delta n_{\mathbf{k}} = |b_{\mathbf{k}}(t)|^2 - |b_{\mathbf{k}}(t_0)|^2 \,. \tag{3.79}$$

To $\mathrm{O}(\epsilon)^2$,

$$\langle |b_{\mathbf{k}}|^2 \rangle = |b_{\mathbf{k}}(t_0)|^2 + \langle |b_{\mathbf{k}}^{(1)}|^2 \rangle + \langle |b_{\mathbf{k}}^{(0)} \bar{b}_{\mathbf{k}}^{(1)}|^2 \rangle + \langle |\bar{b}_{\mathbf{k}}^{(0)} b_{\mathbf{k}}^{(1)}|^2 \rangle + \langle |b_{\mathbf{k}}^{(0)} \bar{b}_{\mathbf{k}}^{(2)}|^2 \rangle + \langle |\bar{b}_{\mathbf{k}}^{(0)} b_{\mathbf{k}}^{(2)}|^2 \rangle \,, \tag{3.80}$$

where $\langle\,\rangle$ denotes averaging over the random phases. Taking each term in turn, using Eqs 3.74, 3.75 and 3.78 and averaging over the phases

$$\begin{aligned} \langle |b_{\mathbf{k}}^{(1)}|^2 \rangle &= \sum_{1,2} \sum_{3,4} b_1^{(0)} b_2^{(0)} \delta_{12}^k \Delta_T(\omega_{12}^k) \bar{b}_3^{(0)} \bar{b}_4^{(0)} \delta_{34}^k \Delta_T(\omega_{34}^k) V_{12}^k \bar{V}_{34}^k \\ &= 2 \sum_{1,2} |V_{12}^k|^2 n_{\mathbf{k}_1} n_{\mathbf{k}_2} \delta_{12}^k \left| \Delta_T(\omega_{12}^k) \right|^2 \end{aligned} \tag{3.81}$$

where the last step follows from $|b_1^{(0)}|^2 |b_2^{(0)}|^2 = n_{\mathbf{k}_1} n_{\mathbf{k}_2}$.

$$\langle |b_{\mathbf{k}}^{(0)} \bar{b}_{\mathbf{k}}^{(1)}|^2 \rangle = \frac{\mathrm{sign} k_x}{\mathrm{i}} \sum_{1,2} V_{12}^k b_{\mathbf{k}}^{(0)} \bar{b}_1^{(0)} \bar{b}_2^{(0)} \delta_{12}^k \Delta_T(\omega_{12}^k) \tag{3.82}$$

By Wick's contraction rule [72], Eq. 3.82 and its complex conjugate, denoted by $\mathrm{c.c.}$, are both zero. The last two terms in Eq. 3.80 provide the contribution

$$\begin{aligned} \langle |\bar{b}_{\mathbf{k}}^{(0)} b_{\mathbf{k}}^{(2)}|^2 \rangle = &- \sum_{1,2} \sum_{3,4} \mathrm{sign} k_x \mathrm{sign} k_{1_x} V_{12}^k \, V_{34}^1 \, b_{\mathbf{k}}^{(0)} b_3^{(0)} b_4^{(0)} b_2^{(0)} \delta_{34}^1 \delta_{12}^k \\ &\times \int_0^T \Delta_T(\omega_{34}^1) \mathrm{e}^{\mathrm{i}\omega_{12}^k t} \, dt + \mathrm{c.c.} \\ &= 2 \sum_{1,2} |V_{12}^k|^2 \delta_{12}^k \mathrm{Re} \left| \Delta_T(\omega_{12}^k) \right|^2 \\ &\times \left[\mathrm{sign}(\omega_{\mathbf{k}} \omega_{\mathbf{k}_2}) n_{\mathbf{k}} n_{\mathbf{k}_1} + \mathrm{sign}(\omega_{\mathbf{k}} \omega_{\mathbf{k}_1}) n_{\mathbf{k}} n_{\mathbf{k}_2} \right] . \end{aligned} \tag{3.83}$$

The term $|\Delta_T(\omega_{12}^k)|^2$ in Eqs 3.81 and 3.83 can be approximated in the long time limit

$\delta T \to \infty$ as,

$$\begin{aligned} |\Delta_T(\omega_{12}^k)|^2 &= \left| \int_0^T \mathrm{e}^{\mathrm{i}\omega_{12}^k t} dt \right|^2 = \frac{|1 - \mathrm{e}^{\mathrm{i}\omega_{12}^k t}|^2}{(\omega_{12}^k)^2} \\ &= \frac{|\mathrm{e}^{\frac{\mathrm{i}}{2}\omega_{12}^k t} - \mathrm{e}^{-\frac{\mathrm{i}}{2}\omega_{12}^k t}|^2}{(\omega_{12}^k)^2} \\ &= \frac{4\sin^2 \frac{(\omega_{12}^k)}{2} T}{(\omega_{12}^k)^2} \\ &\to 2\pi\delta T \delta(\omega_{12}^k) \end{aligned} \tag{3.84}$$

Collecting the terms now from Eqs 3.80 to 3.84, taking the large box limit i.e. $L \to \infty$ and inserting into Eq. 3.79 results in the evolution equation for the energy spectrum $n_{\mathbf{k}}$

$$\frac{\partial n_{\mathbf{k}}}{\partial t} = 4\pi \int \left|V_{12}^k\right|^2 \delta(\mathbf{k} - \mathbf{k}_1 - \mathbf{k}_2)\delta(\omega_{\mathbf{k}} - \omega_{\mathbf{k}_1} - \omega_{\mathbf{k}_2}) \times \left[n_{\mathbf{k}_1} n_{\mathbf{k}_2} - n_{\mathbf{k}} n_{\mathbf{k}_1} \operatorname{sign}(\omega_{\mathbf{k}}\omega_{\mathbf{k}_2}) - n_{\mathbf{k}} n_{\mathbf{k}_2} \operatorname{sign}(\omega_{\mathbf{k}}\omega_{\mathbf{k}_1})\right] d\mathbf{k}_1 d\mathbf{k}_2 \tag{3.85}$$

otherwise known as the wave kinetic equation. The RHS of Eq. 3.85 is called the collision integral and measures the rate of change of the energy spectrum. This can be written in a more general form and because $\hat{\psi}_{-\mathbf{k}} = \bar{\hat{\psi}}_{\mathbf{k}}$ and thus $n_{-\mathbf{k}} = n_{\mathbf{k}}$, only half of the k-space needs to be considered which is taken here as $k_x, k_{1_x}, k_{2_x} \geq 0$

$$\frac{\partial n_{\mathbf{k}}}{\partial t} = \int \left(\mathcal{R}_{12k} - \mathcal{R}_{k12} - \mathcal{R}_{2k1}\right) d\mathbf{k}_1 d\mathbf{k}_2 \tag{3.86}$$

where

$$\mathcal{R}_{12k} = 2\pi \left|V_{12}^k\right|^2 \delta_{12}^k \delta(\omega_{12}^k)(n_{\mathbf{k}_1} n_{\mathbf{k}_2} - n_{\mathbf{k}} n_{\mathbf{k}_1} - n_{\mathbf{k}} n_{\mathbf{k}_2}) \tag{3.87}$$

This form of the wave kinetic equation is also valid if the original variable ψ is complex, as is the case in wave systems such as the nonlinear Schrödinger equation which describes waves in nonlinear optics and Bose-Einstein condensates.

Furthermore, it is often convenient to derive the wave kinetic equation from a Hamiltonian description of the wave system, *especially* if the original variable ψ is complex. Wave turbulence is more commonly described by the Hamiltonian formalism, the advantage being that this approach contains all the necessary information required to study nonlinear interactions of all wave systems without specifically referring to the specific medium. The dispersion relation is the coefficient of the quadratic term of wave

amplitudes in the power series of the Hamiltonian, usually equivalent to the total energy, while the nonlinear interactions are described by the higher terms in the series. Details of the Hamiltonian formalism are given in Appendix A.

3.3 Numerical model

Given the assumptions made in deriving the CHM equation, a simple plane domain can be adopted for its solution. As such, a pseudospectral code with doubly-periodic boundaries has been chosen since the spatial derivatives can be calculated exactly in Fourier space while the nonlinear products can be calculated accurately in physical space. Details of the numerical scheme are given in Appendix B.

Chapter 4

Stability of Rossby Waves

Given that Eq. 3.61 admits Rossby and drift waves with the dispersion relation given by Eq. 3.62, it is natural to ask how stable these waves are to small perturbations. This Chapter revises the linear theory of the modulational instability of a monochromatic wave which was first analysed by Lorenz [38] and Gill [8], highlighting the main points of this theory. The character of the instability is studied using numerical and semi-analytical calculations, focusing on how this changes with the strength of the primary wave.

Direct numerical simulations (DNS), a three-mode truncation (3MT) and a four-mode truncation (4MT) systems are employed to study the nonlinear stage of the instability to determine just how useful the truncated models are in studying the nonlinear dynamics.

4.1 Spectral truncations

Spectral truncations of Eq. 3.61 are employed to assist in the study of the stability properties of Rossby waves by yielding an approximation to the linear growth rate of the instability. This can be compared to the results from the DNS of the full PDE.

4.1.1 Three-mode truncation (3MT)

Given that the nonlinear interaction coefficient Eq. 3.63 is quadratic, wave interactions occur between triads of waves. It follows that the most basic situation is to use a spectral

truncation by restricting Eq. 3.61 to a single triad of three modes by taking a meridional primary wave, $\mathbf{p}$, a small zonal perturbation or modulation, $\mathbf{q}$ and one of the coupled sidebands $\mathbf{p}_- = \mathbf{p} - \mathbf{q}$. Each of these wave vectors is assigned in turn to $\mathbf{k}$ in Eq. 3.61 with the other two and their negatives assuming all possibilities for $\mathbf{k}_1$ and $\mathbf{k}_2$ while neglecting any ψ_k's outside the given triad.

Let the primary wave, $\mathbf{k} = \mathbf{p}$, then assign $\mathbf{q}$ and $\mathbf{p}_-$ to all possibilities for $\mathbf{k}_1$ and $\mathbf{k}_2$. Such possibilities are tabulated in table 4.1 and only those for which the RHS column is equal to $\mathbf{p}$ contribute in summing the nonlinear term i.e. the first and third rows in this case. Since $\psi_{\mathbf{k}}$ is the Fourier transform of a real field, $\psi_{-\mathbf{k}} = \bar{\psi}_{\mathbf{k}}$.

$$\mathbf{k}_3 = \mathbf{k}_1 \pm \mathbf{k}_2 \tag{4.1}$$

and

$$\omega(\mathbf{k}_3) = \omega(\mathbf{k}_1) \pm \omega(\mathbf{k}_2) \tag{4.2}$$

Table 4.1: Three-wave interaction. All possibilities of $\mathbf{q}$ and $\mathbf{p}_-$ assigned to $\mathbf{k}_1$ and $\mathbf{k}_2$ for $\mathbf{k} = \mathbf{p}$.

$\mathbf{k}_1$	$\mathbf{k}_2$	$\mathbf{k}_1 + \mathbf{k}_2$
$\mathbf{q}$	$\mathbf{p}_-$	$\mathbf{p}$
$\mathbf{q}$	$-\mathbf{p}_-$	$2\mathbf{q} - \mathbf{p}$
$\mathbf{p}_-$	$\mathbf{q}$	$\mathbf{p}$
$\mathbf{p}_-$	$-\mathbf{q}$	$\mathbf{p} - 2\mathbf{q}$
$-\mathbf{q}$	$\mathbf{p}_-$	$\mathbf{p} - 2\mathbf{q}$
$-\mathbf{q}$	$-\mathbf{p}_-$	$-\mathbf{p}$
$-\mathbf{p}_-$	$\mathbf{q}$	$\mathbf{k}_1$
$\mathbf{p}_-$	$-\mathbf{q}$	$-\mathbf{p}$

It is convenient to introduce $\Psi_{\mathbf{k}}(t) = \psi_{\mathbf{k}}(t)\mathrm{e}^{i\omega_{\mathbf{k}}t}$. For the mode $\mathbf{p}$, Eq. 3.61 then becomes

$$\partial_t(\Psi_{\mathbf{p}}(t)\mathrm{e}^{-i\omega_{\mathbf{p}}t}) = -i\omega_{\mathbf{p}}\Psi_{\mathbf{p}} + T(\mathbf{p},\mathbf{q},\mathbf{p}_-)\Psi_{\mathbf{q}}\Psi_{\mathbf{p}_-}\mathrm{e}^{i(\omega_{\mathbf{p}}-\omega_{\mathbf{q}}-\omega_{\mathbf{p}_-})t}$$

which can be further simplified to

$$\partial_t\Psi_{\mathbf{p}} = T(\mathbf{p},\mathbf{q},\mathbf{p}_-)\Psi_{\mathbf{q}}\Psi_{\mathbf{p}_-}\mathrm{e}^{i\Delta_- t},$$

where $\Delta_- = \omega_{\mathbf{p}} - \omega_{\mathbf{q}} - \omega_{\mathbf{p}_-}$. Repeating this process for the other two wave vectors yields the following system of ODEs for the wave vector amplitudes,

$$\begin{aligned} \partial_t \Psi_{\mathbf{p}} &= T(\mathbf{p}, \mathbf{q}, \mathbf{p}_-)\, \Psi_{\mathbf{q}} \Psi_{\mathbf{p}_-} \mathrm{e}^{i\,\Delta_- t} \\ \partial_t \Psi_{\mathbf{q}} &= T(\mathbf{q}, \mathbf{p}, -\mathbf{p}_-) \Psi_{\mathbf{p}} \overline{\Psi}_{\mathbf{p}_-} \mathrm{e}^{-i\,\Delta_- t} \\ \partial_t \Psi_{\mathbf{p}_-} &= T(\mathbf{p}_-, \mathbf{p}, -\mathbf{q}) \Psi_{\mathbf{p}}\, \overline{\Psi}_{\mathbf{q}} \mathrm{e}^{-i\,\Delta_- t}. \end{aligned} \tag{4.3}$$

A similar set of equations can be derived for the other natural triad, $(\mathbf{p}, -\mathbf{q}, \mathbf{p}_+)$ where $\mathbf{p}_+ = \mathbf{p} + \mathbf{q}$:

$$\begin{aligned} \partial_t \Psi_{\mathbf{p}} &= T(\mathbf{p}, -\mathbf{q}, \mathbf{p}_+)\, \overline{\Psi}_{\mathbf{q}} \Psi_{\mathbf{p}_+} \mathrm{e}^{i\,\Delta_+ t} \\ \partial_t \Psi_{\mathbf{q}} &= T(\mathbf{q}, -\mathbf{p}, \mathbf{p}_+) \overline{\Psi}_{\mathbf{p}} \Psi_{\mathbf{p}_+} \mathrm{e}^{i\,\Delta_+ t} \\ \partial_t \Psi_{\mathbf{p}_+} &= T(\mathbf{p}_+, \mathbf{p}, \mathbf{q}) \Psi_{\mathbf{p}}\, \Psi_{\mathbf{q}} \mathrm{e}^{-i\,\Delta_+ t}, \end{aligned} \tag{4.4}$$

where $\Delta_+ = \omega_{\mathbf{p}} + \omega_{\mathbf{q}} - \omega_{\mathbf{p}_+}$. If $\Delta_+ = 0$, the triad is exactly resonant. Then Eqs 4.4 form an exactly integrable set of equations which have been extensively studied [73; 74].

4.1.2 Four-mode truncation (4MT)

The next natural step is to retain both triads $(\mathbf{p}, \mathbf{q}, \mathbf{p}_+)$ and $(\mathbf{p}, -\mathbf{q}, \mathbf{p}_-)$ which combines Eqs 4.3 and 4.4 to give

$$\begin{aligned} \partial_t \Psi_{\mathbf{p}} &= T(\mathbf{p}, \mathbf{q}, \mathbf{p}_-)\, \Psi_{\mathbf{q}} \Psi_{\mathbf{p}_-} \mathrm{e}^{i\,\Delta_- t} + T(\mathbf{p}, -\mathbf{q}, \mathbf{p}_+)\, \overline{\Psi}_{\mathbf{q}} \Psi_{\mathbf{p}_-} \mathrm{e}^{i\,\Delta_+ t} \\ \partial_t \Psi_{\mathbf{q}} &= T(\mathbf{q}, \mathbf{p}, -\mathbf{p}_-) \Psi_{\mathbf{p}} \overline{\Psi}_{\mathbf{p}_-} \mathrm{e}^{-i\,\Delta_- t} + T(\mathbf{q}, -\mathbf{p}, \mathbf{p}_+) \overline{\Psi}_{\mathbf{p}} \Psi_{\mathbf{p}_+} \mathrm{e}^{i\,\Delta_+ t} \\ \partial_t \Psi_{\mathbf{p}_-} &= T(\mathbf{p}_-, \mathbf{p}, -\mathbf{q}) \Psi_{\mathbf{p}}\, \overline{\Psi}_{\mathbf{q}} \mathrm{e}^{-i\,\Delta_- t} \\ \partial_t \Psi_{\mathbf{p}_+} &= T(\mathbf{p}_+, \mathbf{p}, \mathbf{q}) \Psi_{\mathbf{p}}\, \Psi_{\mathbf{q}} \mathrm{e}^{-i\,\Delta_+ t}. \end{aligned} \tag{4.5}$$

The linear problem only strictly closes with the inclusion of all the satellites $\pm\mathbf{q} + m\mathbf{p}$ where m is an integer [8]. However, restricting the system to these four modes is deemed sufficient since the higher-order satellites are much-less excited.

4.2 Nonlinearity parameter M

It has been suggested that the character of the instability depends largely on the initial amplitude of the primary wave, $\Psi_0 = \Psi_{\mathbf{p}}|_{t=0}$ [8]. As such, Gill defined a parameter

equivalent to the dimensionless amplitude

$$M = \frac{\Psi_0 p^3}{\beta}. \tag{4.6}$$

which measures the *initial* relative strength of the nonlinear to linear terms at the scale of the primary wave. $M \gg 1$ suggests that the linear β-effect is small and unimportant and when $F = 0$, Eq. 3.35 reduces to the Euler equation in this the limit such that the instability is then equivalent to the plane parallel sinusoidal shear flow or Kolmogorov flow [75; 76]. Most papers on the modulational instability have dealt with this limit [41; 39]. Sometimes this limit is inferred implicitly [63; 41] when scale-separation is imposed by using a modulation wavenumber q much less than the carrier wavenumber p so that $M \to \infty$. Onishchenko *et al* used a 4MT model together with a scale-separation, by expanding in small q, again to give large M. The limit $M \ll 1$ suggests weak nonlinear terms so that the weak turbulence is dominated by resonant wave triads. It has been suggested that typical values for M in the atmosphere are of order O(1) [38; 8].

An instability associated with a single triad is known as the decay instability [35]. For four modes, a primary wave, a modulation and two sidebands, two coupled triads produce independent contributions to the instability [8].

4.3 Decay instability of a Rossby wave

The decay instability defines the instability of one primary wave, $\mathbf{p}$ decaying into two secondary waves [35], $\mathbf{q}$ and $\mathbf{p}_-$. Introducing the vector notation $\mathbf{\Psi} = (\Psi_\mathbf{p}, \Psi_\mathbf{q}, \Psi_{\mathbf{p}_-})$, a monochromatic primary wave is given by $\mathbf{\Psi}_0 = (\Psi_0, 0, 0)$ where Ψ_0 is a complex constant representing the amplitude of the initial primary wave and is an exact solution of the Eq. 3.61. The idea is to determine how stable this solution is to small perturbations, comprised of modes $\mathbf{q}$ and $\mathbf{p}_-$, by taking $\mathbf{\Psi} = \mathbf{\Psi}_0 + \epsilon\mathbf{\Psi}_1$ where the perturbation is composed of modes $\mathbf{\Psi}_1 = (0, \widetilde{\psi}_\mathbf{q}, \widetilde{\psi}_{\mathbf{p}_-})$.

The first step is to linearise Eqs 4.3 for the 3MT by retaining terms up to first order in ϵ, which gives,

$$\begin{aligned} \partial_t \widetilde{\psi}_\mathbf{q} &= T(\mathbf{q}, \mathbf{p}, -\mathbf{p}_-)\Psi_0 \overline{\widetilde{\psi}}_{\mathbf{p}_-} \mathrm{e}^{-i\,\Delta_-\,t} \\ \partial_t \overline{\widetilde{\psi}}_{\mathbf{p}_-} &= T(\mathbf{p}_-, \mathbf{p}, -\mathbf{q})\overline{\Psi}_0\, \widetilde{\psi}_\mathbf{q} \mathrm{e}^{-i\,\Delta_-\,t}. \end{aligned} \tag{4.7}$$

Now solutions are sought of the form

$$\begin{aligned}\widetilde{\psi}_{\mathbf{q}}(t) &= A_{\mathbf{q}}\mathrm{e}^{-i\,\Omega_{\mathbf{q}}\,t}\\ \widetilde{\psi}_{\mathbf{p}_-}(t) &= A_{\mathbf{p}_-}\mathrm{e}^{-i\,\Omega_{\mathbf{p}_-}\,t},\end{aligned}$$

which requires that $\overline{\Omega}_{\mathbf{p}_-} = -\Omega_{\mathbf{q}} + \Delta_-$. Writing Eqs 4.7 in matrix format,

$$\begin{pmatrix} -i\Omega_{\mathbf{q}} & T(\mathbf{q},\mathbf{p},-\mathbf{p}_-)\Psi_0 \\ T(\mathbf{p}_-,\mathbf{p},-\mathbf{q})\overline{\Psi}_0 & i(-\Omega_{\mathbf{q}}+\Delta_-)\end{pmatrix}\begin{pmatrix} A_{\mathbf{q}} \\ \overline{A}_{\mathbf{p}_-}\end{pmatrix} = 0. \tag{4.8}$$

The determinant of this 2×2 matrix must equal zero for non-trivial solutions and gives a quadratic expression for the dispersion relation of the perturbation,

$$\Omega_{\mathbf{q}}(-\Omega_{\mathbf{q}}+\Delta_-) - T(\mathbf{q},\mathbf{p},-\mathbf{p}_-)\,T(\mathbf{p}_-,\mathbf{p},-\mathbf{q})\;|\Psi_0|^2 = 0. \tag{4.9}$$

The roots of this equation are

$$\Omega_\pm = \frac{1}{2}\left(\Delta_- \pm \sqrt{(\Delta_-)^2 - 4\,T(\mathbf{q},\mathbf{p},-\mathbf{p}_-)\,T(\mathbf{p}_-,\mathbf{p},-\mathbf{q})\,|\Psi_0|^2}\right), \tag{4.10}$$

with corresponding eigenvectors

$$\begin{pmatrix} A_{\mathbf{q}} \\ A_{\mathbf{p}_-}\end{pmatrix} = \begin{pmatrix} 1 \\ \frac{T(\mathbf{p}_-,\mathbf{p},-\mathbf{q})\,\Psi_0}{i\,(\overline{\Omega}_{\mathbf{q}}-\Delta_-)}\end{pmatrix}. \tag{4.11}$$

If $\Omega_{\mathbf{q}}$ has a non-zero positive imaginary part, instability occurs with a growth rate of $\gamma_{\mathbf{q}} = -\mathrm{Im}(\Omega_{\mathbf{q}})$. In the case of a triad in exact resonance, $\Delta_- = 0$ and the roots become,

$$\Omega_\pm = \pm\,|\Psi_0|\,\sqrt{T(\mathbf{q},\mathbf{p},-\mathbf{p}_-)\,T(\mathbf{p}_-,\mathbf{p},-\mathbf{q})}\,. \tag{4.12}$$

Substituting Eq. 3.63 back in to Eq. 4.12 gives these roots in terms of the wavenumbers

$$\Omega_\pm = \pm\mathrm{i}\frac{|\Psi_0|\,|\mathbf{p}\times\mathbf{q}|}{\sqrt{(q^2+F)(p_-^2+F)}}\sqrt{(p^2-q^2)(p_-^2-p^2)}\,. \tag{4.13}$$

Thus an instability will occur if $q^2 < p^2 < p_-^2$ or $q^2 > p^2 > p_-^2$.

To investigate the non-resonant instability further i.e when $\Delta_- \neq 0$, it is convenient to perform some rescalings in order to simplify analysis later. Following Gill [8], the ratio of the modulation vector to the primary vector is defined as

$$s = \frac{q}{p} \tag{4.14}$$

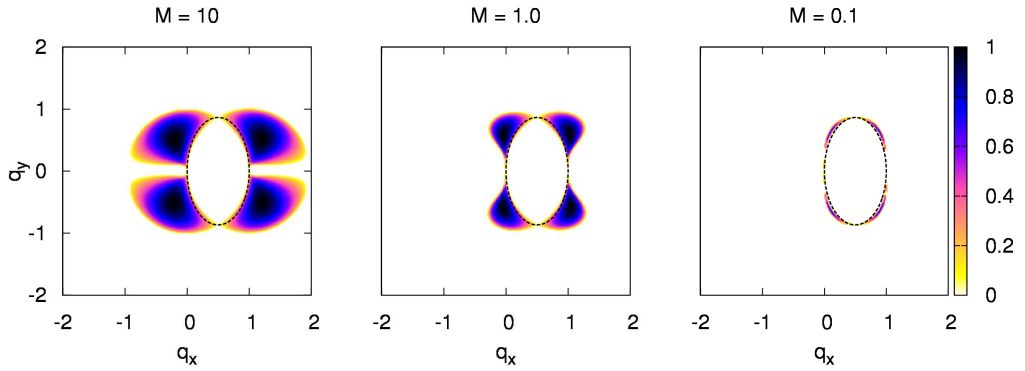

Figure 4.1: The growth rate of the decay instability (the negative imaginary part of the roots of Eq.(4.9)) is plotted as a function of $\mathbf{q}$ for a fixed meridional primary wavevector, $\mathbf{p} = (1, 0)$, for various values of the nonlinearity parameter M.

and the dimensionless primary wave amplitude is given by M defined in Eq. 4.6. The other terms in Eq. 4.9 are non-dimensionalised as $\Omega \to \frac{\beta}{p}\Omega$, $F \to p^2 F$, $\mathbf{p} \to p\,\hat{\mathbf{p}}$ and $\mathbf{q} \to sp\,\hat{\mathbf{q}}$ where $\hat{\mathbf{p}} = (\hat{p}_x, \hat{p}_y)$ and $\hat{\mathbf{q}} = (\hat{q}_x, \hat{q}_y)$ are unit vectors pointing in the directions of $\mathbf{p}$ and $\mathbf{q}$ respectively. Eq. 4.9 can then be rewritten as

$$\Omega_{\mathbf{q}}(-\Omega_{\mathbf{q}} + \hat{\Delta}_-) - M^2\, T(s\,\hat{\mathbf{q}}, \hat{\mathbf{p}}, -\hat{\mathbf{p}}_-)\, T(\hat{\mathbf{p}}_-, \hat{\mathbf{p}}, -\hat{\mathbf{q}}) = 0 \tag{4.15}$$

and the roots become

$$\Omega_{\pm} = \frac{1}{2}\left(\hat{\Delta}_- \pm \sqrt{(\hat{\Delta}_-)^2 - 4\,M^2 T(s\,\hat{\mathbf{q}}, \hat{\mathbf{p}}, -\hat{\mathbf{p}}_-)\, T(\hat{\mathbf{p}}_-, \hat{\mathbf{p}}, -s\hat{\mathbf{q}})}\right). \tag{4.16}$$

Therefore an instability requires that

$$\hat{\Delta}_- < 2M\sqrt{T(s\,\hat{\mathbf{q}}, \hat{\mathbf{p}}, -\hat{\mathbf{p}}_-)\, T(\hat{\mathbf{p}}_-, \hat{\mathbf{p}}, -s\hat{\mathbf{q}})}\,, \tag{4.17}$$

which shows that as $M \to 0$, the instability concentrates on the resonant manifold $\Delta_- = 0$, as illustrated in figure 4.1. The corresponding analysis for the triad $(\mathbf{p}, -\mathbf{q}, \mathbf{p}_+)$ produces identical surfaces reflected about the vertical axis reflecting the instability concentrating on the second resonant manifold, $\Delta_+ = 0$. As $M \to 0$, these two surfaces become disjoint from each other except near the origin $\mathbf{q} = 0$.

4.4 Modulational instability of a Rossby wave

The modulational instability is so-called as it represents a small perturbation or modulation, $\mathbf{q}$ and its sidebands interacting with a primary wave, $\mathbf{p}$. The instability will be derived here for the 4MT model in the same way as for the decay instability in Section 4.3. The primary wave is given by $\mathbf{\Psi}_0 = (\Psi_0, 0, 0, 0)$ where Ψ_0 is a complex constant representing the amplitude of the initial primary wave and is an exact solution of the Eq. 3.61. It will be determined how stable this solution is to small perturbations, comprised of modes $\mathbf{q}$, $\mathbf{p}_-$ and $\mathbf{p}_-$, by taking $\mathbf{\Psi} = \mathbf{\Psi}_0 + \epsilon\mathbf{\Psi}_1$ where the perturbation is composed of modes $\mathbf{\Psi}_1 = (0, \widetilde{\psi}_{\mathbf{q}}, \widetilde{\psi}_{\mathbf{p}_+}, \widetilde{\psi}_{\mathbf{p}_-})$

Linearising Eqs(4.5) for the 4MT model at first order in ϵ gives

$$\begin{aligned}
\partial_t\widetilde{\psi}_{\mathbf{q}} &= T(\mathbf{q},\mathbf{p},-\mathbf{p}_-)\,\Psi_0\,\overline{\widetilde{\psi}}_{\mathbf{p}_-}\,\mathrm{e}^{-i\,\Delta_-\,t} \\
&\quad + T(\mathbf{q},-\mathbf{p},\mathbf{p}_+)\,\overline{\Psi_0}\,\widetilde{\psi}_{\mathbf{p}_+}\mathrm{e}^{i\,\Delta_+\,t} \\
\partial_t\overline{\widetilde{\psi}}_{\mathbf{p}_+} &= T(\mathbf{p}_+,\mathbf{p},\mathbf{q})\,\Psi_0\,\widetilde{\psi}_{\mathbf{q}}\,\mathrm{e}^{-i\,\Delta_+\,t} \\
\partial_t\overline{\widetilde{\psi}}_{\mathbf{p}_-} &= T(\mathbf{p}_-,\mathbf{p},-\mathbf{q})\,\overline{\Psi}_0\,\widetilde{\psi}_{\mathbf{q}}\,\mathrm{e}^{i\,\Delta_-\,t}.
\end{aligned} \tag{4.18}$$

Again seeking solutions of the form:

$$\begin{aligned}
\widetilde{\psi}_{\mathbf{q}}(t) &= A_{\mathbf{q}}\mathrm{e}^{-i\,\Omega_{\mathbf{q}}\,t} \\
\widetilde{\psi}_{\mathbf{p}_+}(t) &= A_{\mathbf{p}_+}\mathrm{e}^{-i\,\Omega_{\mathbf{p}_+}\,t} \\
\widetilde{\psi}_{\mathbf{p}_-}(t) &= A_{\mathbf{p}_-}\mathrm{e}^{-i\,\Omega_{\mathbf{p}_-}\,t},
\end{aligned}$$

requires requires $\Omega_{\mathbf{p}_+} = \Omega_{\mathbf{q}} + \Delta_+$ and $\overline{\Omega}_{\mathbf{p}_-} = -\Omega_{\mathbf{q}} + \Delta_-$. Writing Eqs 4.18 in matrix format

$$\begin{pmatrix}
i\Omega_{\mathbf{q}} & T(\mathbf{q},-\mathbf{p},\mathbf{p}_+)\overline{\Psi}_0 & T(\mathbf{q},\mathbf{p},-\mathbf{p}_-)\Psi_0 \\
T(\mathbf{p}_+,\mathbf{p},\mathbf{q})\Psi_0 & i(\Omega_{\mathbf{q}}+\Delta_+) & 0 \\
T(\mathbf{p}_-,\mathbf{p},-\mathbf{q})\overline{\Psi}_0 & 0 & -i(-\Omega_{\mathbf{q}}+\Delta_+)
\end{pmatrix}
\begin{pmatrix} A_{\mathbf{q}} \\ A_{\mathbf{p}_+} \\ \overline{A}_{\mathbf{p}_-} \end{pmatrix} = 0, \tag{4.19}$$

and setting the determinant of the 3×3 matrix to zero, gives a cubic expression for the

dispersion relation of the modulation,

$$\begin{aligned}
&\Omega_{\mathbf{q}}(\Omega_{\mathbf{q}}+\Delta_+)(-\Omega_{\mathbf{q}}+\Delta_-) \\
&+T(\mathbf{q},-\mathbf{p},\mathbf{p}_+)\,T(\mathbf{p}_+,\mathbf{p},\mathbf{q})\;|\Psi_0|^2\,(-\Omega_{\mathbf{q}}+\Delta_-) \\
&-T(\mathbf{q},\mathbf{p},-\mathbf{p}_-)\,T(\mathbf{p}_-,\mathbf{p},-\mathbf{q})\;|\Psi_0|^2\,(\Omega_{\mathbf{q}}+\Delta_+)=0,
\end{aligned} \tag{4.20}$$

with corresponding eigenvectors

$$\begin{pmatrix} A_{\mathbf{q}} \\ A_{\mathbf{p}_+} \\ A_{\mathbf{p}_-} \end{pmatrix} = \begin{pmatrix} 1 \\ \frac{T(\mathbf{p}_+,\mathbf{p},\mathbf{q})\,\Psi_0}{-i\,(\Omega_{\mathbf{q}}+\Delta_+)} \\ \frac{T(\mathbf{p}_-,\mathbf{p},-\mathbf{q})\,\Psi_0}{i\,(\overline{\Omega}_{\mathbf{q}}-\Delta_-)} \end{pmatrix}. \tag{4.21}$$

Substituting Eq. 3.63 for the interaction coefficient back in to the dispersion relation, Eq. 4.20 and performing some algebra, gives the more usual form of the dispersion for the CHM equation [8; 38; 63; 41; 39; 17]

$$\begin{aligned}
&(q^2+F)\Omega_{\mathbf{q}}+\beta q_x+ \\
&|\Psi_0|^2\,|\mathbf{p}\times\mathbf{q}|^2\,(p^2-q^2)\left[\frac{p_+^2-p^2}{(p_+^2+F)(\Omega_{\mathbf{q}}+\omega)+\beta p_{+_x}}-\frac{p_-^2-p^2}{(p_-^2+F)(\Omega_{\mathbf{q}}+\omega)+\beta p_{-_x}}\right]=0,
\end{aligned} \tag{4.22}$$

which can be solved numerically for $\Omega_{\mathbf{q}}$. Nondimensionalising as before in Section 4.3, the result is

$$(s^2+F)\Omega+s\hat{q}_x+M^2s^2(1-s^2)\,|\hat{\mathbf{p}}\times\hat{\mathbf{q}}|^2\,[T_+-T_-]=0, \tag{4.23}$$

where

$$T_\pm=\frac{|\hat{\mathbf{p}}\pm s\hat{\mathbf{q}}|^2-1}{(|\hat{\mathbf{p}}\pm s\hat{\mathbf{q}}|+F)(-\frac{\hat{p}_x}{1+F}\pm\Omega)+\hat{p}_x\pm s\hat{q}_x}. \tag{4.24}$$

The roots of this equation are controlled by five parameters, M, F, s, θ_p and θ_q with θ_p and θ_q being the angles between the x-axis and the primary wavevector and perturbation wavevector respectively. The structure of the instability is strongly dependent on the value of M and for decreasing M, the instability becomes more concentrated on the resonant manifold as shown in figure 4.2. It is evident that the modulational instability is, in some sense, the nonlinear sum of the decay instabilities for the two triads.

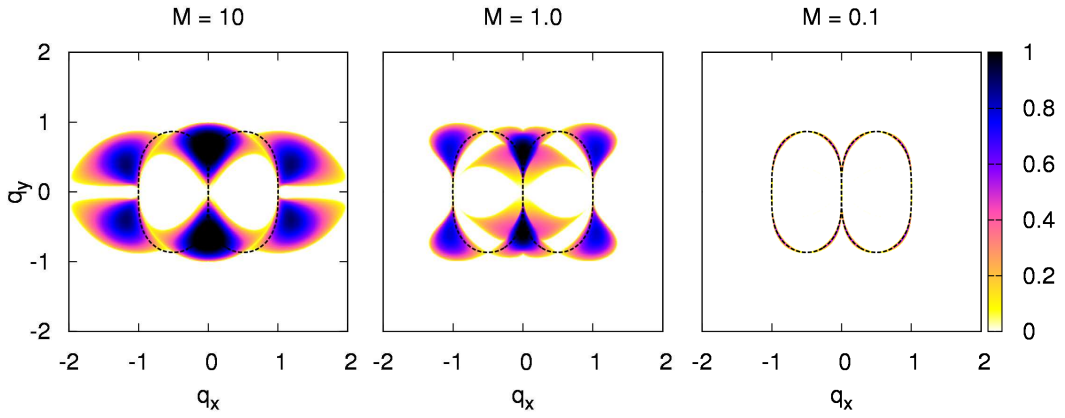

Figure 4.2: Growth rate of the modulational instability (the negative imaginary part of the roots of Eq.(4.23)) as a function of $\mathbf{q}$ for a fixed meridional primary wavevector, $\mathbf{p} = (1, 0)$ and $F = 0$ for various values of the nonlinearity M.

4.5 Comparison of the 3MT and the 4MT models with DNS

Traditionally, four modes have been employed in the study of the modulational instability [8; 20], the justification being that if one of the sidebands is not initially excited, it rapidly becomes so, driven by the instability [20]. It will be clarified here why a single triad and the 3MT is not commonly used to derive the modulational instability.

It has been stated that the modulational instability is a sum of the decay instabilities for the two resonant triads $\Delta_+ = 0$ and $\Delta_- = 0$ and that as $M \to 0$ it collapses to to these resonant manifolds. These two curves are mostly disjoint from each other except at the origin. Thus the two unstable eigenvectors of the instability of the 4MT are equivalent to the eigenvectors of the two decay instability triads. For small M, the maximum growth rate of both the instabilities become identical while for larger M values, that of the modulational instability is typically larger.

In the strong interaction limit, maximum instability is obtained when the primary and secondary waves are perpendicular [8] and the traditional approach is to select a meridional flow such that the primary wavevector, $\mathbf{p}$ is along the x-axis and the perturbation $\mathbf{q}$ along the x-axis. In this situation, looking at figure 4.2, $\mathbf{q}$ is equally close to

both branches of the resonant manifold suggesting that the 4MT should be used since interactions with both manifolds are likely. There is the possibility that $\mathbf{q}$ is off-zonal in that it also has a x-component. An investigation of whether the fundamental mechanism of the modulational instability retains one or both sidebands will be carried out using the 3MT and 4MT models two weakly nonlinear ($M = 0.1$) scenarios:

(i) Pure meridional primary wave, $\mathbf{p} = (10, 0)$ with a pure zonal modulation, $\mathbf{q} = (0, 1)$.

(ii) Pure meridional primary wave, $\mathbf{p} = (10, 0)$ with an off-zonal modulation, $\mathbf{q} = (9, 6)$.

The actual modulational mode that gives the maximum of the instability in this case is $\mathbf{q} = (9.43, 5.35)$ but due to the discreteness of the wavenumbers in the periodic box, this exact wavenumber cannot be selected in the k-space domain and this chosen mode is actually the *only* excited mode in the vicinity of the theoretical value. This sparsity of active modes due to the discreteness of the domain can have a profound effect on numerical simulations of weakly nonlinear regimes [77] if not carefully avoided.

Referring now to case (i) for the zonal modulation, figure 4.3 compares the amplitude of this mode, $|\Psi_{\mathbf{q}}|$ obtained from DNS of Eq. 3.61 to solutions from the 3MT in Eq. 4.3 and the those from the 4MT in Eq. 4.5 with the initial condition being based on the unstable eigenvector of the decay instability. It is clear from figure 4.3(a) that the DNS follow the growth rate predicted by the modulational instability rather than that of the decay instability. Looking more closely at early times in figure 4.3(b), it becomes apparent that while the second sideband is not initially excited, it quickly becomes so [20] with the result that in the time of the order of one inverse of the instability growth rate. Since no other modes are rapidly excited, the 4MT is a better model for this situation up to at least 10 instability times.

For scenario (ii), figure 4.4 compares the amplitude of this mode, $|\Psi_{\mathbf{q}}|$ obtained from DNS of Eq. 3.61 to solutions from the 3MT in Eq. 4.3 and the those from the 4MT in Eq. 4.5 with the initial condition being based on the unstable eigenvector of the decay instability The growth rates of the decay and modulational instability are practically identical and both of the models agree well with DNS up to seven characteristic times. As well as the growth rate, they predict well the maximum amplitude of the zonal jet

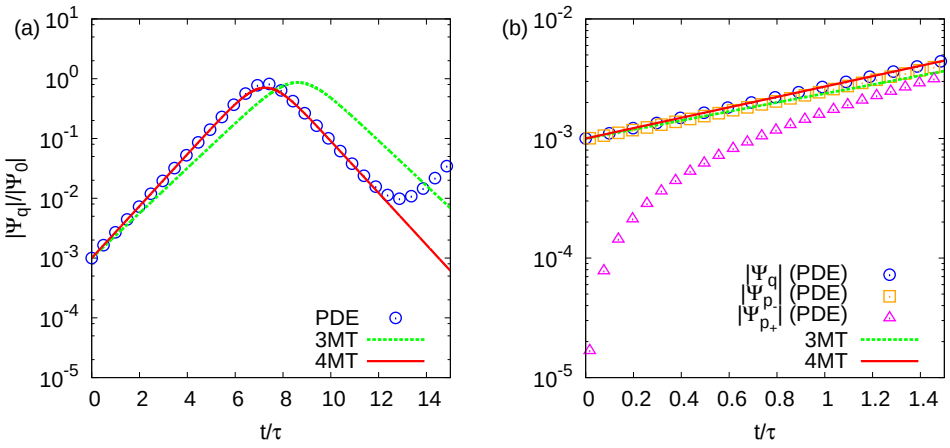

Figure 4.3: Amplitude of the zonal mode with wavenumber $\mathbf{q}$ for $M = 0.1$, $\mathbf{p} = (10, 0)$ obtained from DNS and from solutions of 3MT and 4MT models. Case (i), pure zonal modulation, $\mathbf{q} = (0, 1)$. (a) Long time evolution. (b) Zoomed view of early time evolution.

although the subsequent decrease in amplitude is not as well described as in case (i) by the 4MT model.

From these results it can be concluded that the three-wave interaction is indeed the basic nonlinear process when $M \ll 1$ provided the triad is not degenerate, in the sense that it does not contain quasi-resonant modes which are equidistant from two different resonant manifolds, as happens when the vector $\mathbf{q}$ is zonal. In these cases, the 3MT system is just as good as the 4MT and it describes well the full CHM system for over several characteristic times. On the other hand, the most relevant configuration with $\mathbf{q}$ zonal is in fact, degenerate. In this case, however, the 4MT model works well over many characteristic times whereas the 3MT fails almost immediately. Thus, to have a wider range of applicability, the 3MT model is abandoned and the 4MT model is employed in the study of the modulational instability.

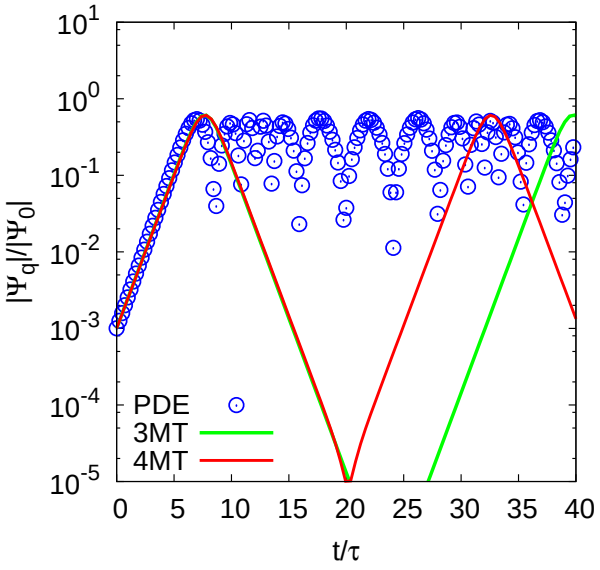

Figure 4.4: As for figure 4.3(a) but now for case (ii), off-zonal modulations, $\mathbf{q} = (9, 6)$.

4.6 Instability for a pure meridional primary wave and a pure zonal modulation

For the situation of a purely meridional primary wave ($\hat{\mathbf{p}} = (1, 0)$) and purely zonal perturbation ($\hat{\mathbf{q}} = (0, 1)$), the analysis is easier to perform and furthermore, it is of physical interest since large scale structures in the atmosphere generally migrate in the zonal direction. The reduced cubic dispersion relation is given by

$$\Omega_{\mathbf{q}}^3 + \frac{s^4\left[2M^2(1-s^2)(1+F)^2(s^2+F+1) - (s^2+F)\right]}{(1+F)^2(s^2+1+F)^2(s^2+F)}\Omega_{\mathbf{q}} = 0, \tag{4.25}$$

which has roots

$$\Omega_{\mathbf{q}} = 0, \tag{4.26}$$

$$\Omega_{\mathbf{q}} = \frac{\pm i s^2}{(1+F)(s^2+1+F)}\left[\frac{2M^2(1-s^2)(1+F)^2(s^2+F+1) - (s^2+F)}{s^2+F}\right]^{1/2} \tag{4.27}$$

An instability exists if the quantity under the square root is positive. Recall that s is the ratio q/p, of the modulus of the modulation wavevector to that of the primary wavevector. Letting $s^2 = y$, a quadratic for the quantity under the square root is obtained which is

positive in the range $s \in (-s_{\max}, s_{\max})$. Solving

$$\frac{2M^2(1-y)(1+F)^2(y+F+1)-(y+F)}{y+F} = 0, \tag{4.28}$$

gives

$$s^2_{\max} = \frac{1+2M^2F(1+F)^2}{2M^2(1+F)^2}\left[-1+\left(1+4\frac{(2M^2(1+F)^3-F)(2M^2(1+F)^2)}{(1+2M^2F(1+F)^2)^2}\right)^{1/2}\right]. \tag{4.29}$$

4.6.1 Infinite deformation radius

When $F = 0$ the analysis becomes particularly simple. For any M, there is always a range, $(0, s_{\max})$, of unstable long wavelength perturbations with $s_{\max}$ given by

$$s_{\max} = \sqrt{\frac{-1+\sqrt{1+16M^4}}{4M^2}}. \tag{4.30}$$

Within this range the growth rate given by Eq. 4.27 is

$$\Omega_{\mathbf{q}} = \frac{s\left(2M^2(1-s^4)-s^2\right)^{1/2}}{(s^2+1)}. \tag{4.31}$$

Taking the derivative of Eq. 4.31 with respect to s, the maximum of the growth rate occurs at $s_0 = \sqrt{y_0}$ where y_0 is the positive root of

$$y^3 + 3y^2 + (1+\frac{1}{M^2})y - 1 = 0. \tag{4.32}$$

The limits of s_0 are $s_0 \to \sqrt{\sqrt{2}-1}$ as $M \to \infty$ and $s_0 = M + O(M^2)$ as $M \to 0$. It would be interesting to know when the maximally unstable zonal perturbation is a local maximum with respect to nearby off-zonal perturbations. This can be done by looking at the sign of the determinant

$$\Delta_M(\hat{q}_x, \hat{q}_y) = \begin{vmatrix} \frac{\partial^2\Omega}{\partial\hat{q}_x^2} & \frac{\partial^2\Omega}{\partial\hat{q}_x\partial\hat{q}_y} \\ \frac{\partial^2\Omega}{\partial\hat{q}_x\partial\hat{q}_y} & \frac{\partial^2\Omega}{\partial\hat{q}_y^2} \end{vmatrix} \tag{4.33}$$

evaluated at $(\hat{q}_x, \hat{q}_y) = (0, s_0)$. This can be done semi-analytically using *Mathematica* and is plotted in the inset of figure 4.5. It is found that $\Delta_M > 0$ with $\frac{\partial^2\Omega}{\partial\hat{q}_x^2} < 0$ (the criterion for a local maximum) for $M > M_c$. $\Delta_M < 0$ with $\frac{\partial^2\Omega}{\partial\hat{q}_x^2} < 0$, the criterion for a

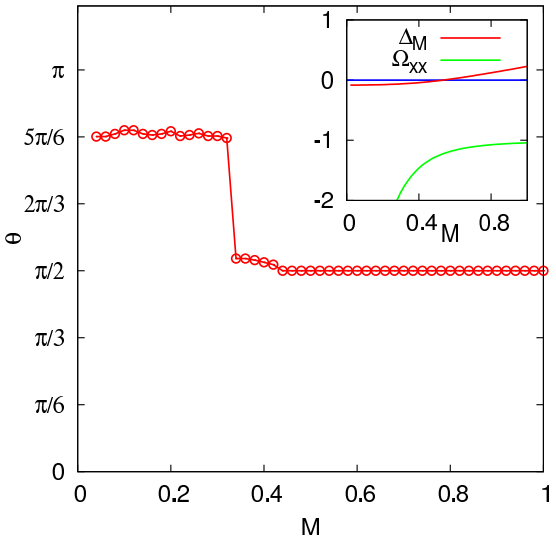

Figure 4.5: Angle, θ, between the $\mathbf{q}$ wave-vector of the maximally unstable perturbation and the x-axis as a function of M. Inset plots Δ_M and Ω_{xx} as a function of M illustrating the transition of the maximum growth rate for on-axis perturbations from a local maximum to a saddle point at $M \approx 0.53$.

saddle, for $M > M_c$. The critical value of M is found numerically to be $M_c \approx 0.534734$. Numerical explorations show that the local maximum found for $M > M_c$, is actually global. Therefore for $M > M_c$, the fastest growing perturbation is indeed zonal. As M decreases below M_c the most unstable perturbation moves to a point with a finite value of q_x. The maximally unstable perturbation for $M < 0.53$ tends to a point on the resonant manifold making an angle of $5\pi/6$ with the x-axis. The dependence of this angle on M is shown in figure 4.5. A clear transition from an axial maximum to an off-axis maximum is clearly visible.

4.6.2 Finite deformation radius

The limiting case of $R \to \infty$ for one-layer QG turbulence has been extensively studied because it makes the governing equations much simpler, even though generally in the real atmosphere and oceans, finite values are more realistic. In the Earth's atmosphere, the deformation radius is approximately $2 - 3 \times 10^6$m [39; 31], about a half to a third

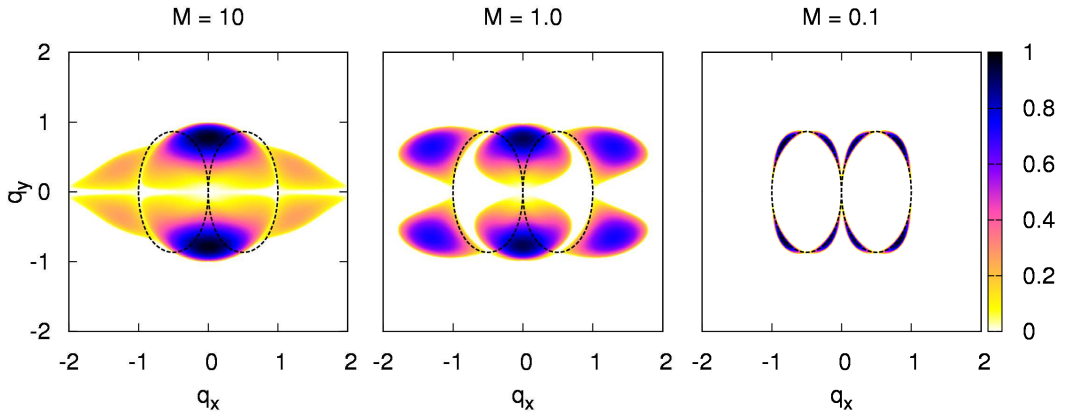

Figure 4.6: Growth rate of the modulational instability (the negative imaginary part of the roots of Eq.(4.23)) as a function of $\mathbf{q}$ for a fixed meridional primary wavevector, $\mathbf{p} = (1, 0)$ and $F = 2$ for various values of the nonlinearity M.

the radius of the Earth which is approximately 6.4×10^6km. The Larmor radius in JET is approximately 6×10^{-3}. However, for finite R the temporal evolution of numerical models is drastically slowed down, making results more difficult to obtain and little is known of the role this length-scale plays in the overall atmospheric dynamics.

Consider now the dependence of the instability on the deformation radius or Larmor radius. Again, the structure of the instability is strongly dependent on the value of M as is shown in figure 4.6 displaying similar behaviour to the $F = 0$ case. When F is finite, there are two regimes, depending on the value of M. For an interval of instability to exist, the requirement is $s^2_{\max} > 0$. Referring to Eq. 4.29, this requires that

$$p(F) = 2M^2(1 + F)^3 - F > 0. \tag{4.34}$$

The discriminant of the corresponding cubic equation, $p(F) = 0$, is $\Delta = -4(-2M^2 + 27M^4)$. In physical situations, $F > 0$ so that two regimes are identified.

- $M > \sqrt{\frac{2}{27}}$

  In this case, $\Delta < 0$ so $p(F) = 0$ has one negative real root, F_1 and $p(F) > 0$ when $F > F_1$. Then for any positive value of F there exists a finite range of s, $s \in (0, s_{\max})$ for which the perturbation is unstable. $s_{\max}$ is given by Eq. 4.29.

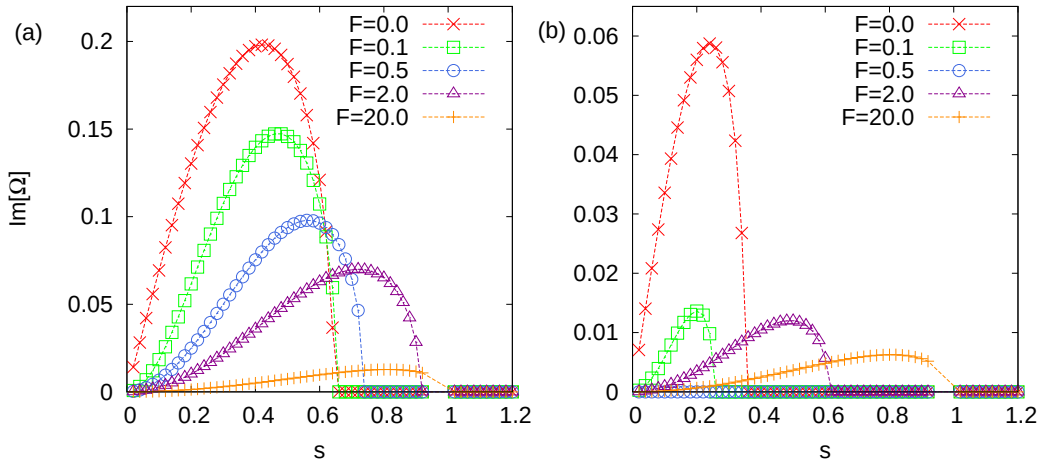

Figure 4.7: Instability growth rate for purely zonal perturbations for different values of the deformation radius with (a) $M = 0.5 > \sqrt{2/27}$ and (b) $M = 0.25 < \sqrt{2/27}$. Note that the growth is completely suppressed with $F = 0.5$ for $M = 0.25$.

In this regime, a finite deformation radius tends to reduce the growth rate of the instability but cannot suppress it as shown in figure 4.7(a).

- $M \leq \sqrt{\frac{2}{27}}$

  In this case, $\Delta > 0$ and $p(F) = 0$ has three real roots, F_1, F_2 and F_3. F_1 is always negative and F_2 and F_3 are always positive. $p(F) < 0$ in the range (F_2, F_3). In this regime, there are critical values of F, F_2 and F_3 such that the range $s \in (0, s_{\max})$ of unstable perturbations only exists if $F < F_2$ or $F > F_3$. F_2 and F_3 are obtained by finding the positive roots of Eq. 4.34 and $s_{\max}$ is again given by Eq. 4.29. In this regime, there is a range of intermediate deformation radii which completely suppress the instability, for example see $F = 0.5$ in figure. 4.7(b).

4.7 Role of the primary wave amplitude

So far, it has been determined that with decreasing nonlinearity $M \to 0$, the most unstable modulation mode moves from zonal to off-zonal for a fixed meridional primary wave. This is the case for both infinite and finite deformation radius. An instability criteria has been defined [63; 41; 39] for a fixed modulation $\mathbf{q}$ which states that the

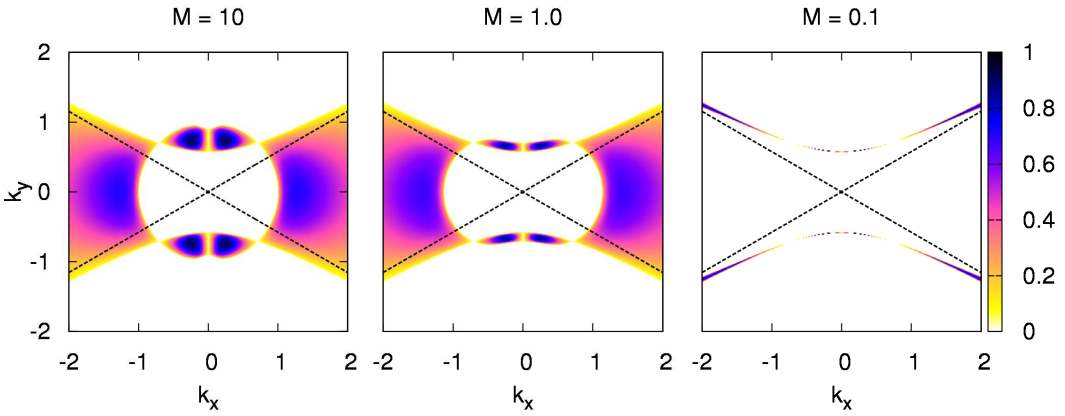

Figure 4.8: Growth rate of the modulational instability, given by Eq. 4.23 as a function of $\mathbf{p}$ for a fixed zonal modulation wavevector, $\mathbf{q} = (\mathbf{0}, \mathbf{1})$ and $F = 0$ for various levels of M. The dashed line is the cone defined by $p_y < \frac{1}{\sqrt{3}} p_x$

primary wave will be unstable if it lies within the cone.

$$F + p_x^2 - 3p_y^2 > 0 \tag{4.35}$$

When $F = 0$, this cone reduces to $p_y < \frac{1}{\sqrt{3}} p_x$. Now plotting the negative imaginary part of the roots of Eq. 4.23 as a function of $\mathbf{p}$ for a fixed zonal modulation $\mathbf{q} = (0, 1)$ and $F = 0$, it is clear from figure 4.8 that the instability region does in fact lie within this cone. As $M \to 0$, a region of stable wavenumbers inside the cone becomes larger such that unstable wavevectors require a larger p_x. Furthermore, for large M, an instability exists for some wavenumbers outside the cone which are very close to the zonal direction. A similar plot for $F = 2$ in figure 4.9 shows that the most unstable wavevectors for a given zonal perturbation are those which lie in the x-axis, i.e. the meridional wavevectors.

4.7.1 Strong nonlinearity $M \gg 1$

The limit of large nonlinearity $M \gg 1$ is a particularly simple and well studied one [75; 38; 8; 63; 41; 39]. the β-effect becomes unimportant and for $F = 0$, this case reduces to the instability of Kolmogorov flow in the Euler equations. Again re-visiting

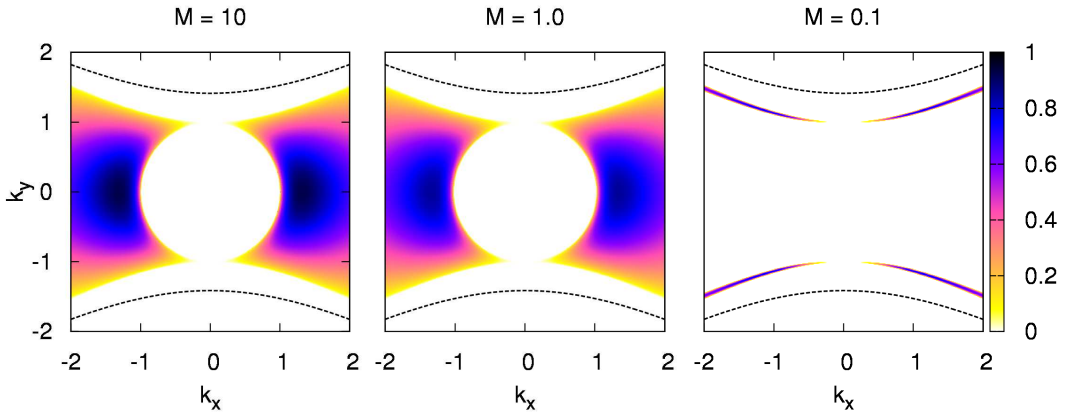

Figure 4.9: Growth rate of the modulational instability, given by Eq. 4.23 as a function of $\mathbf{p}$ for a fixed zonal modulation wavevector, $\mathbf{q} = (\mathbf{0}, \mathbf{1})$ and $F = 2$ for various levels of M. The dashed line is the cone defined by $p_y < \sqrt{\frac{F+p_x^2}{3}}$

the theory of Gill [8], an instability exists in this case when

$$\cos^2\phi < \frac{1+\frac{q^2}{p^2}}{4}, \tag{4.36}$$

where ϕ is the angle between $\mathbf{p}$ and $\mathbf{q}$ and is maximum when $\cos\phi = 0$, that is when the modulation is perpendicular to the primary wave. It must be stressed that the results obtained in the limit $M \to \infty$ should be used with great caution because the most unstable primary wave is not predicted correctly by the 4MT.

4.7.2 Weak nonlinearity $M \ll 1$

In the limit of weak nonlinearity, $M \ll 1$, the dynamics are completely wave dominated [8]. The nonlinear terms allow waves to interact weakly and exchange energy. Since the nonlinearity is quadratic, wave interactions are triadic, i.e. three-wave resonances are allowed by the dispersion relation, Eq. 3.62. Any triad of waves having wavevectors $\mathbf{k}$, $\mathbf{k}_1$ and $\mathbf{k}_2$ interact only if they satisfy the resonance conditions:

$$\mathbf{k} = \mathbf{k}_1 + \mathbf{k}_2 \tag{4.37}$$

$$\omega(\mathbf{k}) = \omega(\mathbf{k}_1) + \omega(\mathbf{k}_2). \tag{4.38}$$

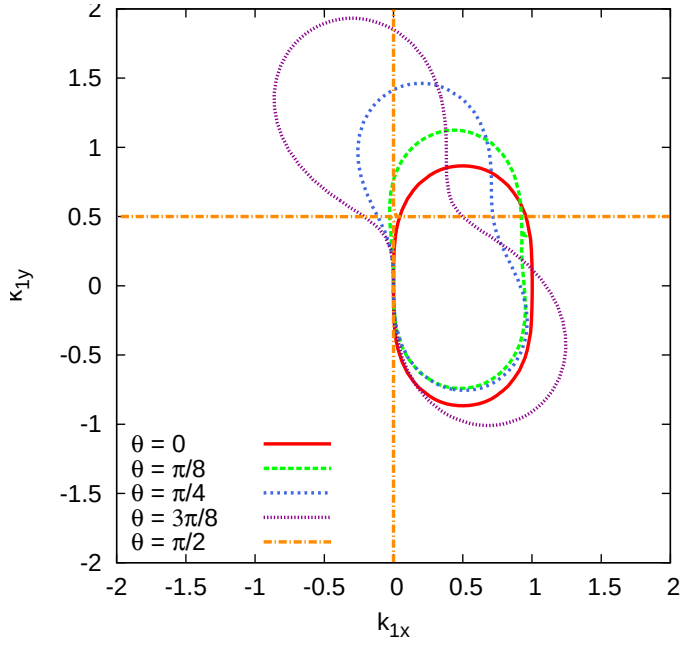

Figure 4.10: Shape of the resonant manifold determined by Eq.(4.39) with $\mathbf{k} = (\cos\theta, \sin\theta)$ for several values of θ for the case $F = 0$.

From Eq. 3.62, this latter relation gives an implicit equation for the resonant manifold of a given $\mathbf{k} = (k_x, k_y)$:

$$\frac{k_{1x}}{k_{1x}^2 + k_{1y}^2 + F} + \frac{k_x - k_{1x}}{(k_x - k_{1x})^2 + (k_y - k_{1y})^2 + F} - \frac{k_x}{k_x^2 + k_y^2 + F} = 0. \qquad (4.39)$$

Because the system is anisotropic, the shape of resonant manifold depends on the direction of $\mathbf{k}$ as shown in figure 4.10. It should be noted, that these resonant manifolds are relevant even for higher levels of nonlinearity because as can be seen in figures 4.2 and 4.6, the unstable modulations still concentrate close to the resonant curves. In fact, figure 4.2 shows two resonant curves corresponding to the two resonant triads,

$$\begin{aligned} \mathbf{k}_1 &= \mathbf{p}, & \mathbf{k}_2 &= \mathbf{q}, & \mathbf{k} &= \mathbf{p} + \mathbf{q} \\ \mathbf{k}_1 &= \mathbf{p}_-, & \mathbf{k}_2 &= \mathbf{q}, & \mathbf{k} &= \mathbf{p} \end{aligned}$$

Out of the four wavenumbers in the truncated system, $\mathbf{p}, \mathbf{q}, \mathbf{p}_-$ and $\mathbf{p}_+$, three are resonant, or nearly resonant and the remaining one is non-resonant ($\mathbf{p}_-$ or $\mathbf{p}_+$). As stated before, this holds true in non-degenerate situations, when $\mathbf{q}$ is not zonal. Then

for $M \to 0$ the amplitude of this non-resonant mode in the instability eigenvector tends to zero, so effectively there are only three active modes, and one can use the results obtained above for the 3MT model. In particular, Eq. 4.13 gives the instability growth rate as

$$\gamma_{\mathbf{q}} = \frac{|\Psi_0||\mathbf{p}\times\mathbf{q}|\sqrt{(p^2-q^2)(p_-^2-p^2)}}{\sqrt{(p_-^2+F)(q^2+F)}}\,, \tag{4.40}$$

which is the expression obtained in [8] in the case $F = 0$, based on the 4MT model. The primary wave is unstable to perturbations if its wavenumber length lies between the wavenumber lengths of the waves it decays into i.e. $q < p < p_+$. This could be interpreted as a dual-cascade whereby in order to decay, the wave must be able to transfer its energy to a larger wave and its enstrophy to a smaller wave. For $F = 0$, the typical instability growth rate is $\gamma_{\mathbf{q}} \sim U_0 p$ where $U_0 = p\psi_0$ is the velocity amplitude of the primary wave [8]. For finite F, the instability is slowed by the factor F/p^2.

Another interesting feature of instability for $M \ll 1$ is evident in figure 4.8 that for fixed zonal $\mathbf{q}$ the unstable region becomes narrow and collapses onto the sides of the cone i.e. onto the lines $p_y = \pm p_x/\sqrt{3}$. This fact can be explained by considering the resonant curve for $q \ll p$ where it behaves as $q_x = -2(p_x p_y/p^4)q_y^3$. For instability, this curve has to pass as close as possible to the vertical, or zonal, axis where $\mathbf{q}$ is also chosen to be. Thus, to minimise the above coefficient $(p_x p_y/p^4)$, for example with respect to p_y for fixed p_x which immediately gives $p_y = \pm p_x/\sqrt{3}$.

For small M the maximally unstable modulation $\mathbf{q}$ is off-zonal, which may be important for determining the final statistical state of the nonlinear evolution. As will be shown in due course, this state appears to have a predominantly off-zonal component even if the initial modulation is chosen to be zonal.

4.8 Modulational instability results

To test the linear predictions and to study the nonlinear evolution, DNS of the CHM system, Eq. 3.35 have been performed using a standard pseudo-spectral method with resolution up to 1024^2, de-aliasing and hyperviscosity parameters $\nu_n = 4.5e^{-30}$. The 4MT system, Eqs 4.5, is solved numerically and compared with DNS. Although the 4MT

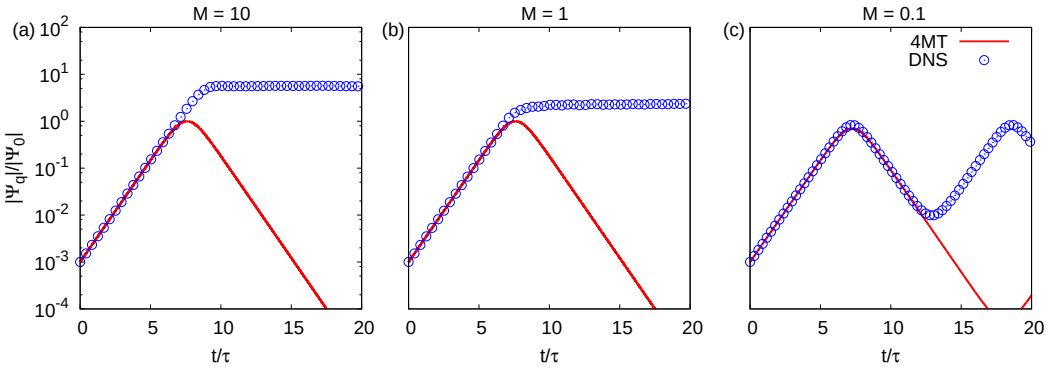

Figure 4.11: Comparison of the growth of the zonal mode $\mathbf{q}$ obtained by DNS versus solving 4MT system. In each case the primary wavenumber is $\mathbf{p} = (\mathbf{10}, \mathbf{0})$ and the modulation wavenumber is $\mathbf{q} = (\mathbf{0}, \mathbf{1})$. The nonlinearity levels are (A) $M = 10$, (B) $M = 1.0$ and (C) $M = 0.1$. In each case time has been scaled by τ,the inverse of the instability growth rate.

was used as the departure point for the linear stability analysis, it is a fully nonlinear set of equations in its own right. In addition to checking the linear instability predictions against DNS, the extent to which the nonlinear dynamics of the 4MT captures the behaviour of the full PDE will also be explored. In all cases, the initial condition is chosen to be along the unstable eigenvector of the 4MT.

4.8.1 Meridional primary wave and zonal modulation

The cases simulated are for $\mathbf{p} = (\mathbf{10}, \mathbf{0})$ and $\mathbf{q} = (\mathbf{0}, \mathbf{1})$. A series of snapshots of the vorticity field for the nonlinearity levels, $M = 10$, $M = 1$ and $M = 0.1$ are shown in figures 4.12, 4.13 and 4.14 respectively. The evolution of the mean zonal velocity $\overline{u}(y)$ averaged over x, obtained from DNS is shown in figure 4.15 for times close to the formation of the jet and the evolution of the amplitude of the zonal mode, $|\psi_{\mathbf{q}}|$ for the same set of nonlinearities are shown in figure 4.11. For comparison, the corresponding values of $|\psi_{\mathbf{q}}|$ obtained from the 4MT.

Th initial stage of the evolution agrees very well with the predicted growth from the linear stability analysis of the 4MT as shown in figure 4.11. In fact for the $M = 0.1$ case, the 4MT works very well even beyond the linear stage in that it predicts the reversal in the growth of the modulation amplitude. The oscillating behaviour of this mode is

evident in the vorticity snapshots of figures 4.14(a)-(d) where the modulation becomes stronger, weakens and subsequently grows again. For $M = 1$, the system's growth does not reverse, but rather experiences a saturation at the level where the 4MT system reaches maximum and reverses. The most surprising behaviour is observed for $M = 10$ where the linear exponential growth continues well beyond the point of reversal of the four-wave system, even though the system is clearly nonlinear at these times and follows a self-similar evolution.

4.8.2 Self-similar jet pinching

The nonlinear dynamics show zonal jets self-focusing and becoming very narrow with respect to the initial modulation wavelength such as those in figures 4.15a and b. This self-focusing was predicted theoretically [63] for large M and $q \ll p$ where self-similar solutions were obtained describing a collapse of the jet width. This feature cannot be described by the 4MT because such an harmonic jet shape involves strong contributions from higher harmonics $\mathbf{p} \pm n\mathbf{q}$.

Figure 4.16 shows the zonal velocity $\overline{u}$ re-scaled with self-similar variables as $\overline{u}(y,t) = a(t)\, f(b(t)y)$ in the run with $M = 10$. The self-similar stage occurs in the time interval corresponding to the overshoot in figure 4.11a, that is, after the 4MT has reached its maximum but before DNS saturates at a plateau. Empirically, the self-similar variables are found to be $a(t) = u_0\, e^{\gamma_{\mathbf{q}} t}$ and $b(t) = e^{1.85t}$.

The nonlinear growth at the self-similar stage continues with the same exponential law, $\mathrm{e}^{\gamma_{\mathbf{q}} t}$, as in the linear dynamics. The self-similarity must stop when the scale separation property breaks down due to the jet narrowing, at which point a roll-up into vortices occurs. For smaller M, the extension of the growth rate beyond the linear stage is not observed and the amplitude of the zonal mode decreases after reaching a maximum in correspondence with the solution of the 4MT. The self-focusing is thereby much reduced and the self-similar stage is not clearly observed.

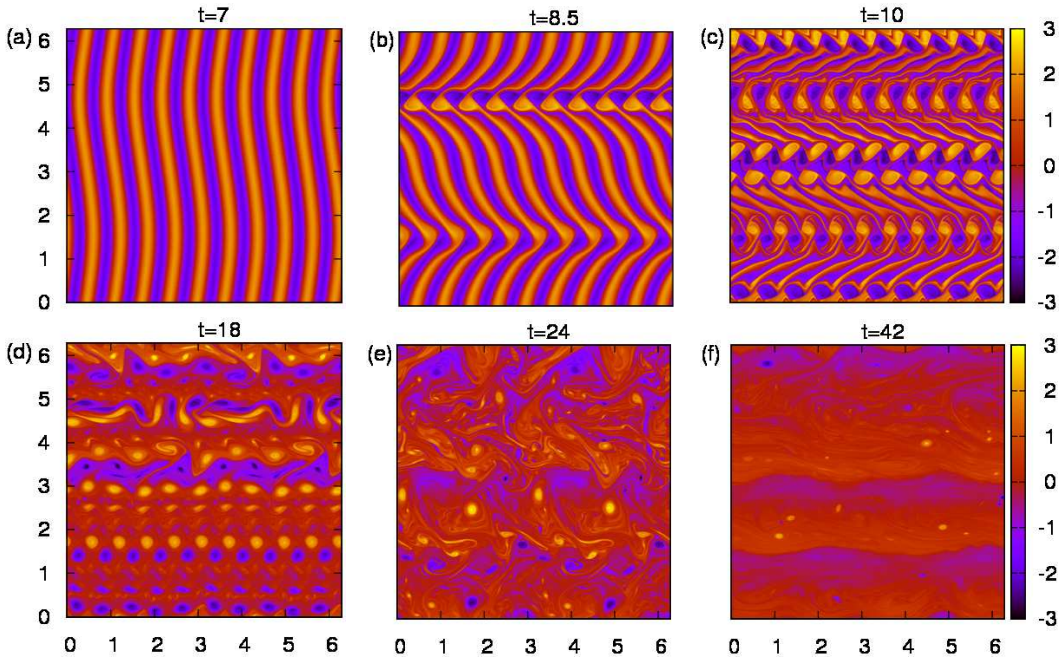

Figure 4.12: Vorticity snapshots showing the linear growth, saturation and transition to turbulence of a zonal perturbation to a meridional primary wave having $M = 10$. The horizontal axis is x and the vertical is y.

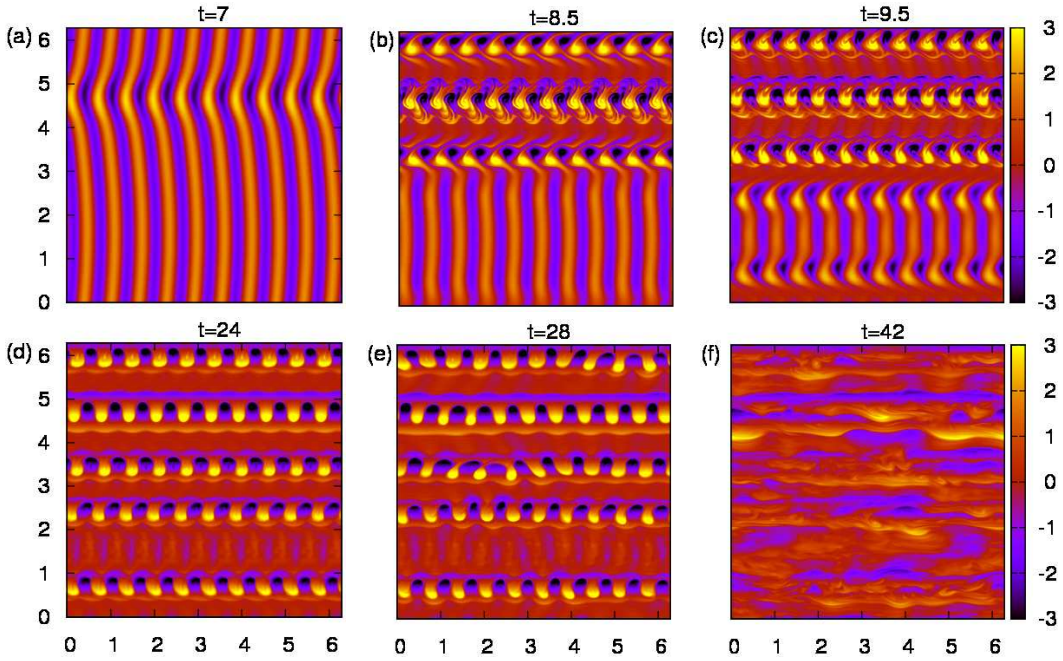

Figure 4.13: Vorticity snapshots showing the linear growth, saturation and transition to turbulence of a zonal perturbation to a meridional primary wave having $M = 1$. The horizontal axis is x and the vertical is y.

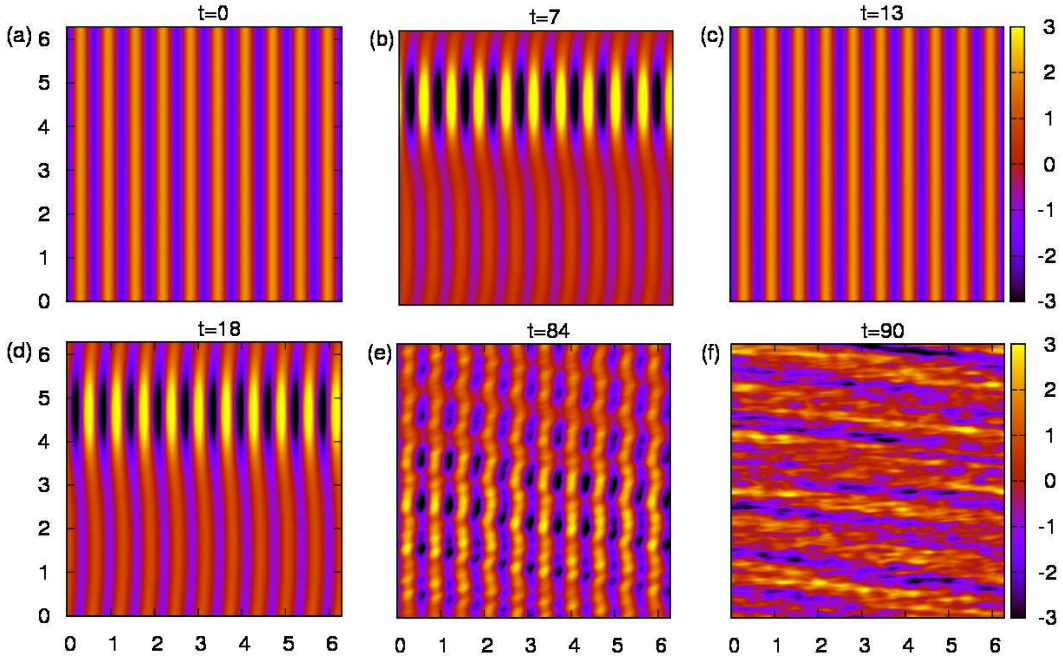

Figure 4.14: Vorticity snapshots showing the growth, growth reversal, saturation and transition to turbulence of a zonal perturbation to a meridional primary wave having $M = 0.1$. The horizontal axis is x and the vertical is y.

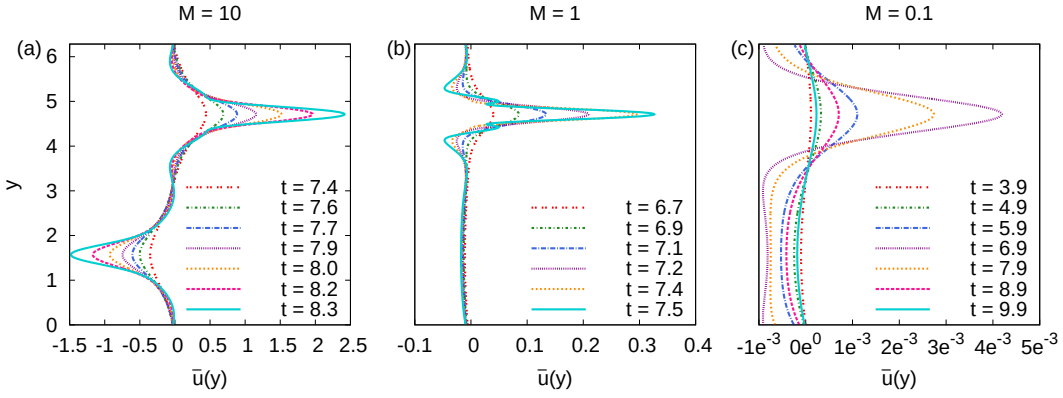

Figure 4.15: Mean zonal velocity profiles for (a) $M = 10$, (b) $M = 1.0$ and (c) $M = 0.1$.

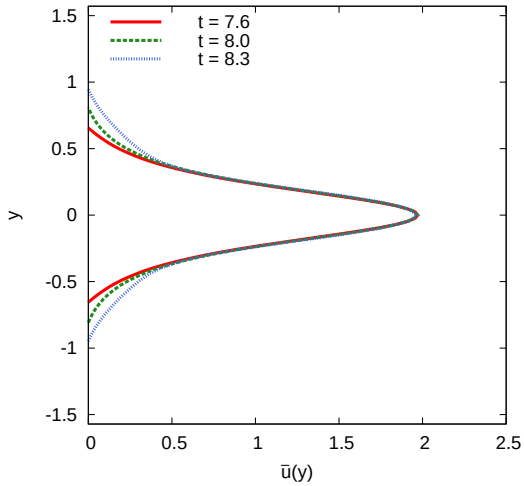

Figure 4.16: Zonal velocity $\overline{u}(y)$ obtained for $M = 10$ re-scaled with self-similar variables: $\overline{u}(y,t) = a(t)\, f(b(t)y)$ with $a(t) = u_0 e^{\gamma_{\mathfrak{q}} t}$ and $b(t) = e^{1.85t}$.

4.8.3 Effect of nonlinearity M

Some clear differences in the qualitative behaviour between the levels of the nonlinearity parameter are evident. The east-west symmetry is larger for weaker waves, evident as the top and bottom half asymmetry in the vorticity in figures 4.12- 4.14 and also in the zonal velocity in figure 4.15. This is as expected because the β-effect, which is the cause of this asymmetry, is less important for large M. Furthermore for this case, the nonlinear evolution is vortex dominated and the vorticity of the initial primary wave rolls into vortices and organises itself into Kármán-like vortex streets. This corresponds to the jet velocity saturating at approximately $t/\tau = 9$ in figures 4.15a and b. At the final stages the vortex streets break up due to a vortex pairing instability which is followed by a transition to turbulence. Such turbulence is anisotropic with a pronounced zonal jet component and a well-formed potential vorticity staircase is evident in figure 4.12(f) [78].

In contrast for weak waves, $M \ll 1$, the nonlinear evolution starts with self-focusing of the primary wave but this is followed by a quasi-oscillatory behaviour where the system returns close to the initial state. The 4MT model captures this effect very well. At later times, there is no vortex roll-up and the nonlinear dynamics are charac-

terised by wave behaviour, as shown in figure 4.14. This oscillation between a Rossby wave and a zonal flow has been reported from numerical studies of a barotropic fluid [79], motivated by observations of such periodic behaviour in the troposphere of the southern hemisphere [80] and similar behaviour has also been noted for the generalised Hasegawa-Mima model [20] for drift turbulence. However, the periodic behaviour is not sustained and a transition to an anisotropic turbulent state occurs. The dominant jet structures observed in such a turbulent state, figure 4.14f, are off-zonal. This effect may be connected to the off-zonal "striations" reported for ocean observations [16] although these ocean striations only become evident in the averaged data since they are sufficiently weak.

For $M \sim 1$ or greater, the vortex streets represent the 2D fine structure of the saturated zonal jets, i.e. at the plateau part of figures 4.11a and b. Such vortex street configurations are more stable than the plane parallel, x-independent, flows with the same zonal velocity profiles. This can be understood heuristically (see, for example [81], chap. 3) by considering the vortices to impart some eddy viscosity to the mean zonal velocity profile. The stability of this mean zonal velocity profile is determined by the Rayleigh-Kuo instability condition [82], given here as

$$\partial_{yy}\overline{u}(y) - \beta > 0, \tag{4.41}$$

details of which are given in Appendix C. These profiles for the various M values are shown in figure 4.15 at selected moments in time. For $M \sim 1$ in figure 4.15a and b, these profiles are seen to cross the x-axis so that condition 4.41 is violated, implying that the zonal flows become stronger than the limiting values imposed by this condition. This could be interpreted as a result of a competition between the instability and the jet sharpening process. For large M the pinching is self-accelerating (self-similar) and it manages to significantly compress/amplify the unstable jet in the finite time needed for the instability to develop (i.e. the inverse growth rate). On the other hand, in the case $M = 0.1$ the jet strength reaches a maximum and then decreases remaining in the stable range according to the criterion 4.41.

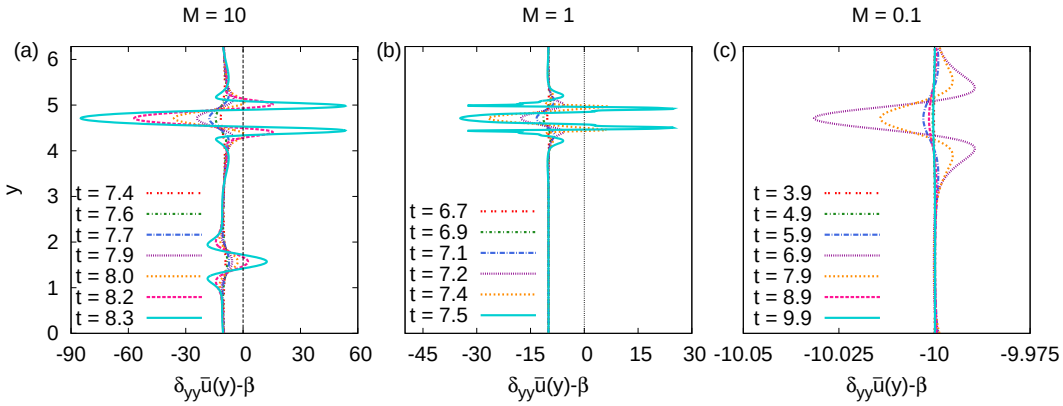

Figure 4.17: The Rayleigh-Kuo profiles, given by Eq. 4.41 for (a) $M = 10$, (b) $M = 1.0$ and (c) M=0.1

4.8.4 Critical nonlinearity M_* and breakdown of 4MT

The results presented show that there are two qualitatively different types of behaviours, namely, vortex roll-up followed by saturation or the oscillatory dynamics, so it would be natural to seek the critical level of nonlinearity which distinguishes between the two. If the maximum jet strength, as predicted by the 4MT, exceeds the value of the Rayleigh-Kuo necessary instability condition 4.41, then the vortex roll-up occurs and the jet strength saturates for a long time (although figure 4.11 shows time as far as 20 characteristic timescales, simulations were actually run until 100 characteristic times). At this point, the behaviour of the system starts to depart from that of the 4MT. If however, the maximum jet strength remains below the Rayleigh-Kuo threshold, then the system's growth reverses and follows the 4MT dynamics for a longer time.

This simple picture permits a qualitative physical estimate for M_* and for the saturated velocity of the jet. Since the x-periodicity is preserved, the spacing of the stable vortex street, i.e. the distance between each vortex is equal to the wavelength of the original primary wave and since the vortices are approximately round, the y-spacing between vortices is equivalent to the x-spacing. Thus, the width of the saturated jet is of the order of the wavelength of the initial primary wave and the jet saturation velocity

is of the order of the velocity amplitude of the initial primary wave,

$$\overline{u}_{max} \sim \frac{M\beta}{p^2}. \tag{4.42}$$

In fact, numerical results for $M = 10$ and $M = 1$ from figures 4.15(a) and (b), give the estimate,

$$\overline{u}_{max} \approx 3\frac{M\beta}{p^2}. \tag{4.43}$$

Estimating $\partial_{yy}\overline{u}(y)$ as $p^2 u_{max}$ and substituting into condition 4.41 arrives at the estimate,

$$\begin{aligned} p^2 u_{max} - \beta &> 0, \\ \frac{3M\beta}{p^2} &> \frac{\beta}{p^2} \\ M &> M_* \sim \frac{1}{3}. \end{aligned} \tag{4.44}$$

Figure 4.18 shows that numerical explorations reveal $M_* \approx 0.25 - 0.35$ but this boundary is not sharp. For $M = 0.25$ the dynamics are definitely wave-dominated, although some elongated, fuzzy vortices are still apparent whereas for $M = 0.35$ streets of round vortices are clearly formed with some wave-like oscillations still present.

4.8.5 Meridional primary wave and off-zonal modulation

It has been established in Section 4.6.1 that there is a critical value of $M = 0.53$, above which, the most unstable modulations are zonal and below which, they are off-zonal. This is very likely to be the reason why the final statistical state of the $M = 0.1$ case shows off-zonal anisotropic flows, even though the initial modulation was purely zonal. In addition, it is quite likely that such weakly-nonlinear systems will select the modulation which is off-zonal already in the initial moments.

It is natural then to consider for weak nonlinearity, a purely meridional primary wave with an off-zonal modulation which corresponds to the fastest growing mode. For $M = 0.1$, a primary wave, $\mathbf{p} = (10, 0)$ gives this modulation for maximum growth to be $\mathbf{q} = (9, 6)$. The growth rate of this case has already been presented in figure 4.4 where after the initial linear growth stage, a periodic oscillation, albeit irregular is observed.

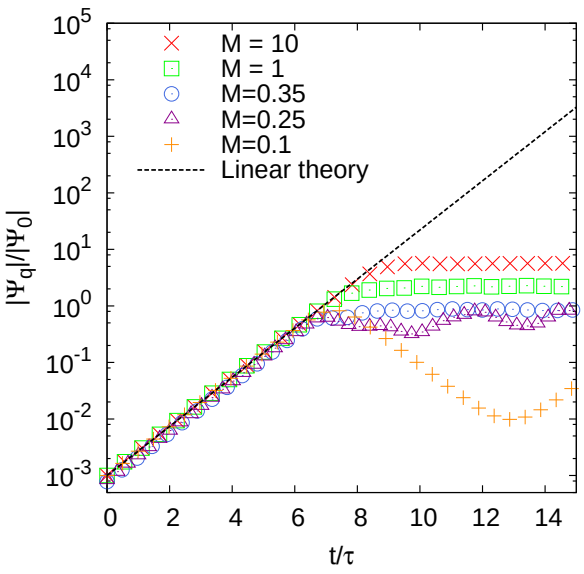

Figure 4.18: Growth of zonal perturbations due to modulational instability of a meridional primary wave having $\mathbf{p} = (10, 0)$ for several different values of M. The amplitude of the zonal mode has been scaled by Ψ_0 and time has been scaled by τ, the inverse of the instability growth rate.

However, these irregular oscillations are clearly non-turbulent, evident in the vorticity snapshots of figure 4.19 which shows quite a regular pattern even at $t/\tau = 100$, by which time the respective $M = 0.1$ system with zonal $\mathbf{q}$ is completely turbulent, see figure 4.14. Another way to see that the dynamics are regular in this case is to look at the 2D k-spectra shown in figure 4.20. At $t/\tau = 0$, the only excited modes are the primary wave $\mathbf{p}$, modulation $\mathbf{q}$ and two satellites $\mathbf{p} \pm \mathbf{q}$ which are marked by red crosses in figure 4.20. At $t/\tau = 60$ a regular "crystalline" structure is evident, corresponding to a discrete set of nodes $n\mathbf{p} + m\mathbf{v}$ (with integer values of m and n) with energy within 1% of the initial primary wave energy. A transition to turbulence does eventually occur after a very long time, and the turbulent state does exhibit off-zonal striations similar to the respective $M = 0.1$ system with zonal initial modulations $\mathbf{q}$.

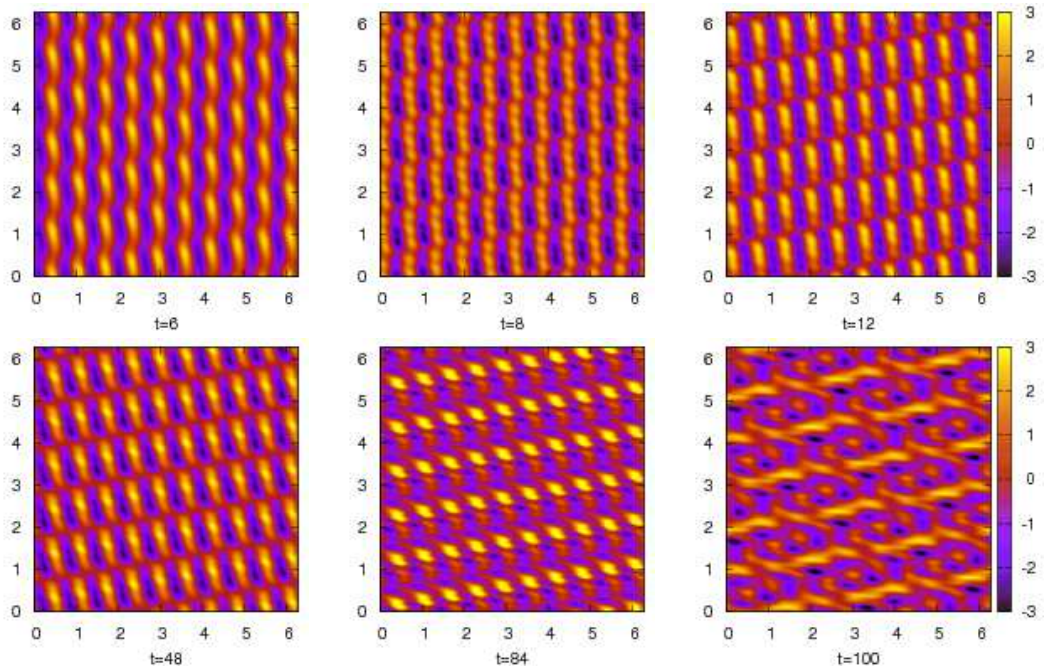

Figure 4.19: Vorticity snapshots for an off-zonal perturbation, $\mathbf{q} = (9, 6)$ to a meridional primary wave, $\mathbf{p} = (10, 0)$ with $M = 0.1$.

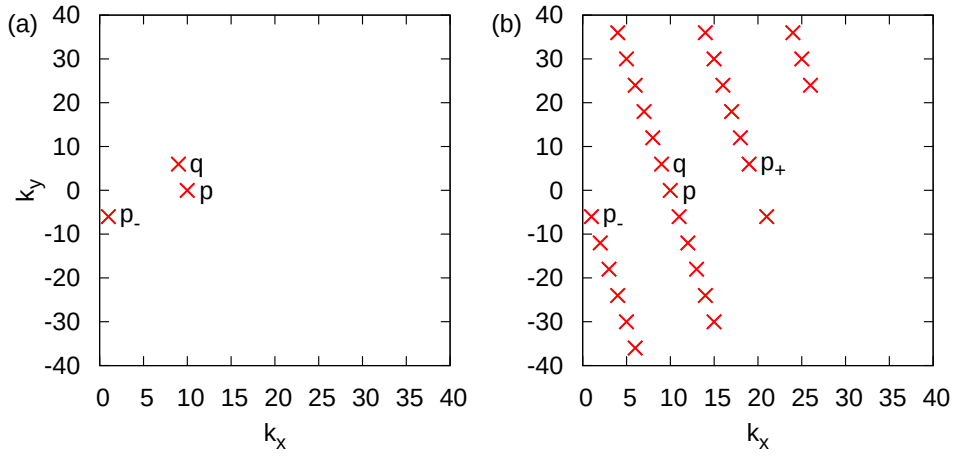

Figure 4.20: Excited modes at $t = 60$ with energy within 1% of the energy of the initial perturbation in run with for, $\mathbf{p} = (10, 0)$, $q = (9, 6)$, $M = 0.1$.

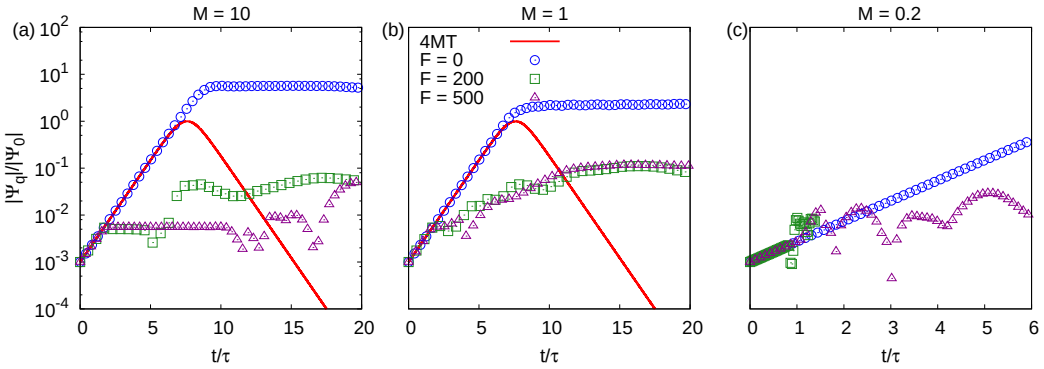

Figure 4.21: Comparison of the growth of the zonal mode $\mathbf{q}$ obtained by DNS versus solving 4MT system for various F. In each case the primary wavenumber is $\mathbf{p} = (\mathbf{10}, \mathbf{0})$ and the modulation wavenumber is $\mathbf{q} = (\mathbf{0}, \mathbf{1})$. The nonlinearity levels are (a) $M = 10$, (b) $M = 1.0$ and (c) $M = 0.2$. In each case time has been scaled by τ,the inverse of the instability growth rate.

4.8.6 Finite deformation radius

The analysis in Section 4.6.2 revealed that the instability growth is suppressed with decreasing deformation radius (increasing F) and this is confirmed in figure 4.21. The predicted linear growth rate is now observed for only one to two timescales. Some vortex streets are still evident for $M = 1$ but they quickly become unstable and within approximately two timescales, the vorticity plots in figure 4.23 show turbulent behaviour.

4.8.7 Stable case

As well as considering in detail various situations where the linear theory based on the 4MT model predicts instability, the linearly stable case has also been investigated.

For small M the zonal mode in the modulationally stable case behaves as expected, following the 4MT theory without growth of the mode as shown in figure 4.24 for $\mathbf{p} = (8, 6)$ and $\mathbf{q} = (0, 1)$. For $M \gg 1$, as expected from the 4MT stability prediction, the zonal mode does not grow initially, for $t/\tau <\sim 1$. After about one timescale however, the mode quickly breaks into growth, increasing, more or less exponentially, by three orders of magnitude. It must be stressed again therefore, that for $M \gg 1$, the 4MT instability predictions should be used with caution.

A steepening of the zonal velocity as predicted [63] for $M \gg 1$, is another feature

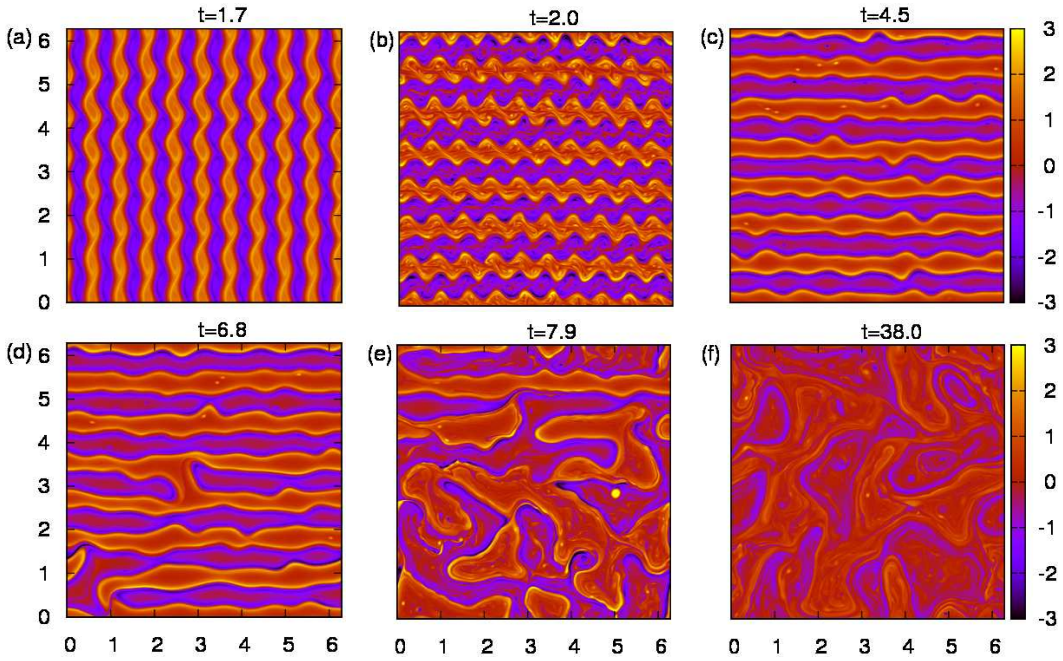

Figure 4.22: Vorticity snapshots showing the transition to turbulence of a zonal perturbation to a meridional primary wave having $M = 10$ and $F = 200$. The horizontal axis is x and the vertical is y.

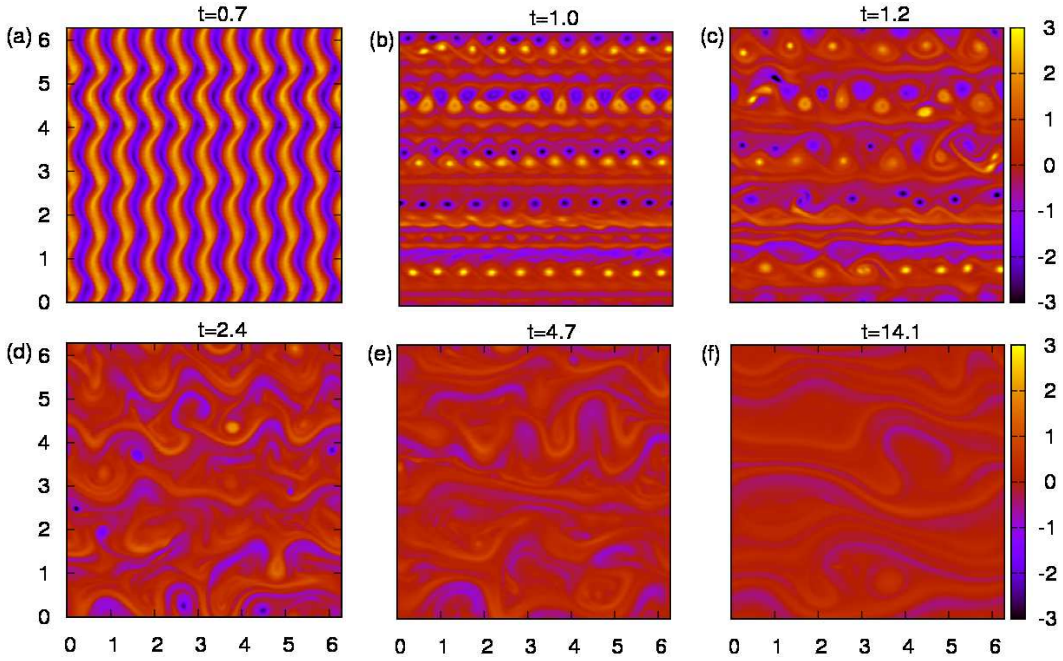

Figure 4.23: Vorticity snapshots showing the transition to turbulence of a zonal perturbation to a meridional primary wave having $M = 1$ and $F = 200$. The horizontal axis is x and the vertical is y.

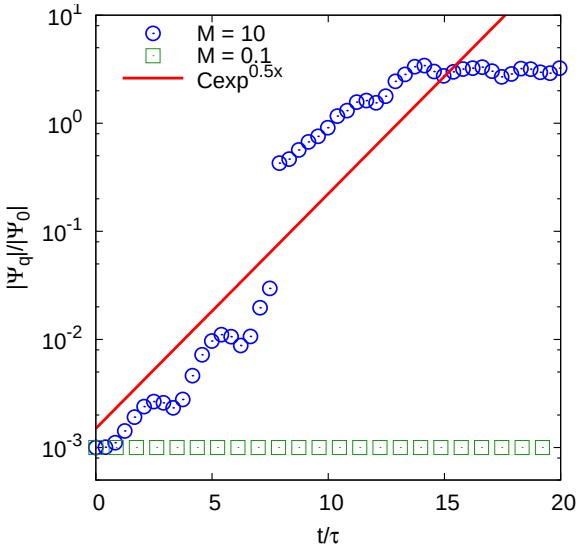

Figure 4.24: Growth of the zonal perturbation $\mathbf{q} = (0, 1)$ obtained by DNS for $\mathbf{p} = (8, 6)$ for $M = 10$ and $M = 0.1$.

of the stable case where the initial sinusoidal profile develops into a triangular Burger's shock-type profile, evident in figure 4.25.

4.9 Summary

The linear theory of the modulational instability [8] of Rossby and drift waves, as described by the CHM equation, has been revisited using a 4MT model. This has been extended to show what part the primary wave amplitude, the nonlinearity level and the deformation or Larmor radius play in the linear and nonlinear dynamics of the system. It has been determined that the most unstable modulation wavevector is off-zonal when the primary wave nonlinearity parameter, M falls below the critical value $M_* = 0.53$ and this point could possibly be used to explain why the observed jets for the $M = 1$ case are off-zonal.

Clarification has been made on the relation between the modulational instability and the decay instability and whether the dominant nonlinear mechanism of the modulational instability is three-wave or four-wave. The decay instability, derived from the 3MT is the basic process when the nonlinearity is low, $M \ll 1$ and the primary wavevector

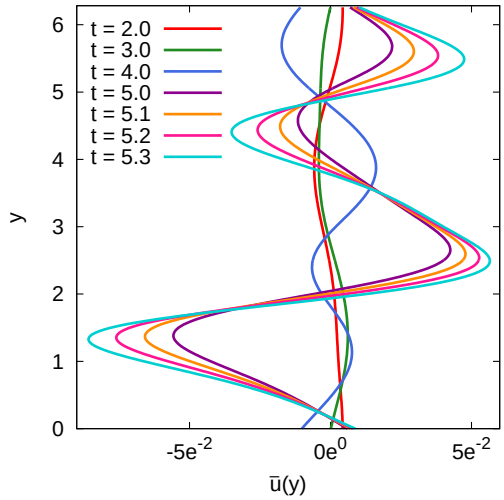

Figure 4.25: Mean zonal velocity profile for the stable configuration $\mathbf{p} = (8, 6)$, $\mathbf{q} = (0, 1)$ and $M = 10$.

and the modulation wavevector belong to the same resonant triad, excluding those which lie close to $\mathbf{k} = 0$, where the two branches of the resonant curve intersect. This however excludes the purely zonal modulations for which the 3MT does not work well. On the other hand, the 4MT models very well the dynamics for low M, including off-zonal modulations. In addition, for $M \gtrsim 1$, the 4MT captures well the initial linear evolution and predicts well the critical level of nonlinearity M_* which separates the regimes of oscillatory nonlinear behaviour from those where saturation is observed. For nonlinearities above M_*, when the jet breaks up into a vortex street, the 4MT fails thereafter, since the system is now vortex-dominated rather than wave-dominated.

For all levels of nonlinearity, the 4MT evolves through an infinite sequence of nonlinear oscillations. This oscillatory behaviour is observed for the full system too, for low nonlinearity levels only, where the initial growth reverses. Conversely, this behaviour does not happen for higher nonlinearities of the full system which rolls-up and then settles into a saturated, more-or-less stable state for a long time.

The formation of narrow zonal jets when $M \gtrsim 1$ agree with theoretical predictions [63]. These jets are more stable than the Rayleigh-Kuo criterion would suggest,

probably because their two-dimensional structure is made-up of stable vortex streets. Such narrow jets represent very effective transport barriers, which exist in the atmosphere and in a magnetically-confined plasma.

Chapter 5

Zonostrophy

The work presented in this chapter focuses on the particular case when the scales are much smaller than the deformation or ion Larmor radius which is the most important and frequently considered limit, at least in the GFD, so that an infinite deformation radius can be assumed or $F = 0$. Taking the respective limit in the general zonostrophy expression obtained in [46], an expression for the zonostrophy for such small scale turbulence is obtained and shown to be positive and scale invariant. The latter observation is necessary in order to apply the generalised Fjørtoft argument developed in [66; 45]. This argument predicts not only zonation but also the anisotropic k-space flow paths of the three invariants during the zonation process.

Having obtained these analytical predictions, DNS of the QG/drift turbulence are carried out to test the conservation of the zonostrophy for different levels of initial nonlinearity, and also to test the predictions of the generalised Fjørtoft argument, by tracking in time the transfer path of the three invariants in k-space.

5.1 Conservation laws

Like all physical systems, wave turbulence systems also conserve energy E and momentum P, where the laws are defined respectively as

$$E = \int |\omega_{\mathbf{k}}| n_{\mathbf{k}} \, d\mathbf{k} \tag{5.1}$$

$$P = \int \mathbf{k} n_{\mathbf{k}} \, d\mathbf{k} \tag{5.2}$$

such that $\omega_{\mathbf{k}}$ can be thought of as the density of the energy and $\mathbf{k}$ the density of the momentum. The enstrophy is equivalent to the x-momentum

$$Q = \int k_x n_{\mathbf{k}} \, d\mathbf{k} \tag{5.3}$$

These are usually the only two conserved quantities of the three-wave kinetic equation although the four-wave kinetic equation also conserves the number of waves. Using Eq. 3.86, the rate of change of energy can be written [33] as

$$\begin{aligned} \frac{\partial E}{\partial t} &= \int \omega_{\mathbf{k}} \frac{\partial n_{\mathbf{k}}}{\partial t} \, d\mathbf{k} \\ &= \int\int\int \left(\omega_{\mathbf{k}} \mathcal{R}_{12k} - \omega_{\mathbf{k}} \mathcal{R}_{k12} - \omega_{\mathbf{k}} \mathcal{R}_{2k1}\right) d\mathbf{k}_1 d\mathbf{k}_2 d\mathbf{k} \\ &= \int \mathcal{R}_{12k} (\omega_{\mathbf{k}} - \omega_{\mathbf{k}_1} - \omega_{\mathbf{k}_2}) d\mathbf{k}_1 d\mathbf{k}_2 d\mathbf{k} \end{aligned} \tag{5.4}$$

where a change of variables $\mathbf{k}_1, \mathbf{k}_2, \mathbf{k} \mapsto \mathbf{k}, \mathbf{k}_1, \mathbf{k}_2$ and $\mathbf{k}_1, \mathbf{k}_2, \mathbf{k} \mapsto \mathbf{k}_2, \mathbf{k}, \mathbf{k}_1$ have been taken for the second and third terms in the parentheses respectively. Similarly for the enstrophy

$$\frac{\partial Q}{\partial t} = \int \mathcal{R}_{12k} (\mathbf{k} - \mathbf{k}_1 - \mathbf{k}_2) d\mathbf{k}_1 d\mathbf{k}_2 d\mathbf{k} \, . \tag{5.5}$$

By virtue of the resonance conditions in Eqs 4.37, the terms within the parentheses of Eqs 5.4 and 5.5 equal zero, showing that energy and enstrophy remain constant in the system. It follows that for any quantity

$$Z = \int \zeta_{\mathbf{k}} n_{\mathbf{k}} \, d\mathbf{k} \tag{5.6}$$

with density $\zeta_{\mathbf{k}}$ is conserved if

$$\zeta(\mathbf{k}) = \zeta(\mathbf{k}_1) + \zeta(\mathbf{k}_2). \tag{5.7}$$

5.2 Conservation of zonostrophy

Such a quantity was found to exist [66; 45; 46] in the early 1990s. By introducing the complex function

$$\zeta_{\mathbf{k}} = \ln Y_{\mathbf{k}}$$

where

$$Y_{\mathbf{k}} = \frac{k_y + \sqrt{3}\, k_x + \mathrm{i}\rho k^2}{k_y - \sqrt{3}\, k_x + \mathrm{i}\rho k^2}\,, \tag{5.8}$$

to a change of variables $(k_x, k_y) \mapsto (m, n)$

$$\begin{aligned} m &= \frac{k_y}{k_x} \qquad\qquad n = k_x + \frac{k_y^2}{k_x} \\ k_x &= \frac{n}{1+m^2} \qquad k_y = \frac{mn}{1+n^2}\,, \end{aligned} \tag{5.9}$$

it was shown that Eq. 5.8 satisfies the condition 5.7. Expanding Eq. 5.8 into real and imaginary parts gives

$$\zeta_{\mathbf{k}} = \mathrm{i}\Big(\mathrm{Arg}[k_y + \sqrt{3}k_x\mathrm{i} + \rho k^2] - \mathrm{Arg}[k_y - \sqrt{3}k_x\mathrm{i} + \rho k^2]\Big) \tag{5.10}$$

$$-\frac{1}{2}\ln[\rho^2 k^4 + (k_y + \sqrt{3}k_x)]^2 + \frac{1}{2}\ln[\rho^2 k^4 + (k_y - \sqrt{3}k_x)^2] \tag{5.11}$$

the imaginary part giving the general form of the zonostrophy density [46] as

$$\Im[\zeta_{\mathbf{k}}] = \arctan\frac{k_y + \sqrt{3}\, k_x}{\rho k^2} - \arctan\frac{k_y - \sqrt{3}\, k_x}{\rho k^2}\,, \tag{5.12}$$

where ρ is the Rossby radius or Larmor radius as defined in table 3.1. Originally however, this density was found in the limiting cases of zonal flows and large scale waves [45].

The present study is concerned with small scale turbulence for which $\rho k \gg 1$ so that the general zonostrophy density can then be expanded in powers of $\frac{1}{\rho}$. Dropping the imaginary symbol for convenience and Taylor expanding Eq. 5.12 gives, up to ninth order

$$\begin{aligned} \zeta_{\mathbf{k}} = \quad & -2\sqrt{3}\frac{k_x}{\rho k^2} + 2\sqrt{3}\frac{k_x}{\rho^3 k^4} \\ & -2\sqrt{3}\frac{k_x}{\rho^5 k^{10}}[k_y^4 + 6k_x^2 k_y^2 + \frac{9}{5}k_x^4] \\ & +2\sqrt{3}\frac{k_x}{\rho^7 k^{14}}[\frac{27}{7}k_x^6 + 27k_x^4 k_y^2 + 15k_x^2 k_y^4 + k_y^6] \\ & -2\sqrt{3}\frac{k_x}{\rho^9 k^{18}}[9k_x^8 + 108k_x^6 k_y^2 + 126k_x^4 k_y^4 + 28k_x^2 k_y^6 + k_y^8] + O(\rho^{-10})\,. \end{aligned}$$

However a Taylor expansion of the frequency $\omega_{\mathbf{k}} = -\frac{\beta}{(k^2+\rho^{-2})}$ in powers of $\frac{1}{\rho}$ is

$$\omega_{\mathbf{k}} = \sum_{n=1}^{\infty} \omega^{(n)} = \sum_{n=1}^{\infty} \frac{(-1)^n \beta \rho^2 k_x}{(\rho k)^{2n}} \tag{5.13}$$

and it is immediately obvious that in the leading order $\zeta_{\mathbf{k}} = \frac{2\sqrt{3}}{\beta\rho}\omega_{\mathbf{k}}$ i.e. in the small scale limit ζ is proportional to the energy and is not an independent invariant. Thus, to find the truly independent invariant in the small scale limit this energy term must be subtracted. To have a simpler expression which is ρ-independent in the leading order, the result is multiplied by $-\frac{5\rho^5}{8\sqrt{3}}$. Re-defined this way, the density of the zonostrophy is

$$\tilde{\zeta}_{\mathbf{k}} = -\frac{5\rho^5}{8\sqrt{3}}(\zeta - 2\sqrt{3}\omega/\beta\rho) =$$
$$k_x^3\left(\frac{5k_y^2 + k_x^2}{k^{10}} - 5\frac{\frac{5}{7}k_x^4 + 6k_x^2k_y^2 + 3k_y^4}{\rho^2 k^{14}} + 5\frac{2k_x^8 + 26k_x^6k_y^2 + 30k_x^4k_y^4 + 6k_x^2k_y^2}{\rho^4 k^{18}}\right),$$

which in the small scale limit or $\rho \to \infty$, becomes

$$\tilde{\zeta}_{\mathbf{k}} = k_x^3 \frac{k_x^2 + 5k_y^2}{k^{10}}. \tag{5.14}$$

For the work which follows, it is Eq. 5.14 which is used to define the zonostrophy density for the small scale turbulence.

5.3 Triple cascade behaviour

5.3.1 Dual cascades in 2D Navier-Stokes turbulence

Fjørtoft [43] deduced the nature of the spectral evolution of the conserved quantities, energy and enstrophy, for two-dimensional turbulence by considering the change in energy at three nonlinearly coupled scales. He argued that when the initial energy is concentrated at the intermediate scale, then for later times, more energy is acquired at the larger scale than at the smaller scale i.e. the energy cascade is an inverse one from larger to small wavenumbers. Conversely, the enstrophy cascade is a direct one to larger wavenumbers or smaller scales. The scenario is now summarised below.

Consider 2D isotropic turbulence described by the Navier-Stokes equations, which is generated at some intermediate forcing scale k_0 and dissipated outside the inertial

ranges at both very large and very small scales for which $k_- \ll k_0$ and $k_+ \gg k_0$ respectively. The expressions for the conserved quantities, energy and enstrophy in the absence of forcing and dissipation are equivalent to those for the CHM model, Eqs 3.55 and 3.58. For steady-state turbulence, the dissipation rates of the energy and enstrophy must be equal the rate at which they are produced. According to Eqs 3.55 and 3.58, the ratio of the k-space densities is k^2 such that the enstrophy dissipation rate μ is related to the energy dissipation rate ε, as $\mu \sim k^2\varepsilon$.

If it is assumed that the energy is dissipated at small scales, k_+ at a rate ε then the enstrophy would have to be dissipated at the rate $k_+^2\varepsilon$. However this is impossible since it is only produced at a rate of $k_0^2\varepsilon \ll k_+^2\varepsilon$. Since the energy must be dissipated at either k_+ or k_- then it can be concluded that it is dissipated at k_- via an inverse cascade through the scales. At these scales, the density of the energy dominates the density of the enstrophy. Similarly, if it is assumed that the enstrophy is dissipated at k_-, then the energy would have to be dissipated at a rate of $\frac{1}{k_-^2}\mu$. Again this rate is greater than $\frac{1}{k_0^2}\mu$, the rate at which it is produced, concluding that the enstrophy must be dissipated at smaller scales or larger wavenumbers k_+, than which it is produced via a direct cascade through the inertial range. At these scales, the enstrophy density exceeds that of the energy.

5.3.2 Triple cascades in weak CHM turbulence

A similar argument can be adopted to determine the direction of the cascade directions of the three conserved quantities of the CHM model by examining in turn the ratio of the densities of each pair of the invariants. It is also required that each of the three densities are positive since positive and negative amounts of the same quantity would lead to a net total of zero of that quantity with the result that the Fjørtoft argument could not be applied. Furthermore, Eqs 5.1, 5.3 and 5.6 show that the three invariants are linearly related to the waveaction spectrum or turbulence intensity n_k so that the density ratios are functions of $\mathbf{k}$ rather than the turbulence intensity.

The turbulence is produced near $\mathbf{k}_0 = (k_{0_x}, k_{0_y})$ and dissipated in regions which are separated in scales from the forcing scale as with the 2D Navier-Stokes turbulence.

To divide the 2D k-space into three non-intersecting regions implies anisotropy where each invariant will evolve to that sector where its density prevails over the others. The boundaries of these sectors are defined where the ratio of each pair of invariants remains constant to its initial value as detailed below.

- **E-Q boundary**: The energy density is $\frac{k_x}{k^2}$ and that of enstrophy is k_x giving the ratio k^2 as with the 2D Navier-Stokes turbulence. Equating this to its initial value gives

$$k^2 \sim k_0^2 \tag{5.15}$$

  which in the 2D k-space amounts to a circle of radius k_0 centered at the origin. Using the same argument as before, energy must be dissipated at the larger scales and enstrophy at the small scales.

- **E-Z boundary**: The zonostrophy density given by Eq. 5.14 can be simplified to

$$\tilde{\zeta} \sim \frac{k_x^3}{k^8} \tag{5.16}$$

  by noting that $k^2 \leq k_x^2 + 5k_y^2 \leq 5k^2$. Thus the ratio of the energy to zonostrophy densities is

$$\frac{k^3}{k_x} \sim \frac{k_0^3}{k_{0_x}}\,. \tag{5.17}$$

  Since it is already known that the energy accumulates at large scales then this boundary slices that region in two. The zonostrophy density is dominant in the region adjacent to the k_x axis and the energy density in the area adjacent to the k_y axis so that the zonostrophy is effectively pushing the energy to zonal scales.

- **Q-Z boundary**: Equating the ratio of the enstrophy density k_x to the zonostrophy density ${k_x}^3/k^8$ to the initial value of this ratio gives the boundary separating the enstrophy and the zonostrophy cascades,

$$\frac{k^4}{k_x} \sim \frac{k_0^4}{k_{0x}}\,. \tag{5.18}$$

These regions are shown in figure 5.1 where it can be seen that the Q-Z boundary cuts the k_x axis at

$$k_x^* \sim \frac{k_0^{\frac{4}{3}}}{k_{0x}^{\frac{1}{3}}}. \tag{5.19}$$

thereby restricting the zonostrophy to not too large wavenumbers unless the initial wavenumber is approximately a zonal scale, $k_{0_y} \gg k_{0_x}$. In particular, if $k_{0_y} = k_{0_x}$ then $k_x^* = 2^{\frac{1}{6}} k_0$, which means that the maximum allowed wavenumber for the zonostrophy cascade is practically the same as the initial scale. In other words, in this case the zonostrophy can only cascade to the larger scales and not to small scales.

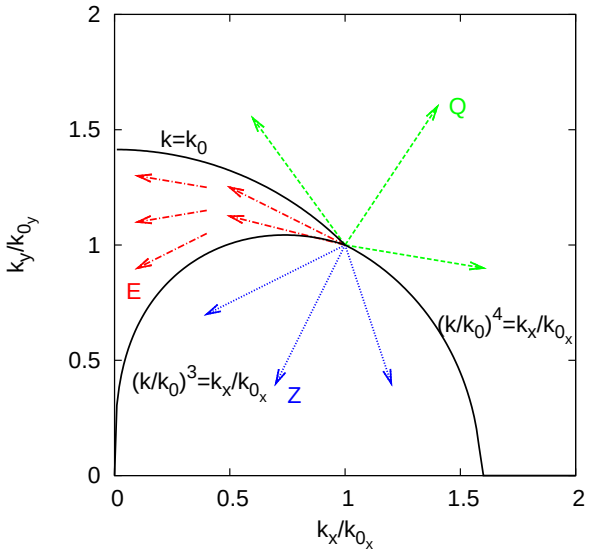

Figure 5.1: Non-intersecting sectors for triple cascade as predicted by the generalised Fjørtoft argument.

5.3.3 Strong turbulence

The foregoing Fjørtoft-type theory assumes zonostrophy conservation which itself has only been proven for the wave kinetic equation. This means that it is valid for weak wave turbulence but not necessarily for strong turbulence.

Suppose that strong turbulence is forced at large $\mathbf{k}$, strong enough so that the nonlinear term of the CHM model, Eq. 3.35 renders the linear term negligible. Since the linear term is the only source of anisotropy in the CHM model, the system is expected to build an isotropic inverse energy cascade identical to that of 2D Navier-Stokes turbulence. As the inverse energy cascade progresses to larger scales, the linear dynamics or the β-effect becomes more and more important so that the nonlinearity of the turbulence is now reduced and behaves increasingly like weak wave turbulence. The wavenumber at which

the inverse cascade of the strong isotropic turbulence transits into weak wave turbulence is the well-known Rhine's scale [49]. This transitional wavenumber can be approximated by equating the characteristic timescales or frequencies from both regimes. In the case of strong turbulence, the eddy turnover time of the inverse energy cascade, τ_{NL} can be estimated from Kolmogorov K41 theory [28; 83] to within a constant by

$$\tau_{NL} = \varepsilon^{-\frac{1}{3}} k^{-\frac{2}{3}} \,. \tag{5.20}$$

The linear timescale is simply the inverse of the linear dispersion relation

$$\tau_L = \frac{k^2}{\beta k_x} \,. \tag{5.21}$$

Equating τ_{NL} and τ_L while ignoring the anisotropy for now (since the initial cascade is isotropic) defines the transitional wavenumber k_β as

$$k_\beta = \left(\frac{\beta^3}{\varepsilon}\right)^{\frac{1}{5}} \,. \tag{5.22}$$

Equating Eqs 5.20 and 5.21, but this time retaining the anisotropy gives

$$k^8 = k_\beta^5 k_x^3 \,, \tag{5.23}$$

the x and y components of k_β then being defined by

$$k_{\beta_x} = k_\beta \cos^{8/5} \alpha \tag{5.24}$$

$$k_{\beta_y} = k_\beta \sin\alpha \cos^{3/5} \alpha \tag{5.25}$$

where $\alpha = \arctan \frac{k_y}{k_x}$. A sketch of this boundary in the 2D k-space is shown in the parametric plot of figure 5.2 which resembles a dumb-bell or is sometimes referred to as the 'lazy 8' curve. For wavenumbers outside the curve, there is strong isotropic turbulence but for those modes smaller than k_β, anisotropic Rossby wave turbulence is the dominant process [49; 84].

If a fully turbulent dispersion relationship $\omega_{NL} = Uk$ is assumed, where U is the fluid velocity, equating its inverse to the linear timescale τ_L retrieves the more commonly known Rhines scale [49; 84]

$$k_\beta^R = \sqrt{\frac{\beta}{U}} \,. \tag{5.26}$$

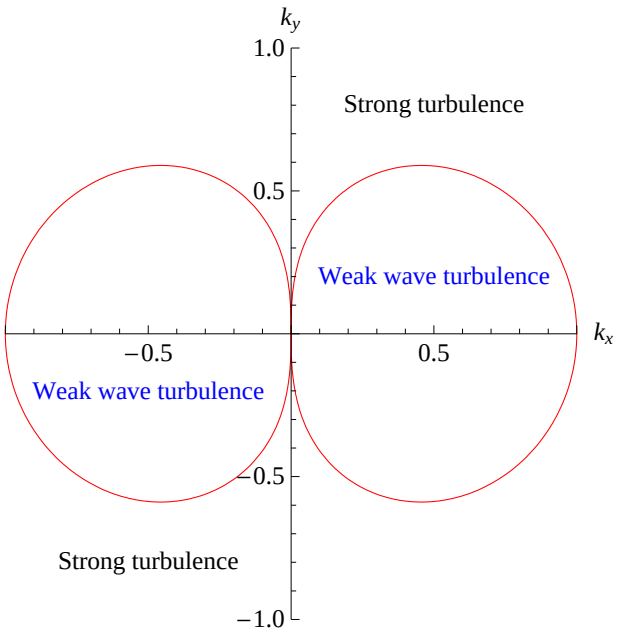

Figure 5.2: Dumb-bell curve in the k-space defining the transition from strong to weak turbulence.

An alternative argument for zonation therefore, in the case of initially strong isotropic turbulence is based on the observation that the weak wave turbulence is less efficient in supporting the energy cascade than the strongly nonlinear interactions. As such, if the forcing scale is far outside the transitional curve, once the inverse energy cascade reaches these scales, it turns and follows the curve towards the zonal scales rather than penetrate the curve.

This condition that the linear wave period and the nonlinear eddy turnover time are balanced *scale-by-scale* could be called a 'critical balance' analogous to the critically-balanced cascade in the weak turbulence of shear Alfvén waves in MHD turbulence [85]. This critical balance picture would mean that the energy cascade path of zonation would be given by Eq. 5.23 which is actually very close to Eq. 5.17, the Fjørtoft predicted path, if $k_0 \sim k_\beta$. If this were in fact the case, then the zonostrophy would flow beneath this path to the weakly nonlinear scales. The zonostrophy would thus be supported at these scales and hence conserved while the energy and enstrophy are still supported at the intermediate and strongly nonlinear scales. Furthermore, if all three invariants are conserved anyway, then the preceding Fjørtoft argument is once again valid.

5.4 Numerical study

The CHM model is employed to numerically test the theoretical predictions of both the conservation of zonostrophy and the triple cascade behaviour of the small scale turbulence. The initial condition is a Gaussian distribution of the stream function defined as

$$\hat{\psi}(\mathbf{k},0) = A\mathrm{e}^{\left(\frac{|\mathbf{k}-\mathbf{k}_0|^2}{k_*^2}+i\phi_{\mathbf{k}}\right)} + \text{image}\,, \tag{5.27}$$

where $\mathbf{k}_0$ is the wavenumber on which the Gaussian is initially centred, A is the constant amplitude, k_* is the variance and $\phi_{\mathbf{k}}$ are random independent phases. The 'image' refers to the mirror-reflected spectrum with respect to the k_x axis.

Zero numerical dissipation has been modelled rather than a forced-dissipated steady state turbulence because there appears to be no physically meaningful dissipation which acts selectively on nearly zonal and nearly meridional scales only. While the triple cascade theory presented in the previous section is based on a forced-dissipative turbulence, it is assumed it is also valid for freely-decaying turbulence as is the case of the dual cascade in 2D Navier-Stokes turbulence. As such, simulations have been carefully monitored to avoid a bottleneck accumulation of turbulence at the maximum wavenumber.

5.4.1 Centroids

To quantify the cascades of the energy, enstrophy and zonostrophy in the time-evolving non-dissipative turbulence the *centroids* or 'centres of mass' of the total of each invariant are introduced and are defined respectively as,

$$\mathbf{k}_E(t) = \frac{1}{E}\int \mathbf{k}\, k^2 |\hat{\psi}_{\mathbf{k}}|^2\, d\mathbf{k}, \tag{5.28}$$

$$\mathbf{k}_Q(t) = \frac{1}{Q}\int \mathbf{k}\, k^4 |\hat{\psi}_{\mathbf{k}}|^2\, d\mathbf{k}, \tag{5.29}$$

$$\mathbf{k}_Z(t) = \frac{1}{Z}\int \mathbf{k}\, \frac{k_x^4}{k^6}(k_x^2+5k_y^2) |\hat{\psi}_{\mathbf{k}}|^2\, d\mathbf{k}. \tag{5.30}$$

Table 5.1: Triple cascade parameters for the weak and strong nonlinearity cases

	Weak	Strong
Resolution	512^2	1024^2
$\mathbf{k}_0$	(20, 20)	(40, 40)
k_*	8	16
A	10^{-6}	5×10^{-7}
λ	0.09	0.7

For the non-dissipative 2D Navier-Stokes or Euler equation, it is actually possible to recast the Fjørtoft argument for the evolving turbulence directly in terms of these centroids in a rigorous way, see Appendix E. However the structure of the CHM is more involved and it is not clear if a generalised Fjørtoft argument is applicable for the triple cascades in terms of the centroids in a rigorous way. This is certainly an interesting question to be addressed in future.

5.4.2 Nonlinearity parameter

The theory is tested for initially weak and strong nonlinearities, a summary of the relevant parameters being presented in table 5.1. A higher resolution is afforded for the stronger nonlinearity since it evolves faster relative to the weaker case which therefore needs to run for longer times. The centre of the initial spectrum and its width are altered accordingly.

The degree of nonlinearity λ, can be approximated by estimated directly the linear and nonlinear terms in Eq. 3.61 but the fact that there will be statistical cancellations in the sum of the nonlinear term due to the the initial random phases must be taken into account. If N is the number of initially excited modes, this is done schematically by

$$\left| \sum_{j=1}^{N} \text{individual-term}_j \right| \sim \sqrt{N} \ |\text{individual-term}| \ .$$

If N is approximated by $2\sqrt{\pi k_*^2}$ the nonlinearity is then defined as

$$\lambda \sim \frac{2\sqrt{2\pi} k_0^3 k_* A}{\beta}, \tag{5.31}$$

which gives $\lambda \sim 0.1$ for the weakly nonlinear case and $\lambda \sim 0.01$ for the strongly nonlinear case. It could be assumed that the phases rapidly become correlated to a certain degree

for the strongly nonlinear case so that the λ estimate in this case would include an extra factor of $\sqrt{N} \sim 100$ which would be an overestimate. It is believed that the previous estimate is more likely so that for the strongly nonlinear case, the turbulence is roughly on the 'lazy-8' curve of figure 5.2.

5.5 Triple cascade results

5.5.1 Weak nonlinearity

With $\lambda \approx 0.09$, the initial turbulence is well within the lazy-8 curve. The conservation of energy, enstrophy and zonostrophy and their associated cascades are shown in figure 5.3. Due to the slow weakly nonlinear evolution of this system, any quantity proportional to the turbulence intensity could appear to be conserved, so in addition to the three invariants, a non-conserved quantity, $\int \psi_{\mathbf{k}}|^2 \, d\mathbf{k}$ is also plotted in figure 5.3(a) to demonstrate the true conservation of the zonostrophy.

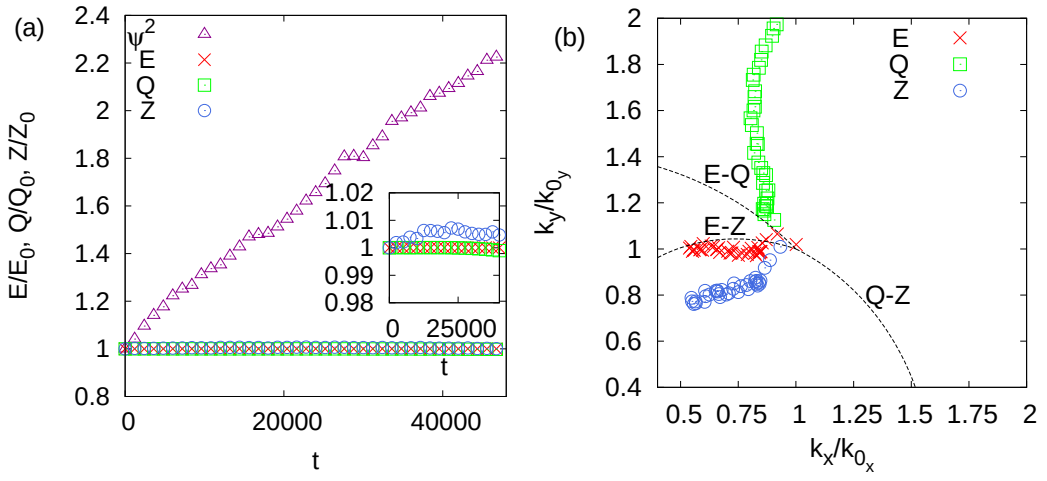

Figure 5.3: Weak nonlinearity. (a) Conservation of energy E, enstrophy Q and zonostrophy Z. Non-conserved quantity ψ^2 is also shown and (b) the cascades of each invariant tracked by their centroids

It is clear that all three invariants, E, Q and Z are well conserved, the energy to within 0.01%, the enstrophy to within 0.15% and the zonostrophy is conserved to within 1%. This is the first numerical demonstration of the conservation of the zonostrophy invariant. It should be remembered that Z is precisely conserved by the wave

kinetic equation, Eq. 3.85 and therefore its conservation by the dynamical CHM equation, Eq. 3.61 is subject to the conditions of applicability of the kinetic equation, namely weak nonlinearity and the random phases. It is not clear *apriori* how well these conditions are satisfied throughout the k-space, particularly near the zonal scales.

The centroids of E, Q and Z are normalised by their initial values so that figure 5.3(b) shows the three centroid paths starting from the same point. Each invariant cascades into its predicted sector. The enstrophy and zonostrophy cascades are well within their respective sector while the energy follows the boundary of its sector with the zonostrophy sector.

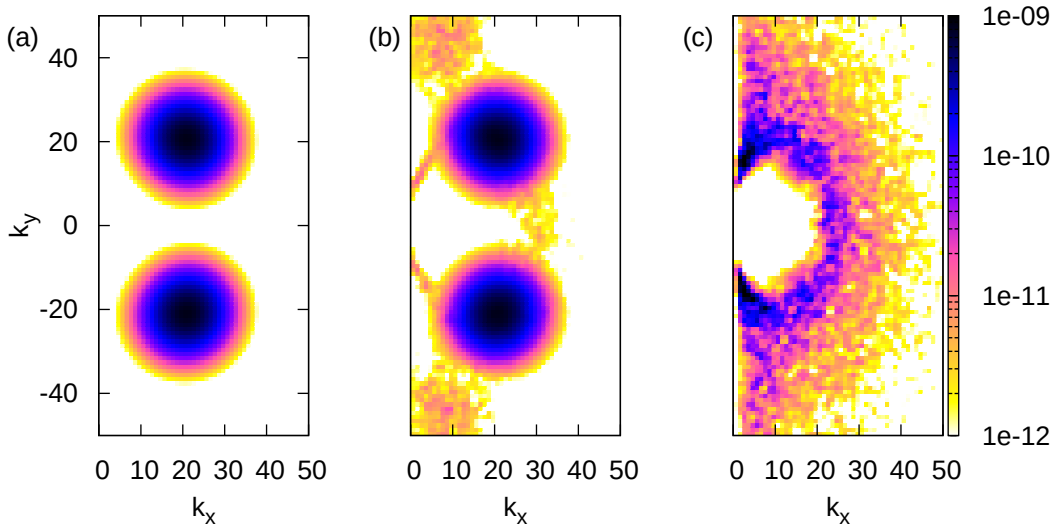

Figure 5.4: Weak nonlinearity. 2D energy spectrum at (a) $t = 0$ (b) $t = 100$ and (c) $t = 40000$

Three successive frames of the energy spectrum in 2D k-space are shown in figure 5.4 and of vorticity distributions in x-space at corresponding times in figure 5.5. The initial spectrum, which represents the Gaussian spot as defined by Eq. 5.27, centered at $\mathbf{k}_0$ and its mirror image in figure 5.4(a), seems to grow branches in panel (b) which stretch toward the origin forming a closed band which subsequently starts shrinking in size. The band is not unlike the lazy-8 curve in figure 5.2 when complemented with the other half of the distribution at $k_x < 0$ although the similarity is only visual rather than quantitative. These features are probably indicative of the structure of the anisotropic

inverse energy cascade process. In the respective vorticity x-plots in figure 5.5, the initial dominant shortwave components are evident in panel (a), propagating at $\pm 45^{\circ}$ corresponding to the position of the initial maxima in the spectrum) which in time evolve into a more disordered turbulent state with a predominant zonal orientation as seen in panel (c).

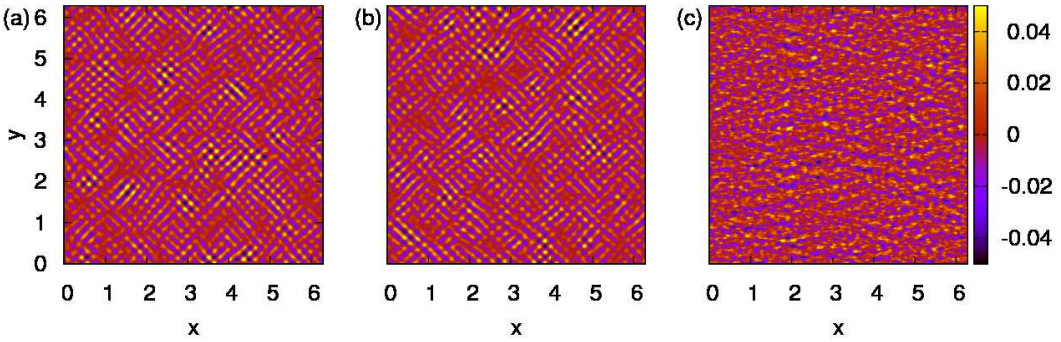

Figure 5.5: Weak nonlinearity. Vorticity distribution at (a) $t = 0$ (b) $t = 100$ and (c) $t = 40000$

5.5.2 Strong nonlinearity

For this case, $\lambda \approx 1$ so that the initial turbulence is near the boundary of the lazy-8 curve. The conservation of each invariant is shown in figure 5.6(a). While the energy and enstrophy are still well conserved, the energy to within 0.2% and the enstrophy to within 1.2% of their initial values, the zonostrophy is not conserved *initially*. It should be remembered however that the zonostrophy is only expected to be conserved for the same conditions as the wave kinetic equation, namely that the nonlinearity be weak. However the zonostrophy growth eventually saturates, so that the zonostrophy is also rather well conserved in the case of stronger nonlinearities. This suggests, as previously mentioned, that for large times the scales that support the zonostrophy invariant are weakly nonlinear, even though the energy scales probably remain moderately nonlinear, and the enstrophy scales are definitely strongly nonlinear.

The cascade paths for E, Q and Z in terms of the respective centroids are plotted in figure 5.6(b). Once again a similar picture to the weakly nonlinear case is observed, namely that the enstrophy and the zonostrophy cascades lie well inside their theoretically

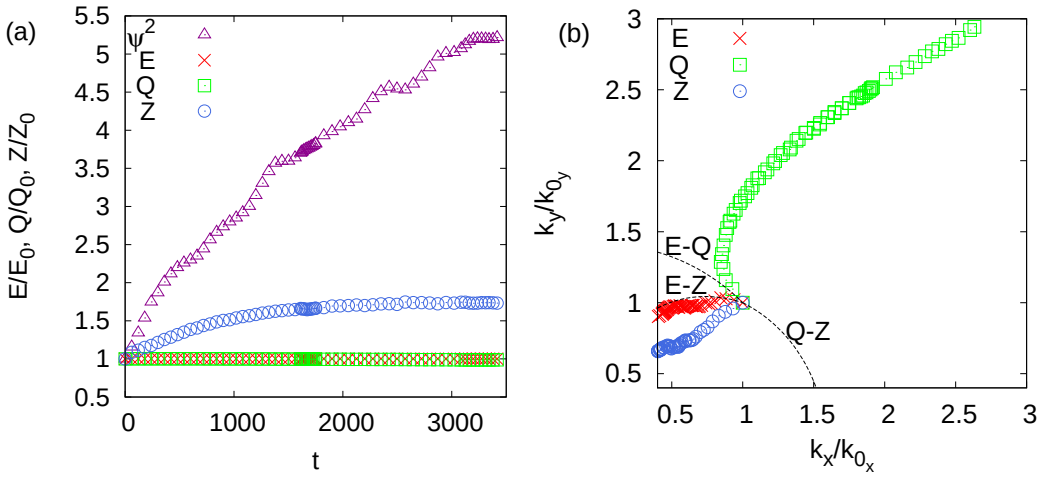

Figure 5.6: Strong nonlinearity. (a) Conservation of energy E, enstrophy Q and zonostrophy Z. Non-conserved quantity ψ^2 is also shown and (b) the cascades of each invariant tracked by their centroids

predicted sectors while the energy cascade again follows the boundary of its sector. It is quite possible that the energy path lies in the critically balanced scales where the nonlinear and the linear time scales are of the same order. However the measurement of the nonlinear time scale is quite ambiguous and it is still unclear if the critical balance approach can be formulated in a more precise way in this case. In any case, it is obvious that even for this strongly nonlinear case, the zonostrophy invariant is conserved for large times and that the triple cascade picture predicted using this invariant provides a reasonable description of the turbulence evolution and an explanation of the zonal jet formation.

The 2D energy spectra in 2D k-space are shown in figure 5.7 and the vorticity distributions in x-space at corresponding times in figure 5.8. The essential features of the evolution of these distributions appear to be similar to those of the weakly nonlinear case with the zonal jets being a little clearer at later times. This can be explained by the fact that the strongly nonlinear system evolves faster than the weakly nonlinear one, figure 5.8(c) is at a more advanced stage of zonation than figure 5.8(c).

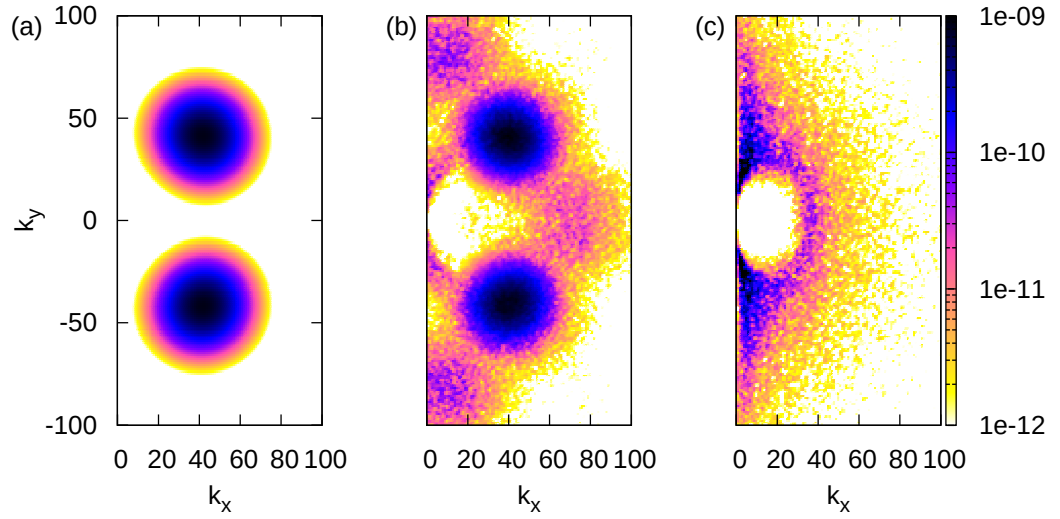

Figure 5.7: Strong nonlinearity. 2D energy spectrum at (a) $t = 0$ (b) $t = 10$ and (c) $t = 3500$

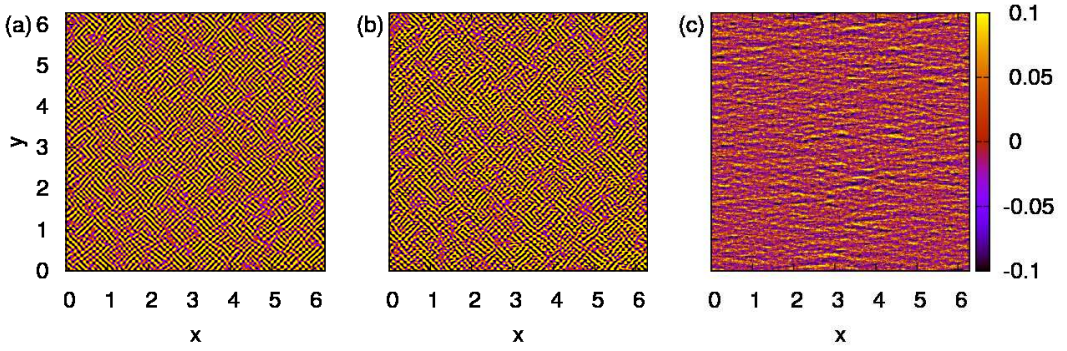

Figure 5.8: Strong nonlinearity. Vorticity distribution at times (a) $t = 0$ (b) $t = 10$ and (c) $t = 3500$

5.6 Summary

The Fjørtoft argument has been used to predict a triple cascade behaviour of the CHM turbulence, in which the energy, the enstrophy and the zonostrophy cascade into their respective non-intersecting predicted sectors in the k-space. These cascades are anisotropic and that of the energy cascade is directed to the zonal scales thus providing a physical explanation into the character of the formation of the zonal jets in such systems.

Numerical proof has been provided of the zonostrophy conservation and of the triple cascade picture for both weak and strong initial nonlinearities. The zonostrophy

invariant is well-conserved for the weakly nonlinear case. Moreover, the zonostrophy conservation is also observed for strong initial nonlinearity after a transient non-conservative time interval. Presumably, this is because the zonostrophy moves in time to the scales that are weakly nonlinear even though the energy and the enstrophy remain in the strongly nonlinear segments of k-space.

It has been demonstrated, using the energy, enstrophy and zonostrophy centroids for tracking the transfers of these invariants in k-space, that all three invariants cascade as prescribed by the triple cascade Fjørtoft argument in both the weakly nonlinear and in the strongly nonlinear cases. The energy appears to be somewhat special among the three invariants in that it tends to cascade along the edge of the sector allowed by the Fjørtoft argument.

Chapter 6

Nonlocal Wave Turbulence

It is now generally accepted in both the fields of plasma physics [86] and in GFD [87], that in the turbulence of Rossby and drift waves, the dominant interaction is with a zonal flow rather than a neighbouring-scale interaction [17], such that studies of drift wave turbulence now imply the study of the drift wave - zonal flow feedback mechanism. Furthermore, observational data from lower hybrid drift waves within the F-layer of the equatorial ionosphere show that the plasma turbulence behaves with a spectrum which indicates that the dominant interaction is a nonlocal one [88].

Rossby waves and drift waves are produced by a primary instability, for example, the ion temperature gradient (ITG) in plasmas or the baroclinic instability in the atmospheres and oceans. Zonal flows are generated via a secondary modulational instability of these waves and they grow by a direct interaction with the small scale waves. The growing zonal flow extracts energy from the wave turbulence, thereby eventually suppressing the turbulence.

One of the reasons that controlled fusion has not been attained to date, is due to the loss of plasma confinement due to turbulent transport. It was discovered however, that under certain circumstances [57] the turbulent transport is greatly reduced, resulting in an enhanced confinement regime. This LH transition is greatly exploited today to yield better plasma confinement. Furthermore, the effect has been observed in numerical simulations of resistive drift wave turbulence at the plasma edge using the modified HW equations [89] and also for full gyrokinetic simulations [90]. However, the underlying

principal mechanism was poorly understood and it is intended here to present a rigorous mathematical description and numerical evidence of the mechanism leading to turbulence suppression and zonal flow saturation.

6.1 Kolmogorov-Zakharov spectra

When Zakharov [67; 68] first derived the weak turbulence spectra, analogous to the Kolmogorov spectra, it assumes as Kolmogorov did, a flux down through the scales of some integral of motion. The first instance of spectral laws for anisotropic media was introduced by Kuznetsov [91] for the ion acoustic waves in a magnetised plasma. The anisotropic spectra of Rossby waves was later studied by Monin and Piterbarg [92] and those of drift waves by Mikhailovski [93; 94]

These spectra are exact solutions of the wave kinetic equation, Eq. 3.85. To obtain the KZ spectra, it must further be assumed that the media is scale invariant. i.e. the dispersion law $\omega_{\mathbf{k}}$ and the nonlinear interaction coefficient V_{12}^{k} in the kinetic equation are invariant to changes in $\mathbf{k}$, formally defined as

$$\begin{aligned} \omega(k) = \text{const}|k|^{a} &\equiv \text{const}|k_x|^{a_x}|k_y|^{a_y}\,, \qquad a = (a_x, a_y) \\ V(qk, qk_1, qk_2) &= q^{b}V(k, k_1, k_2)\,, \qquad b = (b_x, b_y)\,. \end{aligned} \tag{6.1}$$

The two well-known integrals of motion of the CHM model yield the KZ spectra [67; 68]

$$n_E = C_1\mathcal{E}^{\frac{1}{2}}k^{-m_E} \qquad m_E = d + b\,, \quad d = (1,1) \tag{6.2}$$

$$n_Q = C_2\mathcal{Q}^{\frac{1}{2}}k^{-m_Q} \qquad m_Q = d + b + \frac{(1,0) - a}{2}\,, \tag{6.3}$$

where n_E and n_Q are the energy and enstrophy spectra respectively, $\mathcal{E}$ and $\mathcal{Q}$ are the energy and enstrophy flux rates respectively and C_1 and C_2 are constants.

For Rossby and drift waves, conditions 6.1 are true for approximate zonal flows $|k_y| \gg |k_x|$ and then only and if either $\rho k \gg 1$ or $\rho k \ll 1$ The case of interest in this study is that of small scale turbulence so that $\rho k \gg 1$. In this instance, the Rossby or drift dispersion given by Eq. 3.62 is reduced to

$$\begin{aligned} \omega_{\mathbf{k}} &= \frac{\beta k_x}{k_y^2} \\ \implies a &= (1, -2) \end{aligned} \tag{6.4}$$

and the nonlinear interaction coefficient defined in Eq. 3.63 is reduced to

$$\begin{aligned} V_{12}^{k} &= \text{const}|k_x k_{1x} k_{2x}|^{\frac{1}{2}} \left(\frac{1}{k_{1y}} + \frac{1}{k_{2y}} - \frac{1}{k_y} \right) \\ \implies b &= (\frac{3}{2}, -1)\,. \end{aligned} \tag{6.5}$$

Thus the two cascades have exponent $m_E = (\frac{5}{2}, 0)$ and $m_Q = (\frac{5}{2}, 1)$ [92; 93; 94] with corresponding KZ spectra

$$\begin{aligned} n_E &= C_1 \mathcal{E}^{\frac{1}{2}} |k_x|^{-\frac{5}{2}} \\ n_Q &= C_2 \mathcal{Q}^{\frac{1}{2}} |k_x|^{-\frac{5}{2}} |k_y|^{-1}\,. \end{aligned} \tag{6.6}$$

An initial test of the energy KZ spectra given in Eq. 6.6 reveals that it is a solution of the kinetic equation since its collision integral converges and the energy cascade is therefore stationary local. However, subjecting the kinetic equation to finite perturbations leads to divergence of the collision integral at small wavevectors and is there evolutionary nonlocal. Similarly, the collision integral diverges at both large and small wavevectors for the enstrophy spectra [10] given in Eq. 6.6. An extensive examination of KZ spectra in various limiting regimes reveals that the anisotropic KZ spectra of the CHM model are nearly always nonlocal [10], suggesting that drift wave and Rossby wave turbulence are nonlocal. A more detailed analysis of the nature of locality and stability can be found in [95; 96; 33] where the region of locality can be defined by the region of analyticity of the Mellin functions.

In addition, the zonostrophy invariant will lead to yet another KZ spectra for drift wave turbulence defined by

$$n_Z = C_3 \mathcal{Z}^{\frac{1}{2}} k^{-m_Z}\,, \qquad m_Z = d + b + \frac{c-a}{2} \tag{6.7}$$

where $\mathcal{Z}$ is the zonostrophy flux through the scales and

$$\zeta_{\mathbf{k}} = \text{const}\,\mathbf{k}^c \equiv \text{const}|k_x|^{c_x}|k_y|^{c_y}\,, \quad c = (c_x, c_y)\,. \tag{6.8}$$

In the considered limit, $\zeta_{\mathbf{k}} = \frac{k_x^3}{k_y^8}$ so that $c = (3, -8)$ and therefore $m_Z = (\frac{7}{2}, -3)$ and the equivalent spectrum is

$$n_Z = C_3 \mathcal{Z}^{\frac{1}{2}} |k_x|^{-\frac{7}{2}} |k_y|^3\,. \tag{6.9}$$

As a consequence of the nonlocal hypothesis, it was discovered mathematically [10] that two main effects occur:

1. The turbulence spectrum in k-space splits into two unconnected components and as such, intermediate scales die out. One component is a low-frequency turbulence of the zonal flow and the other is a high-frequency short-wavelength jet.

2. The zonal flow must saturate due to the existence of the high-frequency turbulence.

The CHM equation does not contain small scale instabilities of the type which generate Rossby and drift waves, since in the derivation of the HM equation they are filtered out by the adiabatic electrons assumption and a multi-layer model is required in GFD for the baroclinic instability to exist. These instabilities are therefore modelled with a linear forcing term acting like a negative viscosity applied selectively to certain wavenumbers, to numerically investigate this turbulence feedback loop.

6.2 Nonlocal evolution of CHM turbulence

A rigorous mathematical description of the nonlocal turbulence, which was first presented in [9; 10; 11] is reviewed.

To study the nonlocal interaction between wavenumbers $\mathbf{k}$ and zonal flows i.e. waves with a zonal wavenumber, the points of most interest are those two where the resonant manifold crosses the $k_{1_x} = 0$ axis, as shown in figure 4.10. One of those points is the origin which describes the interaction with large-scale zonal flows such that $\mathbf{k}_1 = (0, 0)$. The other point can be determined by setting $k_{1_x} = 0$ in the resonance Eq. 4.37 which gives the wavevector $\mathbf{k}_1 = (0, 2k_y)$ as the other point. The interactions with the wavenumbers in the vicinity of these points give the main contributions to the collision integral, i.e. the RHS of Eq. 3.61.

6.2.1 Nonlocal interaction with large-scale zonal flows

Looking first at the interactions of $\mathbf{k}$ with the large-scale zonal flows near the origin. These large scale waves travel with the x-component of the phase speed,

$$c_{\mathbf{k}} = \frac{\omega_{\mathbf{k}}}{k_x} = -\frac{\beta}{k^2 + F}. \tag{6.10}$$

In the large-scale limit, $k \ll F$, $c_{\mathbf{k}} \to -\beta/F$ and the absolute value of this known as the drift velocity or Rossby velocity. It is convenient therefore to work in a coordinate frame moving with this velocity, in which the Doppler-shifted frequency is given as

$$\Omega_{\mathbf{k}} = \omega_{\mathbf{k}} - c_{\mathbf{k}} k_x = \frac{\beta k_x k^2}{F(k^2 + F)}\,. \tag{6.11}$$

In this moving reference frame, the kinetic equation becomes

$$\frac{\partial n_{\mathbf{k}}}{\partial t} = 4\pi \int \left|V_{12}^k\right|^2 \delta(\mathbf{k} - \mathbf{k}_1 - \mathbf{k}_2)\delta(\Omega_{\mathbf{k}} - \Omega_{\mathbf{k}_1} - \Omega_{\mathbf{k}_2}) \times \\ [n_{\mathbf{k}_1} n_{\mathbf{k}_2} - n_{\mathbf{k}} n_{\mathbf{k}_1} \operatorname{sign}(\omega_{\mathbf{k}}\omega_{\mathbf{k}_2}) - n_{\mathbf{k}} n_{\mathbf{k}_2} \operatorname{sign}(\omega_{\mathbf{k}}\omega_{\mathbf{k}_1})]\; d\mathbf{k}_1 d\mathbf{k}_2. \tag{6.12}$$

The $n_{\mathbf{k}}$ dependence in the collision integral can be simplified by assuming that there are less small scale waves than large-scale zonal waves, i.e. $n_{\mathbf{k}} \ll n_{\mathbf{k}_1}$ and that $k \gg k_1$. As $\mathbf{k}_2 = \mathbf{k} - \mathbf{k}_1$, $\mathbf{k}_2$ can be integrated out. $n_{\mathbf{k}} n_{\mathbf{k}-\mathbf{k}_1}$ can be neglected since it is $\mathrm{O}(n_k^2)$ and thus small compared to the large spectrum at scales $\mathbf{k}_1$ and $\operatorname{sign}(\omega_{\mathbf{k}}\omega_{\mathbf{k}-\mathbf{k}_1}) = 1$ as $\mathbf{k}_1 \to 0$. The term in the square brackets of Eq. 6.12 then reduces to

$$(n_{\mathbf{k}-\mathbf{k}_1} - n_{\mathbf{k}}) n_{\mathbf{k}_1}\,.$$

Defining

$$F(\mathbf{k}, \mathbf{k}_1) = 4\pi \left|V_{\mathbf{k}_1\,\mathbf{k}-\mathbf{k}_1}^k\right|^2 \delta(\Omega_{\mathbf{k}} - \Omega_{\mathbf{k}_1} - \Omega_{\mathbf{k}-\mathbf{k}_1})(n_{\mathbf{k}-\mathbf{k}_1} - n_{\mathbf{k}}) n_{\mathbf{k}_1}\,, \tag{6.13}$$

Eq. 6.12 can be approximated as

$$\frac{\partial n_{\mathbf{k}}}{\partial t} = \int_{\mathbf{k}_1 < \mathbf{k}} F(\mathbf{k}, \mathbf{k}_1)\, d\mathbf{k}_1\,. \tag{6.14}$$

Using the symmetries of $V_{\mathbf{k}_1\,\mathbf{k}-\mathbf{k}_1}^k$ and $\Omega_{\mathbf{k}}$, it can be shown that

$$F(\mathbf{k}, \mathbf{k}_1) = -F(\mathbf{k} - \mathbf{k}_1, -\mathbf{k}_1) \tag{6.15}$$

so that Eq. 6.14 can now be written as

$$\begin{aligned}\frac{\partial n_{\mathbf{k}}}{\partial t} &= \frac{1}{2}\int_{\mathbf{k}_1<\mathbf{k}} F(\mathbf{k},\mathbf{k}_1)\,d\mathbf{k}_1 - \int_{\mathbf{k}_1<\mathbf{k}} F(\mathbf{k}-\mathbf{k}_1,-\mathbf{k}_1)\,d\mathbf{k}_1 \\ &= -\frac{1}{2}\int_{\mathbf{k}_1<\mathbf{k}} F(\mathbf{k},\mathbf{k}_1)\,d\mathbf{k}_1 - F(\mathbf{k}+\mathbf{k}_1,\mathbf{k}_1)\,d\mathbf{k}_1\,. \end{aligned} \tag{6.16}$$

Taylor expanding $F(\mathbf{k}+\mathbf{k}_1,\mathbf{k}_1)$ with respect to $\mathbf{k}_1$,

$$F(\mathbf{k}+\mathbf{k}_1,\mathbf{k}_1) = F(\mathbf{k},\mathbf{k}_1) + \mathbf{k}_1\cdot\nabla_{\mathbf{k}}F(\mathbf{k},\mathbf{k}_1) + \mathrm{O}(k_1^2)\,, \tag{6.17}$$

substituting back in to Eq. 6.16 while neglecting second-order terms gives

$$\frac{\partial n_{\mathbf{k}}}{\partial t} = -\frac{1}{2}\int_{\mathbf{k}_1<\mathbf{k}} \mathbf{k}_1\cdot\nabla_{\mathbf{k}}F(\mathbf{k},\mathbf{k}_1)\,. \tag{6.18}$$

Now Taylor expand $F(\mathbf{k},\mathbf{k}_1)$ with respect to $\mathbf{k}_1$ which is amounts to expanding the $n_{\mathbf{k}-\mathbf{k}_1}$ term. This requires that the argument of the δ-function be Taylor expanded first, noting that $\Omega_{\mathbf{k}_1}\propto k_1^2 k_{1_x}$ as $\mathbf{k}_1\to 0$ and can therefore be neglected,

$$\begin{aligned}\delta(\Omega_{\mathbf{k}}-\Omega_{\mathbf{k}-\mathbf{k}_1}) &= \delta(\Omega_{\mathbf{k}} - (\Omega_{\mathbf{k}} - \mathbf{k}_1\cdot\nabla_{\mathbf{k}}\Omega_{\mathbf{k}} + \mathrm{O}(k_1^2)) \\ &\approx \delta(\mathbf{k}_1\cdot\nabla_{\mathbf{k}}\Omega_{\mathbf{k}}). \end{aligned} \tag{6.19}$$

Performing a similar expansion for the $n_{\mathbf{k}-\mathbf{k}_1}$ term gives

$$F(\mathbf{k},\mathbf{k}_1) \approx 4\pi\left|V^k_{\mathbf{k}_1\,\mathbf{k}-\mathbf{k}_1}\right|^2\delta(\mathbf{k}_1\cdot\nabla_{\mathbf{k}}\Omega_{\mathbf{k}})\mathbf{k}_1\cdot\nabla_{\mathbf{k}}n_{\mathbf{k}}\,, \tag{6.20}$$

and substituting Eq. 6.20 back into Eq. 6.18, the kinetic equation for the small scales can then be written as an anisotropic diffusion equation in $\mathbf{k}$-space:

$$\frac{\partial n_{\mathbf{k}}}{\partial t} = \frac{\partial}{\partial k_i}D_{ij}(k_x,k_y)\frac{\partial n_{\mathbf{k}}}{\partial k_j} \tag{6.21}$$

with the diffusion tensor given by

$$D_{ij}(k_x,k_y) = 2\pi\int_{\mathbf{k}_1<\mathbf{k}}\left|V^k_{\mathbf{k}_1\,\mathbf{k}-\mathbf{k}_1}\right|^2\delta(\mathbf{k}_1\cdot\nabla_{\mathbf{k}}\Omega_{\mathbf{k}}), k_{1_i}k_{1_j}n_{\mathbf{k}_1}d\mathbf{k}_1\,. \tag{6.22}$$

Assume that the scales $k_1 \ll k$, then the integral limits can be extended to infinity in Eq. 6.22 and integration performed with respect k_{1_x}

$$\begin{aligned}D_{ij}(k_x,k_y) &= 2\pi\int_{-\infty}^{\infty}\left|V^k_{\mathbf{k}_1\,\mathbf{k}-\mathbf{k}_1}\right|^2\delta\left(k_{1_x}\frac{\partial\Omega_{\mathbf{k}}}{\partial k_x}+k_{1_y}\frac{\partial\Omega_{\mathbf{k}}}{\partial k_y}\right)k_{1_i}k_{1_j}n_{\mathbf{k}_1}d\mathbf{k}_1 \\ &= 2\pi\int_{-\infty}^{\infty}\left|V^k_{\mathbf{k}_1\,\mathbf{k}-\mathbf{k}_1}\right|^2\left|\frac{\partial\Omega_{\mathbf{k}}}{\partial k_x}\right|^{-1}\delta\left(k_{1_x}+k_{1_y}\frac{\frac{\partial\Omega_{\mathbf{k}}}{\partial k_y}}{\frac{\partial\Omega_{\mathbf{k}}}{\partial k_x}}\right)k_{1_i}k_{1_j}n_{\mathbf{k}_1}d\mathbf{k}_1\end{aligned}$$

Introducing the parameter $\sigma_{\mathbf{k}}$ for brevity, defined as

$$\sigma_{\mathbf{k}} = \frac{\frac{\partial \Omega_{\mathbf{k}}}{\partial k_y}}{\frac{\partial \Omega_{\mathbf{k}}}{\partial k_x}} \tag{6.23}$$

and from the δ-function, if $k_{1_x} = -\sigma_{\mathbf{k}} k_{1_y}$ then, k_{1_x} can be integrated out to give

$$\begin{aligned} D_{ij}(k_x, k_y) &= 2\pi \left| \frac{\partial \Omega_{\mathbf{k}}}{\partial k_x} \right|^{-1} \int_{-\infty}^{\infty} n_{\mathbf{k}_1} d\mathbf{k}_1 \left[\left| V^k_{\mathbf{k}_1\, \mathbf{k}-\mathbf{k}_1} \right|^2 \begin{pmatrix} k_{1_x}^2 & k_{1_x} k_{1_y} \\ k_{1_x} k_{1_y} & k_{1_y}^2 \end{pmatrix} \right] \\ &= 2\pi \left| \frac{\partial \Omega_{\mathbf{k}}}{\partial k_x} \right|^{-1} \int_{-\infty}^{\infty} n_{\mathbf{k}_1} dk_{1_y} \left[\left| V^k_{\mathbf{k}_1\, \mathbf{k}-\mathbf{k}_1} \right|^2 \begin{pmatrix} \sigma_{\mathbf{k}}^2 & -\sigma_{\mathbf{k}} \\ -\sigma_{\mathbf{k}} & 1 \end{pmatrix} k_{1_y}^2 \right]_{k_{1_x} = -\sigma_{\mathbf{k}} k_{1_y}} \end{aligned} \tag{6.24}$$

Since the determinant of the matrix in Eq. 6.24 is zero, the matrix is singular. The eigenvalues are 0 and $1 + \sigma_{\mathbf{k}}^2$ with corresponding eigenvectors $(\frac{1}{\sigma_{\mathbf{k}}}, 1)$ and $(-\sigma_{\mathbf{k}}, 1)$, which suggests that diffusion would only occur in the direction which corresponds to the positive eigenvalue, i.e. in the $(-\sigma_{\mathbf{k}}, 1)$ direction. A change of variables is now sought which would permit this 1D diffusion. Defining the matrix in Eq. 6.24 as

$$\Lambda(k_x, k_y) = \begin{pmatrix} \sigma_{\mathbf{k}}^2 & -\sigma_{\mathbf{k}} \\ -\sigma_{\mathbf{k}} & 1 \end{pmatrix}, \tag{6.25}$$

the general form of Eq. 6.21 is then

$$\left(\frac{\partial}{\partial k_x}, \frac{\partial}{\partial k_y} \right) \Lambda(k_x, k_y) \begin{pmatrix} \frac{\partial}{\partial k_x} \\ \frac{\partial}{\partial k_y} \end{pmatrix} n(k_x, k_y)\,. \tag{6.26}$$

Under a change of variables

$$\begin{aligned} k_x &\mapsto q_1(k_x, k_y) \\ k_y &\mapsto q_2(k_x, k_y)\,, \end{aligned} \tag{6.27}$$

taking into account the derivatives, inverse function and transpose vector, this becomes

$$J \left(\frac{\partial}{\partial q_1}, \frac{\partial}{\partial q_2} \right) |\det J|^{-1} \Lambda(q_1, q_2) J^T \begin{pmatrix} \frac{\partial}{\partial q_1} \\ \frac{\partial}{\partial q_y} \end{pmatrix} |\det J|\, n(q_1, q_2)\,, \tag{6.28}$$

where J is the Jacobian matrix for the change of variables,

$$J = \begin{pmatrix} \frac{\partial q_1}{\partial k_x} & \frac{\partial q_1}{\partial k_y} \\ \frac{\partial q_2}{\partial k_x} & \frac{\partial q_2}{\partial k_y} \end{pmatrix}. \tag{6.29}$$

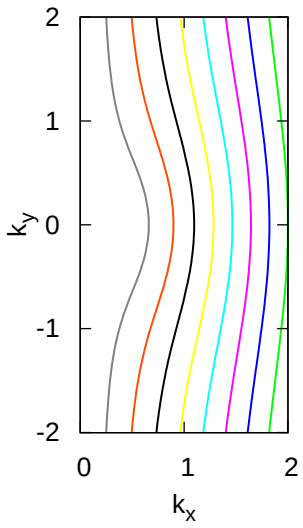

Figure 6.1: The level sets of $\Omega_{\mathbf{k}}$

Ideally, the matrix $J\Lambda J^T$ would be diagonal in order to simplify expression 6.28. However, because Λ is singular, $J\Lambda J^T$ can be further reduced to a 1D diffusion equation. The new variables can be found by denoting

$$J = \begin{pmatrix} a & b \\ c & d \end{pmatrix}$$

so that

$$J\Lambda J^T = \begin{pmatrix} (b - a\sigma_{\mathbf{k}})^2 & (b - a\sigma_{\mathbf{k}})(d - c\sigma_{\mathbf{k}}) \\ (b - a\sigma_{\mathbf{k}})(d - c\sigma_{\mathbf{k}}) & (d - c\sigma_{\mathbf{k}})^2 \end{pmatrix} = \begin{pmatrix} 1 & 0 \\ 0 & 0 \end{pmatrix}.$$

This is true if $b - a\sigma_{\mathbf{k}} = 1$ and $d - c\sigma_{\mathbf{k}} = 0$. The new coordinates then must satisfy the equations

$$\begin{aligned} \frac{\partial q_1}{\partial k_y} - \sigma_{\mathbf{k}} \frac{\partial q_1}{\partial k_x} &= 1 \\ \frac{\partial q_2}{\partial k_y} - \sigma_{\mathbf{k}} \frac{\partial q_2}{\partial k_x} &= 0\,. \end{aligned}$$

By close inspection, these equations are solved for

$$\begin{aligned} q_1(k_x, k_y) &= k_y \\ q_2(k_x, k_y) &= \Omega(k_x, k_y) \end{aligned} \tag{6.30}$$

the Jacobian matrix is

$$J = \begin{pmatrix} 0 & 1 \\ \frac{\partial \Omega_{\mathbf{k}}}{\partial k_x} & \frac{\partial \Omega_{\mathbf{k}}}{\partial k_y} \end{pmatrix} .$$

and the diffusion Eq. 6.21 becomes

$$\frac{\partial n_{\mathbf{k}}}{\partial t} = \frac{\partial \Omega_{\mathbf{k}}}{\partial k_x} \left(\frac{\partial}{\partial k_y} \widetilde{D} \left(\frac{\partial n_{\mathbf{k}}}{\partial k_y} \right)_{\Omega} \right)_{\Omega} \tag{6.31}$$

where $()_\Omega$ means Ω being held constant and the diffusion coefficient is

$$\widetilde{D}_{\mathbf{k}} = 2\pi \left| \frac{\partial \Omega_{\mathbf{k}}}{\partial k_x} \right|^{-2} \int_{-\infty}^{\infty} \left[\left| V^k_{\mathbf{k}_1 \, \mathbf{k}-\mathbf{k}_1} \right|^2 k_{1_y}^2 \right]_{k_{1_x} = -\sigma_{\mathbf{k}} k_{1_y}} n_{\mathbf{k}_1} dk_{1_y} \, . \tag{6.32}$$

Eq. 6.31 therefore describes diffusion in the k_y direction along the curves of constant $\Omega(k_x, k_y)$ which are shown in figure 6.1.

6.2.2 Nonlocal interaction with small scale zonal flows

The other scales of interest for nonlocal interactions are those in the vicinity of $\mathbf{k}_1 \to (0, 2k_y)$. A similar calculation to the previous section will be carried out, assuming that the dominant interaction is now between the small scale Rossby/drift waves $\mathbf{k}$ with the small scale zonal flows $\mathbf{k}_1 \equiv \mathbf{q}$ in this region. The kinetic equation, Eq. 3.85 is now given by

$$\begin{aligned} \frac{\partial n_{\mathbf{k}}}{\partial t} &= \int_{|q_x|<k_x} F(\mathbf{k}, \mathbf{q}) \, d\mathbf{q} \\ &= -\int_{|q_x|<k_x} F(\mathbf{k}-\mathbf{q}, -\mathbf{q}) \, d\mathbf{q} \\ &\approx -\int_{|q_x|<k_x} \left[F(\mathbf{k}-\mathbf{q}_*, -\mathbf{q}) - (\mathbf{q}-\mathbf{q}_*) \cdot \left(\nabla_{\mathbf{q}} F(\mathbf{k}-\mathbf{q}_*, -\mathbf{q}) \right) |_{\mathbf{q}=\mathbf{q}_*} \right] d\mathbf{q} \, . \end{aligned} \tag{6.33}$$

In the last step, the first argument of $F(\mathbf{k}-\mathbf{q}_*, -\mathbf{q})$ is Taylor expanded, retaining first-order terms in $\mathbf{q}$ only. For brevity of notation, let

$$\tilde{\mathbf{k}} = \mathbf{k} - \mathbf{q}_* = (k_x, -k_y) \tag{6.34}$$

and recalling that

$$F(\tilde{\mathbf{k}}, -\mathbf{q}) = 4\pi \left| V^{\tilde{\mathbf{k}}}_{-\mathbf{q}, \tilde{\mathbf{k}}+\mathbf{q}} \right|^2 \delta(\Omega_{\tilde{\mathbf{k}}} - \Omega_{-\mathbf{q}} - \Omega_{\tilde{\mathbf{k}}+\mathbf{q}}) (n_{\tilde{\mathbf{k}}+\mathbf{q}} - n_{\tilde{\mathbf{k}}}) n_{-\mathbf{q}} \, , \tag{6.35}$$

then only the δ-function and the n-terms within the parentheses need to be expanded in the Taylor expansion of $F(\tilde{\mathbf{k}}, -\mathbf{q})$, since $V^{-\mathbf{q}}_{\tilde{\mathbf{k}}-\mathbf{q},\mathbf{k}}$ and $n_{-\mathbf{q}}$ vary rapidly near $\mathbf{q} = \mathbf{q}_*$. Taylor expanding the argument of the δ-function at $\mathbf{q} = \mathbf{q}_*$ gives,

$$\begin{aligned}\Omega_{\tilde{\mathbf{k}}} - \Omega_{-\mathbf{q}} - \Omega_{\tilde{\mathbf{k}}+\mathbf{q}} = \quad & \Omega_{\tilde{\mathbf{k}}} - \Omega_{-\mathbf{q}_*} + (\mathbf{q}-\mathbf{q}_*)\cdot\nabla\Omega(-\mathbf{q}) \\ & -\Omega_{\mathbf{k}} + (\mathbf{q}-\mathbf{q}_*)\cdot\nabla\Omega(\tilde{\mathbf{k}}+\mathbf{q})\,. \end{aligned} \tag{6.36}$$

When calculated explicitly, $\Omega_{\tilde{\mathbf{k}}} - \Omega_{\mathbf{k}} = 0$ and $\Omega_{-\mathbf{q}_*} = 0$ leaving,

$$\begin{aligned} & q_x\left[\frac{\partial\Omega}{\partial q_x}(-q_x,-q_y) + \frac{\partial\Omega}{\partial q_x}(k_x+q_x,-k_y+q_y)\right]_{(q_x,q_y)=(0,2k_y)} \\ +(q_y-2k_y)&\left[\frac{\partial\Omega}{\partial q_y}(-q_x,-q_y) + \frac{\partial\Omega}{\partial q_y}(k_x+q_x,-k_y+q_y)\right]_{(q_x,q_y)=(0,2k_y)}\,. \end{aligned} \tag{6.37}$$

Now calculating each of the four derivatives explicitly

$$q_x\left[-\frac{4\beta k_y}{F(4k_y^2+F)} + \frac{\beta(k^4+F(3k_x^2-k_y^2))}{F(k^2+F)^2})\right] + (q_y-2k_y)\left[0+\frac{2\beta k_x k_y}{(k^2+F)^2}\right]\,.$$

The last term $\frac{2\beta k_x k_y}{(k^2+F)^2} \equiv \frac{\partial\Omega_{\mathbf{k}}}{\partial k_y}$ so the δ-function is reduced to

$$\delta\left(\frac{\partial\Omega_{\mathbf{k}}}{\partial k_y}\left(q_y - 2k_y + \xi_{\mathbf{k}} q_x\right)\right) = \left|\frac{\partial\Omega_{\mathbf{k}}}{\partial k_y}\right|^{-1}\delta\left(q_y - 2k_y + \xi_{\mathbf{k}} q_x\right)\,, \tag{6.38}$$

where

$$\xi_{\mathbf{k}} = \frac{3F(k_x^2-k_y^2) + k_x^4 - 3k_y^4 + 6k_x^2k_y^2}{2k_xk_y(4k_y^2+F)}\,. \tag{6.39}$$

Expanding $n_{\tilde{\mathbf{k}}+\mathbf{q}} - n_{\tilde{\mathbf{k}}}$ from Eq. 6.35 gives,

$$\begin{aligned} n_{\tilde{\mathbf{k}}+\mathbf{q}} - n_{\tilde{\mathbf{k}}} &= n_{\tilde{\mathbf{k}}+\mathbf{q}_*} - n_{\tilde{\mathbf{k}}} + (\mathbf{q}-\mathbf{q}_*)\cdot\nabla_{\mathbf{q}} n(\tilde{\mathbf{k}}+\mathbf{q}_*)|_{\mathbf{q}=\mathbf{q}_*} + \mathrm{O}(|\mathbf{q}-\mathbf{q}_*|^2) \\ &\approx n_{\mathbf{k}} - n_{\tilde{\mathbf{k}}} + q_x\frac{\partial n_{\mathbf{k}}}{\partial q_x} + (q_y-2k_y)\frac{\partial n_{\mathbf{k}}}{\partial q_y}\,. \end{aligned} \tag{6.40}$$

The leading order term of Eq. 6.40 contributes to the leading order term of the kinetic equation for the nonlocal interaction of small scale Rossby/drift turbulence with small scale zonal flows. The integration limits can again be extended to infinity if it is assumed that $|k_x| \ll k$ and combining Eqs 6.33, 6.38 and 6.40, the kinetic equation for this nonlocal interaction is given by

$$\frac{\partial n_{\mathbf{k}}}{\partial t} = Y_{\mathbf{k}}[n(k_x,-k_y) - n(k_x,k_y)] \tag{6.41}$$

where

$$\begin{aligned} Y_{\mathbf{k}} &= 4\pi \left|\frac{\partial \Omega_{\mathbf{k}}}{\partial k_y}\right|^{-1} \int_{-\infty}^{\infty} dq_x dq_y \left|V^{\tilde{\mathbf{k}}}_{-\mathbf{q},\tilde{\mathbf{k}}+\mathbf{q}}\right|^2 \delta\left(q_y - 2k_y + \xi_{\mathbf{k}} q_x\right) n(q_x, q_y) \\ &= 4\pi \left|\frac{\partial \Omega_{\mathbf{k}}}{\partial k_y}\right|^{-1} \int_{-\infty}^{\infty} dq_x dq_y \left|-V^{k}_{\mathbf{q},\mathbf{k}-\mathbf{q}}\right|^2 \delta\left(q_y - 2k_y - \xi_{\mathbf{k}} q_x\right) n(-q_x, q_y) \\ &= 4\pi \left|\frac{\partial \Omega_{\mathbf{k}}}{\partial k_y}\right|^{-1} \int_{-\infty}^{\infty} \left[\left|V^{k}_{\mathbf{q},\mathbf{k}-\mathbf{q}}\right|^2 n_{\mathbf{q}}\right]_{q_y=2k_y} dq_x \,. \end{aligned} \tag{6.42}$$

Assuming that the spectrum is symmetric about the k_y axis, the integration variable has been re-labeled $q_x \to -q_x$ in Eq. 6.42 and the δ-function has been used to integrate out q_y to leading order. However, Eq. 6.41 actually suggests a relaxation of the spectrum to a symmetric equilibrium $n(k_x, -k_y) - n(k_x, k_y)$.

In order to show some redistribution of the spectral energy density in this particular nonlocal interaction, it is therefore necessary, to consider the contribution from the next-order terms from Eq. 6.33,

$$\frac{\partial n_{\mathbf{k}}}{\partial t} = \int_{|q_x|<k_x} \left[(\mathbf{q} - \mathbf{q}_*) \cdot \left(\nabla_{\mathbf{q}} F(\mathbf{k} - \mathbf{q}_*, -\mathbf{q})\right)|_{\mathbf{q}=\mathbf{q}_*}\right] d\mathbf{q} \,. \tag{6.43}$$

which effectively means retaining the next order terms from Eq. 6.40. Following the same procedure as in Section 6.2.1, this second order contribution can again be presented as an anisotropic diffusion equation in $\mathbf{k}$-space

$$\frac{\partial n_{\mathbf{k}}}{\partial t} = \frac{\partial}{\partial k_i} B_{ij}(\mathbf{k}) \frac{\partial n_{\mathbf{k}}}{\partial k_j} \tag{6.44}$$

with the diffusion tensor $B(\mathbf{k})$ given by,

$$B(\mathbf{k}) = 4\pi \left|\frac{\partial \Omega_{\mathbf{k}}}{\partial k_y}\right|^{-1} \int_{-\infty}^{\infty} dq_x dq_y \quad \left|V^{\tilde{\mathbf{k}}}_{-\mathbf{q},\tilde{\mathbf{k}}+\mathbf{q}}\right|^2 \delta\left(q_y - 2k_y + \xi_{\mathbf{k}} q_x\right) n(q_x, q_y) \times \begin{pmatrix} q_x^2 & q_x(q_y - 2k_y \\ q_x(q_y - 2k_y) & (q_y - 2k_y)^2 \end{pmatrix} . \tag{6.45}$$

Again using the symmetries of the interaction coefficient, $V^{\tilde{\mathbf{k}}}_{-\mathbf{q},\tilde{\mathbf{k}}+\mathbf{q}}$, changing the integration variable to $-q_x$ and using the δ function to leading order to integrate out k_y, this can be simplified to

$$B(\mathbf{k}) = 4\pi \left|\frac{\partial \Omega_{\mathbf{k}}}{\partial k_y}\right|^{-1} \int_{-\infty}^{\infty} dq_x \left[\left|V^{k}_{\mathbf{q},\mathbf{k}-\mathbf{q}}\right|^2 n(-q_x, q_y)\, q_x^2\right]_{q_y=2k_y} \begin{pmatrix} 1 & -\xi_{\mathbf{k}} \\ -\xi_{\mathbf{k}} & \xi_{\mathbf{k}}^2 \end{pmatrix} . \tag{6.46}$$

Since the diffusion tensor is again singular, Eq. 6.44 can be reduced to a 1D diffusion equation by an appropriate change of variables. Introducing the variables

$$\begin{aligned} k_x &\mapsto s_1(k_x, k_y) \\ k_y &\mapsto s_2(k_x, k_y)\,, \end{aligned} \tag{6.47}$$

taking into account the derivatives, inverse function and transpose vector, when transformed, the general form of Eq. 6.44 is given by

$$J\left(\frac{\partial}{\partial s_1}, \frac{\partial}{\partial s_2}\right) |\det J|^{-1} \begin{pmatrix} 1 & -\xi_{\mathbf{k}} \\ -\xi_{\mathbf{k}} & \xi_{\mathbf{k}}^2 \end{pmatrix} (s_1, s_2) J^T \begin{pmatrix} \frac{\partial}{\partial s_1} \\ \frac{\partial}{\partial s_y} \end{pmatrix} |\det J|\, n(s_1, s_2)\,, \tag{6.48}$$

where J, the Jacobian matrix for the change of variables is

$$J = \begin{pmatrix} \frac{\partial s_1}{\partial k_x} & \frac{\partial s_1}{\partial k_y} \\ \frac{\partial s_2}{\partial k_x} & \frac{\partial s_2}{\partial k_y} \end{pmatrix} = \begin{pmatrix} a & b \\ c & d \end{pmatrix}. \tag{6.49}$$

The matrix in expression 6.48 can be reduced to a 1D diffusion equation if

$$J \begin{pmatrix} 1 & -\xi_{\mathbf{k}} \\ -\xi_{\mathbf{k}} & \xi_{\mathbf{k}}^2 \end{pmatrix} J^T = \begin{pmatrix} (a - b\xi_{\mathbf{k}})^2 & (a - b\xi_{\mathbf{k}})(c - d\xi_{\mathbf{k}}) \\ (a - b\xi_{\mathbf{k}})(c - d\xi_{\mathbf{k}}) & (c - d\xi_{\mathbf{k}})^2 \end{pmatrix} = \begin{pmatrix} 1 & 0 \\ 0 & 0 \end{pmatrix}.$$

This is true if $a - b\xi_{\mathbf{k}} = 1$ and $c - d\xi_{\mathbf{k}} = 0$. The new coordinates then must satisfy the equations

$$\begin{aligned} \frac{\partial s_1}{\partial k_x} - \xi_{\mathbf{k}} \frac{\partial s_1}{\partial k_y} &= 1 \\ \frac{\partial s_2}{\partial k_x} - \xi_{\mathbf{k}} \frac{\partial s_2}{\partial k_y} &= 0\,, \end{aligned}$$

and have been calculated [11] to be

$$\begin{aligned} s_1(k_x, k_y) &= k_x \\ s_2(k_x, k_y) \equiv \widetilde{Z}_{\mathbf{k}} &= \arctan\left(\frac{(k_y + \sqrt{3}\,k_x)\sqrt{F}}{k^2}\right) - \arctan\left(\frac{(k_y - \sqrt{3}\,k_x)\sqrt{F}}{k^2}\right) \\ &\quad -\frac{2\sqrt{3\,F}k_x}{k^2 + F}\,, \end{aligned} \tag{6.50}$$

which is an equivalent expression to that of zonostrophy density defined in Eq. 5.12. The

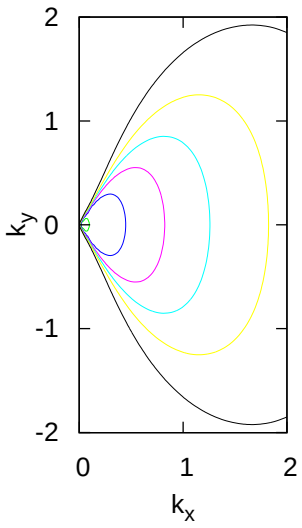

Figure 6.2: The level sets of $\widetilde{Z}_{\mathbf{k}}$

diffusion equation, Eq. 6.44 is now reduced to

$$\frac{\partial n_{\mathbf{k}}}{\partial t} = \frac{\partial \widetilde{Z}_{\mathbf{k}}}{\partial k_y} \frac{\partial}{\partial k_x} \left| \frac{\partial \widetilde{Z}_{\mathbf{k}}}{\partial k_y} \right|^{-1} \widetilde{B}_{\mathbf{k}} \frac{\partial n_{\mathbf{k}}}{\partial k_x} \tag{6.51}$$

where

$$\widetilde{B}(\mathbf{k}) = 4\pi \left| \frac{\partial \Omega_{\mathbf{k}}}{\partial k_y} \right|^{-1} \int_{-\infty}^{\infty} dq_x \left[\left| V^k_{\mathbf{q},\mathbf{k}-\mathbf{q}} \right|^2 n(-q_x, q_y)\, q_x^2 \right]_{q_y = 2k_y} . \tag{6.52}$$

Eqs 6.51 and 6.52 describe diffusion in the k_x direction along curves of constant $\widetilde{Z}_{\mathbf{k}}$ which are shown in figure 6.2.

6.2.3 Turbulence suppression loop

The mathematically predicted evolution of the turbulence spectrum, Eq. 6.31 provides some insight into the features of the nonlocal turbulence. The energy of the small scale waves with dispersion $\omega_{\mathbf{k}}$ is defined as,

$$E = \int |\omega_{\mathbf{k}}| n_{\mathbf{k}} d\mathbf{k} \,. \tag{6.53}$$

As the spectrum of these small scales diffuses along the curves of constant $\Omega_{\mathbf{k}}$, it loses energy since $\omega_{\mathbf{k}}$ decreases along these curves. However for an unforced, dissipationless turbulence, the total energy of the system must be conserved, therefore this energy

from the small scales has to go somewhere and must therefore be transferred to larger scales. Neither is there dissipation at these large scales so the energy spectrum will accumulate there. Furthermore, since the diffusion coefficient $\widetilde{D}_{\mathbf{k}}$ given by Eq. 6.32 is directly proportional to k_y, the rate of transfer of energy from the small wavepackets to the large scales is also increased.

For a forced and dissipative turbulence regime, the evolution of the spectrum will be determined by the forcing and dissipation terms, collectively denoted as $\Gamma_{\mathbf{k}}$, added to the RHS of Eq. 6.31 i.e.

$$\frac{\partial n_{\mathbf{k}}}{\partial t} = \frac{\partial \Omega_{\mathbf{k}}}{\partial k_x}\left(\frac{\partial}{\partial k_y}\widetilde{D}\left(\frac{\partial n_{\mathbf{k}}}{\partial k_y}\right)_{\Omega}\right)_{\Omega} + \Gamma_{\mathbf{k}} n_{\mathbf{k}}\,. \tag{6.54}$$

Recall from Eq. 6.32 that the diffusion coefficient, $\widetilde{D}$ depends on the spectrum of the zonal flow, $n_{\mathbf{k}_1}$. If this spectrum is given then $\widetilde{D}$ is a fixed function of k_y and Ω. The spectrum $n_{\mathbf{k}}$ evolves along the curves of constant Ω and it's magnitude is controlled by the maximum value of $\Gamma_{\mathbf{k}}$ on that curve, growing exponentially if $\Gamma_{\mathbf{k}} > 0$ and being damped exponentially if $\Gamma_{\mathbf{k}} < 0$ [9; 10]. Positive values of $\Gamma_{\mathbf{k}}$ occur near the maximum of the forcing while negative $\Gamma_{\mathbf{k}}$ occurs far away from this maximum where dissipation terms are dominant.

For positive $\Gamma_{\mathbf{k}}$, the spectrum $n_{\mathbf{k}}$ grows on the curve of constant $\Omega_{\mathbf{k}}$ but this growth cannot be sustained indefinitely as it has already been stated that diffusion of the spectrum along these curves results in energy transfer to large scales. Since this results in augmented diffusion to the dissipation region, the growth of the spectrum due to positive $\Gamma_{\mathbf{k}}$ is gradually relaxed until a balance is achieved between the growth and the diffusion. Consequently, the large scale zonal flow saturates at a level which can be estimated by balancing the forcing and diffusion terms of Eq. 6.54, which gives

$$n_{\mathbf{p}} \sim \frac{\beta\,\Gamma_{max}}{p^3 |V^k_{1\,2}|^2} \tag{6.55}$$

where for large scales $p_x \sim p_y \sim p$. Again, using the fact that $n_{\mathbf{p}} = \frac{E_{\mathbf{p}}}{\omega_{\mathbf{p}}}$ whereby in the large-scale limit,

$$E_{\mathbf{p}} \approx \frac{F}{p^2}\psi^2 \tag{6.56}$$

and $U_{ZF} = \frac{\partial \psi}{\partial y} \sim p\psi$, another expression can be obtained for $n_{\mathbf{p}}$

$$n_{\mathbf{p}} \sim \frac{F^2 U_{ZF}^2}{p^5 \beta}\,. \tag{6.57}$$

Equating Eqs 6.55 and 6.57 and deducing from Eq. 3.68 that $|V_{12}^k|^2 \sim \frac{\beta p^3}{F}$, then the large scale zonal flow is estimated to saturate at the velocity

$$U_{ZF} \sim \sqrt{\beta\, \Gamma_{max} L}\,, \tag{6.58}$$

where $L \sim \frac{2\pi}{p}$.

This estimate, Eq. 6.58 is valid for weak turbulence only, $U_{ZF} \sim \beta$, since it's derivation stems from the kinetic equation. For strong turbulence, the β term is negligible and Eq. 6.58 is invalid. An alternative zonal flow saturation velocity for the strong turbulence regime will be determined in the next section.

6.3 WKB approach to zonal flow growth

The foregoing rigorous mathematical theory is based on the wave kinetic equation and is therefore valid only in the weak wave turbulence regime which requires that the quasi-zonal scale turbulence be weak. However an alternative theory which is similar to Wentzel-Kramers-Brillouin (WKB) theory and which does not require a weak turbulence assumption, was introduced in [97], extended in [33] and is now presented. The presentation of both theories provides a unified picture of both strong and weak wave turbulence regimes.

Consider a drift-wave packet (DWP) propagating on the background zonal flow with a velocity profile $U(y)$ which varies randomly in y. The correlation length L corresponds to a typical wavelength profile in $U(y)$. Again nonlocal drift turbulence is assumed, so that interactions between the drift waves themselves are negligible in comparison to their interactions with the zonal flow.

By averaging the Fourier transformed CHM Eq. 3.61 over the characteristic times of the small scales the evolution equation for the slow large scales, i.e. the zonal flow is obtained. The evolution equation for the small scale drift and Rossby waves is obtained

by multiplying Eq. 3.61 by $\hat{\psi}_{\mathbf{k}}$ and averaging over the fast times of the small scales. The resulting spectrum evolution is given by [97]

$$\left(\frac{\partial}{\partial t}+\frac{\partial\bar{\omega}_{\mathbf{k}}}{\partial\mathbf{k}}\frac{\partial}{\partial\mathbf{x}}+\frac{\partial\bar{\omega}_{\mathbf{k}}}{\partial\mathbf{x}}\frac{\partial}{\partial\mathbf{k}}\right)n_{\mathbf{k}}=0 \tag{6.59}$$

where the term within the parentheses is a time derivative along the wave rays [98] defined as

$$D_t=\frac{\partial}{\partial t}+\frac{\partial\mathbf{x}}{\partial t}\cdot\nabla+\frac{\partial\mathbf{k}}{\partial t}\cdot\nabla_k \tag{6.60}$$

and $\bar{\omega}_{\mathbf{k}}$ is the total frequency of the drift wave packet due to its own linear dispersion plus that due to the motion of the large scale zonal flow [97]. It is defined as

$$\bar{\omega}_{\mathbf{k}}=\frac{k_x(Uk^2+\beta)}{k^2+F}\,. \tag{6.61}$$

It then follows from Eqs 6.59 and 6.60 that

$$\frac{\partial k_y}{\partial t}=-\frac{\partial\bar{\omega}}{\partial y}=\frac{k_x k^2 U'}{k^2+F} \tag{6.62}$$

where $' \equiv \frac{\partial}{\partial y}$ and

$$\frac{\partial y}{\partial t}=\frac{\partial\bar{\omega}}{\partial k_y}=\frac{2k_xk_y(F\,U-\beta)}{(k^2+F)^2}\,. \tag{6.63}$$

6.3.1 Weak zonal flow

Assuming that the zonal flow is sufficiently weak, i.e $U \ll \beta$, the DWP can travel through many correlation lengths in the y-direction. The DWP will experience a random walk in k_y so that the evolution of the mean waveaction $n_{\mathbf{k}}$ will be described by a diffusion equation,

$$n=\frac{\partial}{\partial k_y}\left(D_{rw}\frac{\partial n_k}{\partial k_y}\right)+\gamma_k n \tag{6.64}$$

where γ_k describes the instability in the unstable region where $\gamma_k > 0$ and $\gamma_k < 0$ in the dissipative region. The diffusion coefficient D_{rw} can be estimated from a standard random walk argument

$$D_{rw}=\left(\frac{1}{\partial_t k_y}\right)^2\tau \tag{6.65}$$

where τ is the correlation time estimated as

$$\tau_{rw}=\frac{L}{\partial_t k_y}\,. \tag{6.66}$$

Inserting Eq. 6.63 into Eq. 6.66 and then into Eq.6.65, the random walk diffusion coefficient is estimated to be

$$D_{rw} = \frac{k^4 U^2}{2(FU - \beta)} \tag{6.67}$$

where the estimates $k_x \sim k_y (\sim k\sqrt{2})$ and $U' \sim U/L$ have been used. Then the characteristic time of the diffusion process is

$$\tau_{dif} = \frac{k_y^2}{D} = \frac{F|U - \beta|L}{k^2 U^2}\,. \tag{6.68}$$

Assuming that the zonal flow is excited by drift wave turbulence via an inverse cascade until a saturated value is reached, the saturation value can be determined by balancing the diffusion and instability terms in Eq. (6.64) which gives

$$\frac{D}{k_y^2} = \gamma_{max}, \tag{6.69}$$

where γ_{max} is the maximum value of the growth rate of the underlying instability. Substituting Eq. 6.67 into Eq. 6.69, the estimated saturation velocity of the zonal flow is

$$U_{dif} = \frac{\sqrt{\beta \gamma_{max} L}}{k}. \tag{6.70}$$

This estimate coincides with Eq. (6.58) obtained in the previous section if $k \sim 1$.

6.3.2 Strong zonal flow

In the case of a strong zonal flow the β-effect is less important so that the DWP will travel through $\mathrm{O}(1)$ correlation lengths, getting carried from the unstable region to the dissipative region in a shorter time than it would take to cross one zonal flow oscillation of length L. The characteristic time for these rapid distortions follows from Eq. 6.62

$$\tau_{rd} \sim \frac{k_y}{\frac{\partial k_y}{\partial t}} \sim \frac{(k^2 + F)L}{k^2 U}. \tag{6.71}$$

This rapid distortion will occur when $\tau_{rd} < \tau_{dif}$ or equivalently

$$U_{rd} > \frac{\beta F}{k^2}\,. \tag{6.72}$$

It follows that the rapid distortion will replace the diffusive regime if Eq. 6.70 is greater than Eq. 6.72 giving the following condition for when rapid distortion is expected,

$$L\gamma_{max} > \frac{k^2 \beta}{(k^2 + F)^2}\,. \tag{6.73}$$

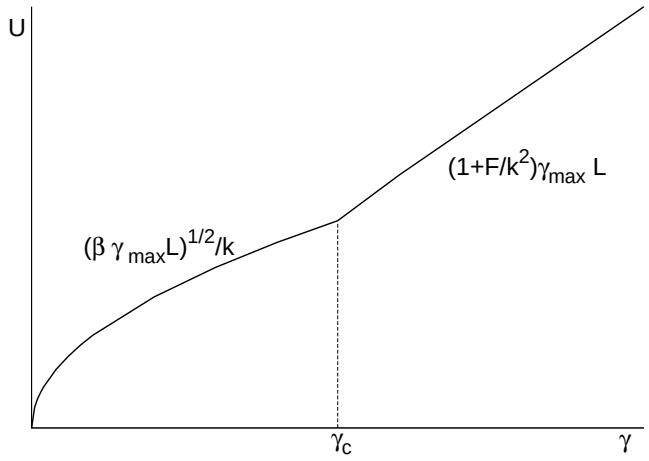

Figure 6.3: Zonal flow velocity U as a function of the instability growth rate γ

From Eq. 6.72, it can be said that when $k \lesssim \sqrt{F}$, rapid distortion occurs when $U \gtrsim \beta$ so the assumption of $U \ll \beta$ in obtaining the weak zonal flow saturation estimate is justified. Considering the specific limit when $U = \frac{\beta}{F}$, there will be stagnation points because according to Eq. 6.62, $\frac{\partial y}{\partial t} = 0$ at these points. Saturation of the rapid distortion zonal flow growth, U_{rd} can be estimated by assuming the inverse of its characteristic time, $\gamma_{max} \sim \frac{1}{\tau_{rd}}$ which gives

$$U_{rd} = \left(1 + \frac{F}{k^2}\right) L\gamma_{max} \tag{6.74}$$

From Eq. (6.73) it is clear that transition between the diffusive and rapid distortion regimes for zonal flow saturation occurs when the strength of the instability reaches $\gamma_c = \frac{k^2\beta}{(k^2+F)^2 L}$ at a zonal flow velocity $U = \frac{\beta F}{k^2}$ as shown in figure 6.3.

6.4 Instability forcing

This drift/Rossby wave turbulence hypothesis is now tested numerically. As previously mentioned, the CHM equation does not contain small scale instabilities so a linear forcing term must be added to the RHS of Eq. 3.35 in order to generate the waves. For the instability forcing $\gamma_{\mathbf{k}}$, the simplest form is sought which retains the key features of the

relevant primary instabilities mentioned above, namely that they act at small scales and primarily generate meridional waves. In various physical situations, the region of instability which leads to drift waves turns out to be approximately the same [10; 99; 100] and also coincides with the region determined by the linear instability analysis of the two-layer QG PV model. Forcing can be included in the CHM model therefore by simply adding a linear forcing term to the original equation. The forced CHM equation is now written as

$$(\partial_t - \mathcal{L})\,(\Delta\psi - F\psi) + \beta\partial_x\psi + (\partial_x\psi)\partial_y\Delta\psi - (\partial_y\psi)\partial_x\Delta\psi = 0, \tag{6.75}$$

where $\Gamma_{\mathbf{k}} = \gamma_{\mathbf{k}} - \nu_m k^{2m}$ with $\gamma_{\mathbf{k}}$ is the instability forcing term and ν_m a hyperviscosity coefficient. Dissipation $\nu_m(-\Delta)^m$ is a typical hyperviscosity for turbulence simulations with $m \in \mathbb{N}$. A dimensionless parameter is introduced

$$\chi = \frac{\gamma_{max}\sqrt{F}}{\beta} \tag{6.76}$$

which measures the nonlinearity of the system assuming that the instability saturates at a level determined by the amplitude of the nonlinear term in Eq. 6.75 and where $\gamma_{max} = \max(\gamma_{\mathbf{k}})$. Results are presented for an idealised forcing and a more physical instability forcing.

6.4.1 Idealised forcing

The instability forcing is required to act at small scales and to generate the meridional drift or Rossby waves. For simplicity, forcing at a single mode, $\mathbf{k}$ at the scale of the ion gyroradius or deformation radius was chosen with $\gamma_{\mathbf{k}} > 0$ and constant.

Eq. 6.75 has exact plane wave solutions

$$\psi = \exp^{(-i(\omega_{\mathbf{k}}t - \mathbf{k}\cdot\mathbf{x}) + \gamma_{\mathbf{k}}t - \nu_m k^{2m}t)} \tag{6.77}$$

with the dispersion relation $\omega_{\mathbf{k}}$ given by Eq. 3.62. In order to introduce mode coupling and allow the development of turbulence with a single-mode forcing, the numerical simulations are started from an initial condition consisting of spatial white noise of very low amplitude.

Results presented here are for $\gamma = 1.2$, $m = 8$, $\nu_m = 1.0 \times 10^{-29}$ and $F = 2500$ for various β. The k-space has been divided into the zonal sector for which $|k_x| < |k_y|$

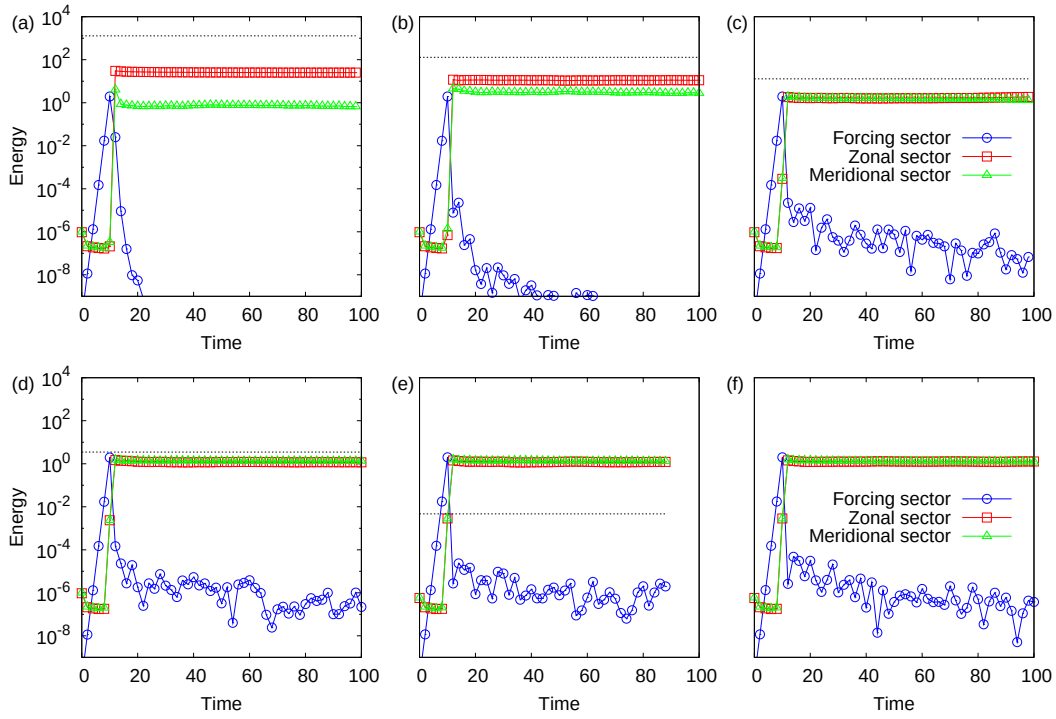

Figure 6.4: The evolution of the energy contained in the forcing mode, zonal and meridional sectors for (a) $\chi = 2.4 \times 10^{-7}$, (b) 2.4×10^{-6} and (c) 2.4×10^{-5}, (d) 2.4×10^{-4}, (e) 2.4×10^{-2} and (f) $\chi \to \infty$ respectively.

and a meridional sector for which the opposite is true, minus the forcing mode. Figure 6.4 shows the evolution of the energy contained in the forcing mode, zonal and meridional sectors. The energy of the forced mode grows exponentially while the initial energies of the zonal and meridional sectors remains constant at the level of the background noise. After $t = 10$, when the amplitude of the forcing mode reaches a high enough level to trigger nonlinear mode coupling, a sharp growth of the zonal and meridional energies takes place. A short time after however, the energies in the forcing mode and in the meridional sector are suddenly suppressed while that of the zonal energy remains at the highest level attained. A steady state is reached whereby the energy of the forcing mode is fully suppressed while that of the zonal energy subsequently saturates at the highest level. The horizontal dashed line is the saturation estimate of the zonal energy, based on Eq. 6.58. In this case, although it is of the correct order, the estimate is a little high

but it should be noted that it is an approximate estimate not taking into account some constant factors.

It is clear that as the level of nonlinearity is reduced, the greater the energy in the zonal sector and also the better the suppression of the small scale turbulence.

The corresponding 2D energy spectrum is shown in figure 6.5. In panel (a), the wave amplitude of the forcing mode at $(50, 0)$ has reached a high enough level to become modulationally unstable [63; 39; 5]. This triggers the nonlinear interactions, initially with modes which lie on the resonant (blue, dotted) curve which grow from the background noise. The maximally unstable perturbations to the LHS of the resonant curve have a significant zonal component and are equivalent to those in figure 4.6. The observed rapid decrease in the meridional energy corresponds to the zonal flow-induced diffusion along the (red, solid) curves of constant Ω which is evident in figure 6.5(b). While the diffusion is not *exactly* along the curves, the deviation could be attributed to the fact that the scale-separation between the forcing and zonal modes is not as pronounced as is assumed in the derivation of Eq. 6.31. Diffusion along the (green, dashed) curves of constant $\widetilde{Z}_{\mathbf{k}}$ shows evidence of interactions with small scale zonal flows and again highlights the importance of the zonostrophy invariant in drift and Rossby wave turbulence theory [11].

6.4.2 Baroclinic / ITG instability forcing

An expression for $\gamma_{\mathbf{k}}$ which is more physically relevant can be obtained by considering the linear dynamics of a higher level model which does contain an intrinsic instability. Such models are the two-layer model in GFD or in the case of plasmas the two-field Hasegawa-Wakatani (HW) model.

It is the baroclinic instability in the stratified atmosphere which generates Rossby waves. This instability is the main source of the large cyclones and anticyclones which constitute the transient midlatitude weather systems [21; 19] and numerical weather prediction experts are continually seeking to improve the parametrisation of these processes in their models. Analysis of a mean zonal baroclinic flow in its simplest configuration as a two-layer QG model [81] derives an expression for the baroclinic instability. Two layers of equal height and with a vertical, but no horizontal, shear between them is assumed.

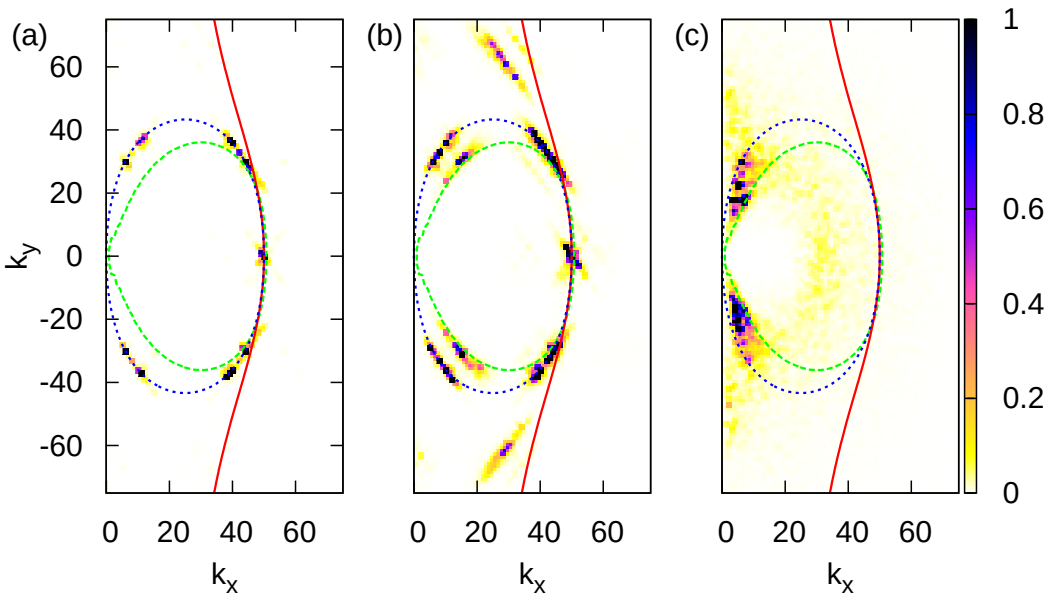

Figure 6.5: The 2D energy spectrum at times (a) 11.2, (b) 11.4 and (c) 20 for $\chi = 6 \times 10^{-4}$, normalised by the maximum energy 0.05, 0.05 and 0.2 respectively.

$U(y)$ is the constant mean flow. By analysing the baroclinic mode, an exponentially growing modal solution is found to exist due to the vertical shear, which represents the baroclinic instability. The growth rate of this unstable mode is defined as [21; 81]

$$\gamma_{\mathbf{k}} = U k_x \sqrt{\frac{F - k^2}{F + k^2}}. \tag{6.78}$$

A full derivation of this instability is given in Appendix D. The expression in Eq. 6.78 is used in the numerical simulations and is shown graphically in figure 6.6. Points to note are that the growth rate ($\gamma_{\mathbf{k}} > 0$) is in a region adjacent to the k_x axis and it reaches a maximum on this axis. The $\gamma_{\mathbf{k}} = 0$ contour line passes through $k = 0$ and $\gamma \to -\infty$ as $|k| \to \infty$.

Analogous to this is the ITG instability which is the most important instability for fusion turbulence. The centre of a magnetically confined plasma could reach a temperature of $10 - 20keV$ with colder edge temperatures of the order $1eV$. This large thermodynamic gradient in a tokamak plasma is a perfect source of free energy for instabilities. It arises in magnetically confined plasmas due to the particles in the hotter

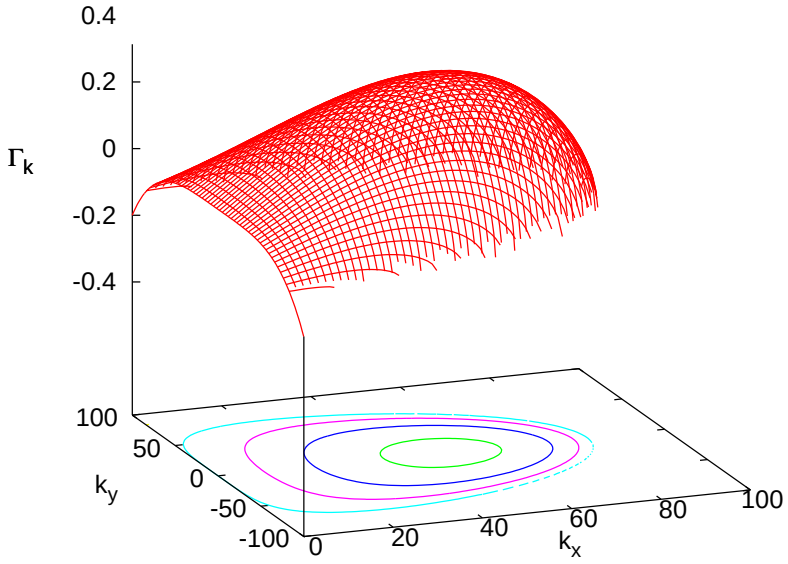

Figure 6.6: Graphical representation for $\Gamma_{\mathbf{k}} = \gamma_{\mathbf{k}} - \nu_2 k^4$ for $U = 0.01$, $F = 7000$ and $\nu_2 = 2. \times 10^{-9}$. The outermost contour is $\Gamma = 0$.

side of the plasma having higher kinetic energy which eventually causes perturbations along the temperature gradient. The higher drift velocity of these particles across the magnetic field adds to the perturbations which then can become unstable. The typical expression for the ITG instability [101] is

$$\gamma_{\mathbf{k}} = \text{const} \frac{v_{t_i}}{\sqrt{RL_T}} \tag{6.79}$$

where v_{t_i} is the ion thermal velocity, R is the tokamak major radius and $L_T = \frac{\nabla T}{T}$ and T is temperature. It can be derived from the electrostatic gyrokinetic equation [101].

The initial condition this time is gaussian, centered at the maximum of the forcing mode. Results presented here are for $U = 0.01$, $m = 2$, $\nu_m = 2.0 \times 10^{-9}$ and $F = 7000$ for various β. Figure 6.7 shows the time evolution of the energy contained within each sector where the forcing sector now encompasses the modes within the variance of the Gaussian distribution.

As before, the energy of the forcing sector grows exponentially at the beginning. The energies in the zonal and meridional sectors also grow from the outset. The forcing energy continues to grow until the resonant nonlinear interactions occur and the forcing

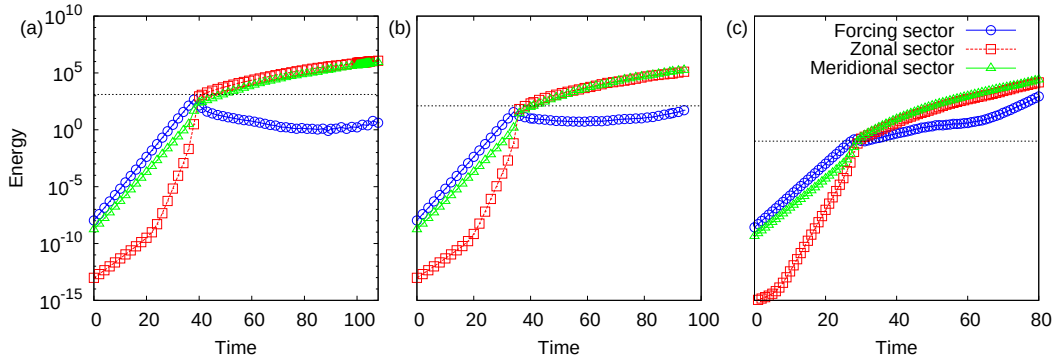

Figure 6.7: The evolution of the energy contained in the forcing mode, zonal and meridional sectors for (a) $\chi = 2.5 \times 10^{-5}$, (b) 2.5×10^{-4} and (c) 25.

is subsequently suppressed. The zonal energy is the dominant sector. Saturation of the zonal flow energy is not observed here but a definite reduction in its growth rate is. Panels (a), (b) and (c) of figure 6.7 show that as the nonlinearity becomes stronger, the energies in the zonal and meridional sectors become more-or-less equal. The horizontal dashed line in the plots represents an approximate saturated value as estimated from Eq. 6.58. It is clearly a very good estimate of the ideal level where saturation would be deemed to occur, according to the point where the growth rate slows down at $t \approx 40$. This estimate decreases with β.

The initial resonant interactions are again evident in the 2D energy spectrum plots in figure 6.8(a). Subsequently in frame (b) the small scale spectrum begins to diffuse along the open curves of constant $\Omega_{\mathbf{k}}$ and also diffusion along the shell-like curve of constant $\widetilde{Z}_{\mathbf{k}}$ to large scales, showing the two unconnected components of the turbulence spectrum. Finally in panel (c), the energy has been suppressed at the forcing modes and is now concentrated around the zonal modes. The corresponding vorticity plots in figure 6.4.2 show these zonal-type structures at late times.

For higher levels of nonlinearity measure, as expected, the vorticity plots are characterised by vortices rather than zonal structures. The β term can be neglected so that large scale condensation occurs in large round vortices rather than zonal flows. Equivalent to Euler turbulence. Thus don't see large suppression of the forcing.

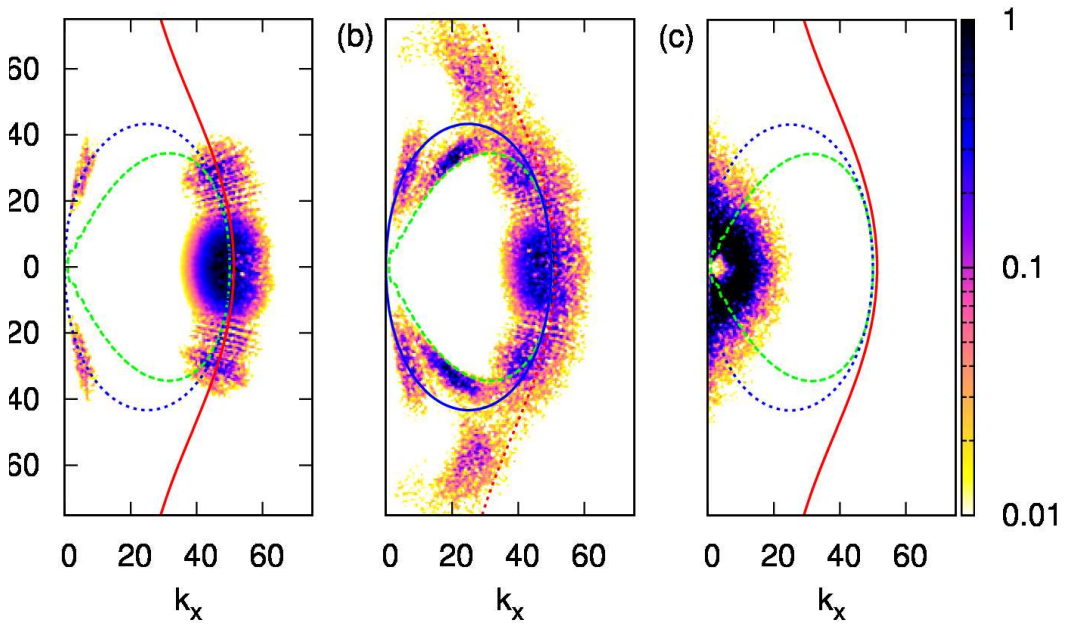

Figure 6.8: The 2D energy spectrum for $\chi = 2.5 \times 10^{-5}$ at times (a) 38.6, (b) 39.2 and (c) 70 normalised by the maximum energy 0.25, 0.25 and 5 respectively.

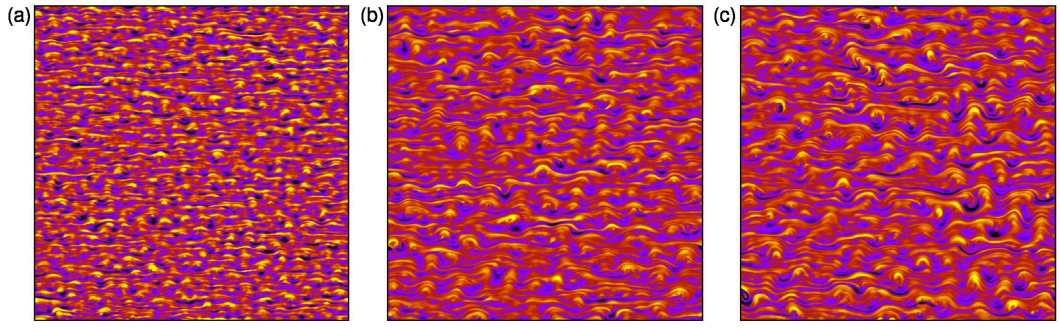

Figure 6.9: Vorticity snapshots for $\chi = 2.5 \times 10^{-5}$ at times (a) 80, (b) 100 and (c) 108 normalised by the maximum vorticity 1500, 2000 and 2000 respectively. Horizontal axis is x and the vertical y.

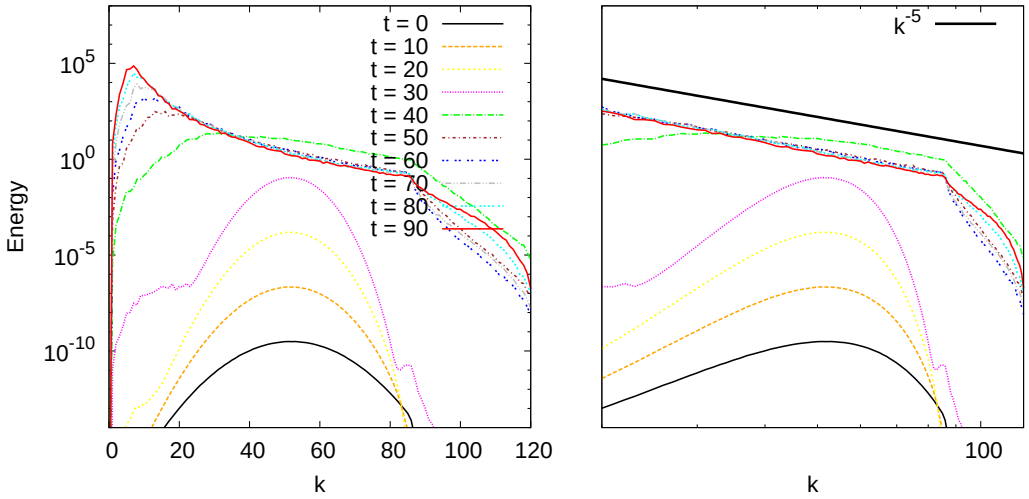

Figure 6.10: The 1D averaged spectra for $\chi = 2.5 \times 10^{-5}$

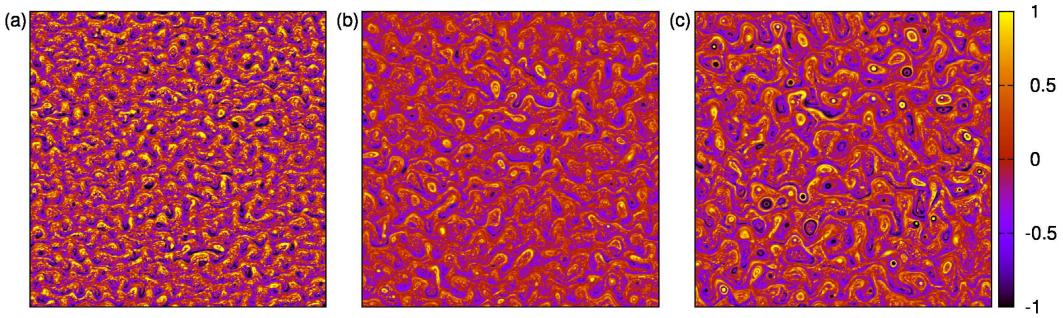

Figure 6.11: Vorticity plots for $\chi = 2.5 \times 10^{-4}$ at times (a) 65, (b) 80 and (c) 95 normalised by the maximum vorticity 500, 1000 and 1000 respectively. Horizontal axis is x and the vertical y.

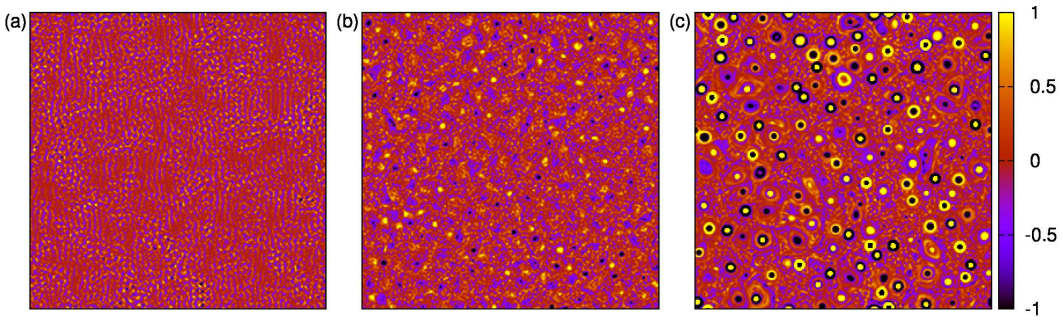

Figure 6.12: Vorticity plots for $\chi = 25$ at times (a) 30, (b) 60 and (c) 80 normalised by the maximum vorticity 50, 500 and 750 respectively. Horizontal axis is x and the vertical y.

The averaged spectra shown in figure 6.10 show a tendency to a k^{-5} law. This isotropic power law was originally proposed by Rhines [49] who then dismissed it as being physically impossible. However, there are arguments, based on data from the Voyager spacecraft, that this spectrum exists for the zonal flows on Jupiter and Saturn [102], albeit for the zonal component of the wavenumber only.

6.5 Summary

The feedback loop and the nonlocal turbulence hypothesis of drift and Rossby waves with zonal flows has been investigated and numerically validated. This is one candidate for the explanation of the LH transition previously mentioned. The instability, modelled here as forcing at the scale of the ion Larmor or deformation radius, generates the small scale drift or Rossby waves, whose energy initially grows exponentially. The nonlinear evolution of the energy spectrum progresses as diffusion along 1D curves in k-space, the diffusion coefficient increasing as it does so, resulting in an increased rate of diffusion to the large scales. The increasing diffusion battles with the growth of the instability until a balance is reached whereby the instability is effectively suppressed and the large scale zonal flow saturates at a level of the order defined by Eq. 6.58.

The idealised forcing produces well the saturation mechanism albeit that the actual level of saturation is not exactly realised. With the baroclinic or ITG forcing

applied, the level of where the zonal flow should saturate is well-approximated although an exact saturation is not observed without the need to apply large scale dissipation.

Whether or not these results could be of use to real tokamak experiments depends on whether the weak turbulence regime is observed. The strong turbulence scaling in Eq. 6.72, appropriate for $U \gtrsim \frac{\beta}{F}$ has been widely used in tokamak theory [103] for some time now. On the other hand, the weak turbulence estimate in Eq. 6.70 is more recent [33] and should be used when $U \lesssim \frac{\beta}{F}$. Zonal flows in the DIIID and JET tokamaks have been reported with $U \sim 5 - 35\,\mathrm{km\,sec}^{-1}$ [104; 105], whereas $\frac{\beta}{F}$ for both systems could range from $5\,\mathrm{km\,sec}^{-1}$ in the core to $100\,\mathrm{km\,sec}^{-1}$ in the pedestal regions. Thus, both the weak and the strong turbulent regimes should be realistically realisable.

Chapter 7

Conclusion

Several aspects of Rossby and drift wave - zonal flow turbulence have been studied through the medium of the CHM equation. These include the modulational instability and the inverse cascade mechanisms for zonal flow generation and the examination of the nonlocal hypothesis of this turbulence [9; 10; 11] which also demonstrates the famous feedback loop [17].

The MI study has confirmed that the dominant nonlinear mechanism is a three-wave one for weak primary waves. However, the 3MT fails when the modulation wavevector is zonal for low nonlinearity since it is equally close to both branches of the resonant curve. The 4MT is more robust in that it is sufficiently accurate for all levels of nonlinearity and both zonal and off-zonal perturbations. However, for strong nonlinearity, even the 4MT fails at the point of saturation since the system is now vortex-dominated rather than wave-dominated. Knowledge that truncated models predict such features well is useful for parametrisation of larger models.

An investigation into the role of the primary wave amplitude has shown that below a critical level of nonlinearity, the most unstable perturbation shifts from zonal to off-zonal. It would be interesting to investigate this effect to determine if it relates to recent observations of quasi-zonal striations, or latent jets [106], within the World Ocean Database [16], and to determine exactly the nonlinearity level of that data, which is likely to be low.

The formation of narrow zonal jets when nonlinearity $M \gtrsim 1$ is also observed.

For strong primary waves, these narrow zonal jets further roll up into Kármán-like vortex streets. It would be interesting to study in more detail how the transport properties are affected by both zonal and off-zonal jets that arise in the strongly and weakly nonlinear cases respectively. In particular, it would be interesting to establish the difference between the transport barriers provided by coherent vortex streets and the barriers provided by random jets at the later stages.

While the presence of baroclinic dynamics will change the overall dynamics of the system, it would be interesting to establish the relationship of the modulational instability with recent work on a two-layer model [106] of ocean Rossby waves, where the authors also suggest the need to study these unstable modes within boundaries.

A more accurate, albeit still idealised, model for plasmas is the modified HM equation which differs from the CHM equation in that it has an extra term which subtracts the zonal average of the field variable in order to model the effect of averaging over the magnetic surface [107]. This modification has a profound effect on the modulational instability [20; 107] so it would be interesting to apply the work carried out here to the modified equation to determine the similarities and differences between the two systems.

Some insight into the characterisation of the cascades in CHM turbulence has been provided. While it has been predicted for some time that the Rossby and drift wave turbulence conserve a third invariant [45; 46; 47], these are the first numerical proofs that zonostrophy is actually conserved in the weakly nonlinear regime. It is also, surprisingly, observed for strong initial nonlinearity after a transient non-conservative time interval, probably because the zonostrophy cascades to scales which are weakly nonlinear while the energy and the enstrophy remain in the strongly nonlinear segments of k-space.

Qualitative results of the triple cascade of the three conserved quantities, which follow the path of their centroids, reveal that the energy, enstrophy and the zonostrophy cascade into the sectors as predicted by the Fjørtoft argument. They revealed that the zonostrophy pushes the energy to the zonal scales.

Further theoretical and numerical studies would be helpful to help establish the conditions under which the zonostrophy is conserved. In particular, the extent to which the statistical properties of the system are important, for example random phases, in

addition to weak nonlinearity of the zonostrophy supporting scales. It would also be interesting to study the behaviour of zonostrophy in the other setups within the CHM model such as the modulational instability and truncated systems of coupled resonant triads.

Helicity, an extra inviscid invariant of 3D turbulence, plays a similar role to zonostrophy in QG turbulence in that it can alter the energy cascade. Perhaps the centroid-tracking technique could be employed in a study of helicity to provide more insight into these cascades.

Numerical calculations have shown evidence of the mechanism of the drift and Rossby wave - zonal flow turbulence feedback loop. This loop is characterised by the zonal flows growing from the unstable drift or Rossby waves. The zonal flows extract sufficient energy from the wave turbulence, eventually causing suppression of that turbulence. The zonal flows themselves reach saturation.

The saturation of the zonal flow and suppression of the turbulence is realised particularly well for the idealised single-mode forcing. This is quite remarkable since it occurs in a very basic model, without the need to switch-off the forcing or to use large scale dissipation. The fact that the proposed mechanism works so transparently in a model as simple as the CHM model is encouraging, suggesting that for more realistic applications to plasma physics, including tokamak theory, the mechanism should be fully realisable.

Furthermore, the calculations appear to favour the nonlocal hypothesis of drift and Rossby wave - zonal flow turbulence as predicted in [9; 10; 11]. The mathematical predictions for the diffusion routes of the turbulence spectrum in k-space are very close to the numerical evolution of the spectrum. It should be straightforward to determine whether or not the results obtained could be of use to real tokamak experiments by ascertaining whether or not the weak turbulence regime is observed in tokamaks.

Further investigation is required into the baroclinic or ITG-type forcing with either a modified HM model or the modified Hasegawa-Wakatani model ([89]) since neither a sharp switch-off of the turbulence nor saturation of the zonal flow is observed in this case. This work could provide reference points for future studies of even more realistic nonlinear

models which intrinsically include the linear instability, namely the two-layer GFD model or the Hasegawa-Wakatani model in plasmas, since current theoretical, experimental and numerical research is heavily focused on understanding and parametrising these zonal flows and their interaction with the drift wave and Rossby wave turbulence.

Appendix A

Hamiltonian formalism of Wave Turbulence

The diagonalised Hamiltonian wave equations in terms of canonical variables are given by

$$\frac{\partial a_{\mathbf{k}}}{\partial t} = -\mathrm{i}\frac{\delta \mathcal{H}}{\delta \bar{a}_{\mathbf{k}}} \tag{A.1}$$

where the complex wave amplitudes $a_{\mathbf{k}}$ is defined in Eq. 3.66 and the overbar denotes the complex conjugate and $\mathcal{H}$ denotes the Hamiltonian. This is expanded in a power series of $a_{\mathbf{k}}$

$$\mathcal{H} = \mathcal{H}_0 + \mathcal{H}_1 + \mathcal{H}_2 + \mathcal{H}_3 + \mathcal{H}_4 + \dots .$$

The derivative of the zeroth order term $\mathcal{H}_0 = 0$ and therefore does not contribute to the equation of motion, Eq. A.1. The first order $\mathcal{H}_1$ term insinuates the system is in equilibrium with minimal contribution to the Hamiltonian [31]. The quadratic term of the Hamiltonian is therefore the first important one in the expansion and has the linear dispersion frequency of a single mode as its coefficient

$$\mathcal{H}_2 = \sum_{\mathbf{k}} \omega_{\mathbf{k}} a_{\mathbf{k}} \bar{a}_{\mathbf{k}} \,. \tag{A.2}$$

The higher-order terms $\mathcal{H}_3$ and $\mathcal{H}_4$, etc describe three-wave and four-wave processes respectively, etc. providing information regarding the wave-wave interactions in the tur-

bulence and are defined as

$$\begin{aligned}\mathcal{H}_3 &= \sum_{\mathbf{k}\,\mathbf{k}_1,\mathbf{k}_2} (V_{12}^k \bar{a}_{\mathbf{k}} a_{\mathbf{k}_1} a_{\mathbf{k}_2} + \text{c.c.})\, \delta(\mathbf{k}-\mathbf{k}_1-\mathbf{k}_2) d\mathbf{k}\, d\mathbf{k}_1\, d\mathbf{k}_2 \qquad \text{(A.3)}\\ \mathcal{H}_4 &= \sum_{\mathbf{k}\,\mathbf{k}_1,\mathbf{k}_2,\mathbf{k}_3} (W_{23}^{\mathbf{k}1} \bar{a}_{\mathbf{k}} \bar{a}_{\mathbf{k}_1} a_{\mathbf{k}_2} a_{\mathbf{k}_3} + \text{c.c.})\, \delta(\mathbf{k}+\mathbf{k}_1-\mathbf{k}_2-\mathbf{k}_3) d\mathbf{k}\, d\mathbf{k}_1\, d\mathbf{k}_2\, d\mathbf{k}_1\,,\end{aligned}$$

where V_{12}^k and W_{23}^{k1} denote three and four-wave interaction coefficients respectively.

For the Rossby wave and drift wave systems, the quadratic nonlinear term insinuates a three-wave process so that the leading term of the interaction Hamiltonian in this case is given by $\mathcal{H}_3$ so that

$$\mathcal{H} = \sum_{\mathbf{k}} \omega_{\mathbf{k}} a_{\mathbf{k}} \bar{a}_{\mathbf{k}} + \sum_{\mathbf{k}\,\mathbf{k}_1,\mathbf{k}_2} (V_{12}^k \bar{a}_{\mathbf{k}} a_{\mathbf{k}_1} a_{\mathbf{k}_2} + \text{c.c.})\, \delta(\mathbf{k}-\mathbf{k}_1-\mathbf{k}_2) d\mathbf{k}\, d\mathbf{k}_1\, d\mathbf{k}_2 \qquad \text{(A.4)}$$

and $\omega_{\mathbf{k}}$ and V_{12}^k are defined in Eqs 3.62 and 3.68 respectively. The leading term of Eq. A.4 is equivalent to Eq. A.2

In addition to these generalised symmetric equations of motion, they can also be expressed in Poisson bracket format. In the early 1980s, both Zakharov [108] and Weinstein [109] independently presented the Hamiltonian structure for drift and Rossby waves with non-canonical variables. Equivalent to Liouville's theorem in this format, the CHM Eq. 3.35 is equivalent to [109; 108; 31]

$$\frac{\partial W}{\partial t} = \{W, \mathcal{H}\} \qquad \text{(A.5)}$$

where

$$W = \nabla \psi_{\mathbf{k}} - F\psi_{\mathbf{k}}\,. \qquad \text{(A.6)}$$

and $\mathcal{H}$ is defined as

$$\mathcal{H} = \frac{1}{2}\int_{\mathbf{k}} (\nabla \psi_{\mathbf{k}})^2 + F\psi_{\mathbf{k}}^2\, dx\, dy \qquad \text{(A.7)}$$

and is equivalent to the total energy of the system (see Eq. 3.55).

The Poisson bracket for the functionals $A = A(\psi)$, $B = B(\psi)$ is defined by

$$\{A, B\} = \int qJ\left(\frac{\delta A}{\delta W}\frac{\delta B}{\delta W}\right) dx\, dy\,, \qquad \text{(A.8)}$$

where J is the Jacobian, q is the potential vorticity (PV) defined by

$$q = \nabla^2 \psi_{\mathbf{k}} - F\psi_{\mathbf{k}} + \beta y\,, \qquad \text{(A.9)}$$

and $\frac{\delta}{\delta W}$ denotes the variational derivative with respect to the functional $W(\psi)$.

Eq. A.5 is relevant also for hydrodynamic turbulence i.e in the limit $\beta \to 0, F \to 0$ where in this case the Hamiltonian and vorticity are reduced to $H = \frac{1}{2}\int_{\mathbf{k}}(\nabla\psi_{\mathbf{k}})^2$ and $q = \nabla^2\psi_{\mathbf{k}}$ respectively.

Appendix B

Numerical Model

Re-writing the dynamical Eq. 3.61 and dropping the subscript $\mathbf{k}$ and hat notation for brevity, solving the CHM equation is reduced to solving a simple PDE.

$$\psi_t + i\omega\psi + \mathcal{N}(\psi) = 0, \tag{B.1}$$

where the subscript t denotes the time derivative and $\mathcal{N}(\psi) = \frac{1}{2}\sum_{\mathbf{k}_1,\mathbf{k}_2} T(\mathbf{k},\mathbf{k}_1,\mathbf{k}_2)\,\psi_1\,\psi_2$ is short-hand for the nonlinear term on the RHS of Eq. 3.61.

B.1 Timestepping method

When the PDE is expressed as a sum of the Fourier modes with time-dependent coefficients, a set of ordinary differential equations (ODEs) for the mode amplitudes is yielded. This system of ODEs tends to be stiff [110] due to the linear part occurring on a much shorter timescale than the nonlinear part for which the usual methods of time discretisation require a very small timestep.

Employing the Integrating factor (IF) method for solving ODEs, Eq. B.1 can be re-written as

$$\frac{\partial}{\partial t}(e^{i\omega t}\psi) = e^{i\omega t}\mathcal{N}(\psi). \tag{B.2}$$

IF methods improve the stiffness by effectively removing the stiff linear part from the equation so combining a standard third-order Runge-Kutta method [111] to solve Eq. B.2,

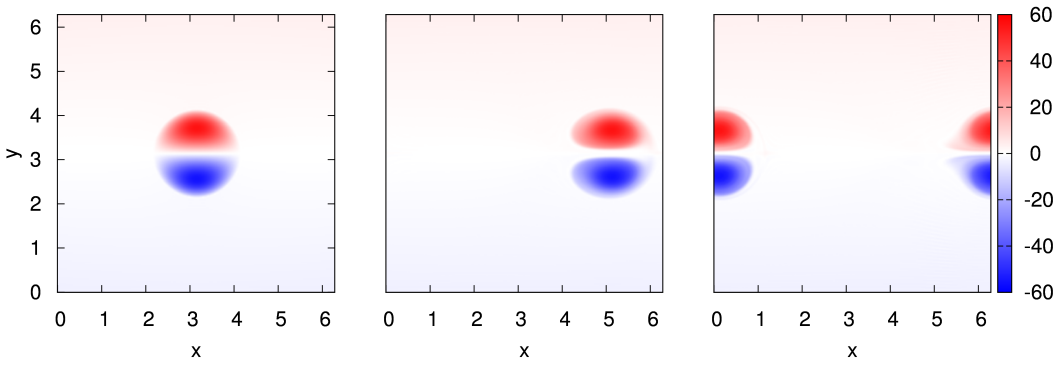

Figure B.1: Modon test case - snapshots of vorticity

the timestepping method is defined as

$$\psi(t+dt) = \psi_0 e^{-i\omega dt} + \frac{2}{9} dt\mathcal{N}(\psi_0)e^{-i\omega dt} + \frac{1}{3} dt\mathcal{N}(\psi_1)e^{-\frac{1}{2}i\omega dt} + \frac{4}{9} dt\mathcal{N}(\psi_2)e^{-\frac{3}{4}i\omega dt} \quad \text{(B.3)}$$

where ψ_0 is the initial stream function, ψ_1 and ψ_2 are intermediate values defined at $t + \frac{1}{2}dt$ and $t + \frac{3}{4}dt$ respectively. Using the Euler method, these are defined as,

$$\psi_1 = \psi_0 e^{-\frac{1}{2}i\omega dt} + \frac{1}{2} dt\mathcal{N}(\psi_0)e^{-\frac{1}{2}i\omega dt} \quad \text{(B.4)}$$

and

$$\psi_2 = \psi_0 e^{-\frac{3}{4}i\omega dt} + \frac{3}{4} dt\mathcal{N}(\psi_1)e^{-\frac{1}{4}i\omega dt}. \quad \text{(B.5)}$$

A de-aliasing technique was applied.

B.2 Modons

Perhaps it is not so well-known that the CHM equation also admits a di-polar vortex solution, called a *modon* [112; 4][1] which travels in the x-direction at a constant velocity u.

The solution is given by

$$\psi(r,\theta) = \begin{cases} \dfrac{u+\kappa}{b^2}\left(a\dfrac{J_1(br)}{J_1(ba)} - r\left(\dfrac{b^2}{s^2}+1\right)\right)\sin\alpha, & r < a, \\ \dfrac{u+\kappa}{s^2} a \dfrac{K_1(sr)}{K_1(sa)}\sin\alpha, & r > a, \end{cases} \quad \text{(B.6)}$$

[1] Many thanks to Bill Dorland for suggesting this as a test case for the code

where $\tan\alpha = y/x$. J_1 is the first-order Bessel function of the second kind and K_1 is a first-order modified Bessel function of the second kind. a is the radius of the dipolar vortex and s and κ are constants which satisfy $u = \frac{\kappa}{s^2-1}$.

The continuity of $\partial\psi/\partial t$ at $r = a$ gives the eigenvalue b

$$\sum_{n=1}^{\infty} \frac{1}{(ba)^2 - z_n^2} = \frac{1}{2\rho a}\left(\frac{1}{\rho a} - \frac{K_1'(\rho a)}{K_1(\rho a)}\right) \tag{B.7}$$

where z_n is the monotonically increasing sequence of zeros of $J_1(r)$. See [112; 4] for further details.

It can be clearly seen from figure B.1 that the modon travels in the x-direction, as expected. The velocity has been checked as calculated from the dispersion relation.

Appendix C

Rayleigh-Kuo Instability Criterion

Stationary flows may be unstable to a small perturbation. An analysis is presented here for the stability criterion of a stationary flow, governed by the barotropic vorticity equation. This work by Kuo [82] was an extension to the work of Rayleigh [113; 81] to take into account the inclusion of β, the variation of the Coriolis parameter into the governing equations of large scale atmospheric motion. The barotropic vorticity equation, expressed in terms of the streamfunction ψ is

$$\partial_t \Delta\psi + \beta\partial_x\psi + (\partial_x\psi)\partial_y\Delta\psi - (\partial_y\psi)\partial_x\Delta\psi = 0\,, \tag{C.1}$$

which is equivalent to Eq. 3.35 in the $F \to 0$ limit. Assume there is a small-amplitude streamfunction perturbation, $\widetilde{\psi}(x, y, t)$ on an otherwise stationary background flow, $\psi_0(y)$ such that

$$\psi = \psi_0 + \widetilde{\psi} \tag{C.2}$$

with $\widetilde{\psi} \ll \psi_0$. To linearise Eq. C.1 substitute Eq. C.2 for ψ, neglect terms nonlinear in the perturbation since they are small and remembering that $\psi_0 = \psi_0(y)$,

$$\partial_t \Delta\widetilde{\psi} + \beta\partial_x\widetilde{\psi} + (\partial_x\widetilde{\psi})\partial_y\Delta\psi_0 - (\partial_y\psi_0)\partial_x\Delta\widetilde{\psi} = 0\,. \tag{C.3}$$

Since

$$U_0 = -\frac{\partial\psi_0}{\partial y}\,, \tag{C.4}$$

Eq. C.3 can be rewritten as

$$\partial_t \Delta\widetilde{\psi} + U_0 \partial_x \Delta\widetilde{\psi} + \beta \partial_x \widetilde{\psi} - U_{0_{yy}} \partial_x \widetilde{\psi} = 0\,. \tag{C.5}$$

Now seek normal mode solutions of the form

$$\widetilde{\psi}(x, y, t) = \mathrm{Re}[\Psi(y) e^{i(k_x x - \omega t)}]\,. \tag{C.6}$$

Inserting Eq. C.6 into Eq. C.5 and factoring out $e^{i(k_x x - \omega t)}$, results in

$$\left(U_0 - \frac{\omega}{k_x}\right)(\Psi_{yy} - k^2\Psi) + (\beta - U_{0_{yy}})\Psi = 0\,. \tag{C.7}$$

Multiplying Eq. C.7 by $\bar{\Psi}$, where the bar denotes the conjugate, integrating over y and separating the real and imaginary parts gives,

$$\int_{-\infty}^{\infty} \left(k^2|\Psi|^2 - |\Psi_y|^2\right) dy = \int_{-\infty}^{\infty} \frac{\beta - U_{0_{yy}}}{U_0 - \frac{\omega}{k_x}} |\Psi|^2 dy\,. \tag{C.8}$$

The LHS of Eq. C.8 is real. The RHS can have real and imaginary parts and upon integration, equating real and imaginary parts gives

$$0 = \int_{-\infty}^{\infty} \frac{(\beta - U_{0_{yy}})\mathrm{Im}[\omega]}{\left|U_0 - \frac{\omega}{k_x}\right|^2} |\Psi|^2 dy\,. \tag{C.9}$$

Since $\mathrm{Im}[\omega] \neq 0$ for an instability to exist and all other terms in the integrand are positive, except $\beta - U_{0_{yy}}$, this expression must change sign so that it would have positive and negative contributions to result in zero. The necessary condition for an instability is therefore, that $\beta - U_{0_{yy}}$ crosses zero.

Appendix D

Baroclinic Instability

The simplest model which admits vertical shear is the two-layer QG PV model. A simple sketch in figure D.1 shows this idealised set-up which is typical of the stratification in the troposphere of mid-latitudes [81]. The density in the upper layer is less than that of the lower layer $\rho_1 < \rho_2$, there is no horizontal shear and for simplicity, let the layers be of equal depth, $H_1 = H_2 = H$. The upper layer has a constant velocity $U(y)$ in the positive x-direction while the lower layer has velocity $-U(y)$.

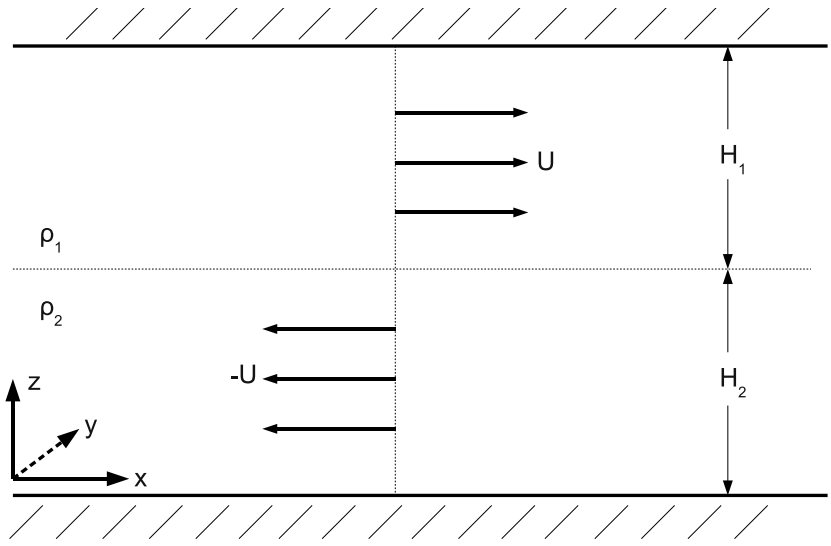

Figure D.1: Idealisation of a baroclinic two-layer fluid

The derivation of the QG PV equation is presented in many texts [81; 19] and is simply stated here for an inviscid two-layer model. Define the baroclinic deformation radius, $R = \frac{\sqrt{g'H}}{2f_0}$ where $g' = g\frac{\rho_1 - \rho_2}{\rho_0}$ is the reduced gravity due to the density difference across the interface between the layers, g is the usual gravitational acceleration and f_0 is the leading order term of the Coriolis parameter. In this two-layer model, the PV is denoted as q_n where $n = 1, 2$ for the respective layers and Eq. A.9 is generalised as

$$q_n = \nabla^2\psi_n + \beta y + (-1)^n \frac{f_0^2}{g'H_n}(\psi_1 - \psi_2) \tag{D.1}$$

$$\frac{\partial q_n}{\partial t} + J[\psi_n, q_n] = \frac{\partial q_n}{\partial t} + \frac{\partial \psi_n}{\partial x}\frac{\partial q_n}{\partial y} - \frac{\partial \psi_n}{\partial y}\frac{\partial q_n}{\partial x} = \mathcal{F}_n = 0 \tag{D.2}$$

Consider a perturbation to the stationary state so that

$$\begin{aligned} \psi_n &= \bar{\psi}_n + \widetilde{\psi}_n \\ q_n &= \bar{q}_n + \widetilde{q}_n \end{aligned} \tag{D.3}$$

where $\widetilde{\psi}_n \ll \bar{\psi}_n$ and since U is constant, the mean fields are related as

$$\begin{aligned} \bar{\psi}_n &= (-1)^{n+1} U y \\ \bar{q}_n &= \beta y - (-1)^{n+1}\frac{Uy}{R^2} \end{aligned} \tag{D.4}$$

i.e. independent of x. Linearising Eqs D.2 by neglecting terms of order two in the perturbation and noting that $(-1)^{n+1}U = \frac{\partial \bar{\psi}_n}{\partial y}$ and $\widetilde{v}_n = \frac{\partial \widetilde{\psi}_n}{\partial x}$ where $\widetilde{v}_n$ is the y-velocity component of the perturbation, yields

$$\begin{aligned} \frac{\partial \widetilde{q}_1}{\partial t} + U\frac{\partial \widetilde{q}_1}{\partial x} + \widetilde{v}_1\frac{\partial \bar{q}_1}{\partial y} &= \frac{\partial \widetilde{q}_1}{\partial t} + U\frac{\partial \widetilde{q}_1}{\partial x} + \widetilde{v}_1\left(\beta + \frac{U}{R^2}\right) = 0 \\ \frac{\partial \widetilde{q}_2}{\partial t} - U\frac{\partial \widetilde{q}_2}{\partial x} + \widetilde{v}_2\frac{\partial \bar{q}_2}{\partial y} &= \frac{\partial \widetilde{q}_2}{\partial t} - U\frac{\partial \widetilde{q}_2}{\partial x} + \widetilde{v}_2\left(\beta - \frac{U}{R^2}\right) = 0\,, \end{aligned} \tag{D.5}$$

where the y derivatives have been calculated explicitly from Eqs D.4. Now seek normal mode solutions of the form

$$\begin{aligned} \widetilde{\psi}_n(x, y, t) &= \mathrm{Re}[\Psi_n(x, y)e^{i(\mathbf{k}\cdot\mathbf{x} - \omega t)}] \\ \widetilde{q}_n(x, y, t) &= \nabla^2\widetilde{\psi}_n + \beta y + (-1)^n\frac{f_0^2}{g'H_n}(\widetilde{\psi}_1 - \widetilde{\psi}_2)\,. \end{aligned} \tag{D.6}$$

Introducing Eqs D.6 into Eqs D.5, noting that $\Psi = \Psi(x, y)$ and factoring out $e^{i(\mathbf{k}\cdot\mathbf{x}-\omega t)}$ gives,

$$\omega k^2\Psi_1 + \frac{\omega}{2R^2}(\Psi_1 - \Psi_2) - U\left[k_x k^2\Psi_1 - \frac{k_x}{2R^2}(\Psi_1 - \Psi_2)\right] + k_x(\beta + \frac{U}{R^2})\Psi_1 = 0$$
$$\omega k^2\Psi_2 + \frac{\omega}{2R^2}(\Psi_1 - \Psi_2) + U\left[k_x k^2\Psi_2 - \frac{k_x}{2R^2}(\Psi_1 - \Psi_2)\right] + k_x(\beta - \frac{U}{R^2})\Psi_2 = 0 \quad \text{(D.7)}$$

which can be re-arranged to

$$\begin{aligned}\left(\frac{\omega}{k_x}k^2 - U\right)\left[k^2\Psi_1 + \frac{1}{2R^2}(\Psi_1 - \Psi_2)\right] + \left(\beta + \frac{U}{R^2}\right)\Psi_1 &= 0 \\ \left(\frac{\omega}{k_x}k^2 + U\right)\left[k^2\Psi_2 - \frac{1}{2R^2}(\Psi_1 - \Psi_2)\right] + \left(\beta - \frac{U}{R^2}\right)\Psi_2 &= 0\,. \end{aligned} \quad \text{(D.8)}$$

In a baroclinic fluid, it is often convenient to transfer the layer amplitudes into respective vertical modal amplitudes [81] defined as

$$\begin{aligned}\Phi_0 &= \frac{1}{2}(\Psi_1 + \Psi_2) \\ \Phi_1 &= \frac{1}{2}(\Psi_1 - \Psi_2)\,. \end{aligned} \quad \text{(D.9)}$$

Taking the sum and difference of Eqs D.8 gives the equations for the modal amplitudes,

$$\begin{aligned}\left[\frac{\omega}{k_x}k^2 + \beta\right]\Phi_0 - Uk^2\Phi_1 &= 0 \\ \left[\frac{\omega}{k_x}\left(k^2 + \frac{1}{R^2}\right) + \beta\right]\Phi_1 - U(k^2 - \frac{1}{R^2})\Phi_0 &= 0 \end{aligned} \quad \text{(D.10)}$$

Substituting the first equation into the other yields the general dispersion relation.

$$\left[\frac{\omega}{k_x}k^2 + \beta\right]\left[\frac{\omega}{k_x}(k^2 + \frac{1}{R^2}) + \beta\right] - Uk^2\left(k^2 - \frac{1}{R^2}\right) = 0 \quad \text{(D.11)}$$

Then solving for ω when $\beta = 0$ gives

$$\omega = Uk_x\sqrt{\frac{\frac{1}{R^2} - k^2}{\frac{1}{R^2} + k^2}}\,, \quad \text{(D.12)}$$

which in the longwave limit $k < \frac{1}{R}$ is an imaginary quantity corresponding to an exponentially growing mode [81].

Appendix E

Fjørtoft argument in terms of the centroids

Consider an evolving hydrodynamic 2D turbulence in the absence of forcing and dissipation. Here the Fjørtoft argument will be re-formulated in terms of the energy and enstrophy centroids in the Fourier k-space and in the physical l-space where $\mathbf{l} = (x, y)$. This formulation will be rigorous and is useful for visualising the directions of the energy and enstrophy transfer. In contrast with the version of the Fjørtoft argument given in Section 5.4.1, this formulation is for a non-dissipative turbulence rather than a forced and dissipated system.

The energy and the enstrophy k-centroids are defined respectively as

$$k_E = \frac{1}{E}\int_0^\infty k\, E_k\, dk \tag{E.1}$$

$$k_Q = \frac{1}{Q}\int_0^\infty k^3\, E_k\, dk \tag{E.2}$$

and their l-centroids as

$$l_E = \frac{1}{E}\int_0^\infty \frac{1}{k}\, E_k\, dk \tag{E.3}$$

$$l_Q = \frac{1}{Q}\int_0^\infty k\, E_k\, dk \equiv \frac{k_E E}{Q}\,, \tag{E.4}$$

where E_k is the energy density at k and recall that $Q = \int k^2 E_k$.

Assuming now that all the integrals defining E, Q, k_E, k_Q, $\mathbf{l}_E$ and $\mathbf{l}_Q$ converge, the Cauchy-Schwartz inequality which states that

$$\left|\int_0^\infty f(k)g(k)\,dk\right| \leq \left|\int_0^\infty f^2(k)\,dk\right|^{\frac{1}{2}} \left|\int_0^\infty g^2(k)\,dk\right|^{\frac{1}{2}} \tag{E.5}$$

for any functions $f(k)$ and $g(k)$. Only positive functions will be dealt with here so the absolute value brackets may be omitted.

Consider the following integrals, applying the Cauchy-Schwartz inequality E.5 to them and use Eqs E.1 - E.4 to simplify.

$$\begin{aligned}
\int_0^\infty kE\,dk &= \int_0^\infty (kE^{\frac{1}{2}})(E^{\frac{1}{2}})\,dk \leq \left(\int_0^\infty k^2E\,dk\right)^{\frac{1}{2}} \left(\int_0^\infty E\,dk\right)^{\frac{1}{2}} \\
\implies k_E E &\leq Q^{\frac{1}{2}}E^{\frac{1}{2}} \\
\implies k_E &\leq \sqrt{\frac{Q}{E}} \quad \text{and} \qquad \text{(E.6)} \\
l_Q &\leq \sqrt{\frac{E}{Q}}. \qquad \text{(E.7)}
\end{aligned}$$

$$\begin{aligned}
\int_0^\infty k^2E\,dk &= \int_0^\infty (k^{\frac{3}{2}}E^{\frac{1}{2}})(k^{\frac{1}{2}}E^{\frac{1}{2}})\,dk \leq \left(\int_0^\infty k^3E\,dk\right)^{\frac{1}{2}} \left(\int_0^\infty kE\,dk\right)^{\frac{1}{2}} \\
\implies Q &\leq (k_Q Q)^{\frac{1}{2}}(k_E E)^{\frac{1}{2}} \\
\implies k_E k_Q &\geq \frac{Q}{E} \qquad \text{(E.8)}
\end{aligned}$$

Combining inequalities E.8 and E.6 gives

$$k_Q \geq \sqrt{\frac{Q}{E}} \tag{E.9}$$

and from E.6 and E.9 it is clear that during the system's evolution the energy centroid $k_E(t)$ is bounded from above and the enstrophy centroid $k_Q(t)$ is bounded from below by the same wavenumber $k = \sqrt{Q/E}$. Furthermore, inequality E.8 means that if $k_E(t)$ happened to move to small k's then $k_Q(t)$ *must* move to large k's, i.e. roughly speaking there cannot be inverse cascade of energy without a forward cascade of enstrophy. There is no complimentary restriction which would oblige $k_E(t)$ to become small when $k_Q(t)$

becomes large so the k-centroid part of the Fjørtoft argument is asymmetric, and one has to consider the l-centroids to make it symmetric.

Now splitting $\int kE\,dk$ another way gives,

$$\begin{aligned}
\int_0^\infty kE\,dk &= \int_0^\infty (k^{\frac{3}{2}}E^{\frac{1}{2}})(k^{-\frac{1}{2}}E^{\frac{1}{2}})\,dk \leq \left(\int_0^\infty k^3E\,dk\right)^{\frac{1}{2}}\left(\int_0^\infty k^{-1}E\,dk\right)^{\frac{1}{2}} \\
\implies k_EE &\leq (k_QQ)^{\frac{1}{2}}(l_EE)^{\frac{1}{2}} \\
\implies k_E &\geq \frac{E}{Q}\,. \qquad \text{(E.10)}
\end{aligned}$$

Combining inequalities E.10 and E.7 gives

$$l_E \geq \sqrt{\frac{E}{Q}}\,. \qquad \text{(E.11)}$$

Inequality E.10 now imposes the restriction of an inverse energy cascade if the enstrophy undergoes a direct one.

Bibliography

[1] J. G. Charney, "On the scale of atmospheric motions," *Geophys. Public*, vol. 17, pp. 3–17, 1948.

[2] A. Hasegawa and K. Mima, "Pseudo-three-dimensional turbulence in magnetised nonuniform plasma," *Phys. Fluids*, vol. 21, pp. 87–92, 1978.

[3] J. Pedlosky, *Geophysical Fluid Dynamics*. Springer, 1987.

[4] W. Horton and A. Hasegawa, "Quasi-two-dimensional dynamics of plasmas and fluids," *Chaos*, vol. 4, pp. 227–251, 1994.

[5] C. P. Connaughton, S. V. Nadiga, B. T.and Nazarenko, and B. E. Quinn, "Modulational instability of Rossby and drift waves and generation of zonal jets," *J. Fluid Mech.*, vol. 654, pp. 207–231, 2010.

[6] S. V. Nazarenko and B. E. Quinn, "Triple cascade behaviour in QG and drift turbulence and the generation of zonal jets," *Physical Review Letters*, vol. 203, p. 118501, 2009.

[7] S. V. Nazarenko and B. E. Quinn, "Triple cascade behaviour in QG and drift turbulence and the generation of zonal jets," in *IUTAM Symposium on Turbulence in the Atmosphere and Oceans* (D. Dritschel, ed.), vol. 28 of *IUTAM Bookseries*, (Cambridge), pp. 265–288, Springer Science+Business Media, 2010.

[8] A. E. Gill, "The stability of planetary waves on an infinite beta-plane," *Geophys. Fluid Dyn.*, vol. 6, pp. 29–47, 1974.

[9] A. M. Balk, S. V. Nazarenko, and V. E. Zakharov, "On the nonlocal turbulence of drift type waves," *Phys. Lett. A*, vol. 146, pp. 217–221, 1990.

[10] A. M. Balk, V. E. Zakharov, and S. V. Nazarenko, "Nonlocal turbulence of drift waves," *Sov. Phys. JETP*, vol. 71, pp. 249–260, 1990.

[11] S. V. Nazarenko, "On the nonlocal interaction with zonal flows in turbulence of drift and Rossby waves," *Sov. Phys. JETP*, vol. 71, pp. 604–607, 1991.

[12] A. A. Simon, "The structure and temporal stability of Jupiter's zonal winds: A study of the north tropical region," *Icarus*, vol. 141, p. 29, 1999.

[13] A. Sanchez-Lavega, J. F. Rojas, and P. V. Sada, "Saturn's zonal winds at cloud level," *Icarus*, vol. 147, pp. 405–420, 2000.

[14] B. Galperin, H. Nakano, H.-P. Huang, and S. Sukoriansky, "The ubiquitous zonal jets in the atmospheres of giant planets and earth's oceans," *Geophys. Res. Lett.*, vol. 131, p. L13303, 2004.

[15] J. M. Lewis, "Clarifying the dynamics of the general circulation: Phillips's 1956 experiment," *Bull. Amer. Met. Soc.*, vol. 79, no. 1, 1988.

[16] N. A. Maximenko, O. V. Melnichenko, P. P. Niiler, and H. Sasaki, "Stationary mesoscale jet-like features in the ocean," *Geophys. Res. Lett.*, vol. 35, p. L08603, 2008.

[17] P. H. Diamond, S.-I. Itoh, K. Itoh, and T. S. Hahm, "Zonal flows in plasma - a review," *Plasma Phys. Control. Fusion*, vol. 47, no. 5, pp. R35–R161, 2005.

[18] M. E. McIntyre, "Potential vorticity inversion and the wave-turbulence jigsaw: some recent clarifications," *Adv. Geosci.*, vol. 15, pp. 47–56, 2008.

[19] B. Cushman-Roisin, *Introduction to Geophysical Fluid Dynamics*. Prentice-Hall Inc., 1994.

[20] G. Manfredi, C. M. Roach, and R. O. Dendy, "Zonal flow and streamer generation in drift turbulence," *Plasma Phys. Control. Fusion*, vol. 43, pp. 825–837, 2001.

[21] I. N. James, "Suppression of baroclinic instability in horizontally sheared flows," *J. Atmo. Sci.*, vol. 44, no. 24, p. 3710, 1987.

[22] D. L. Hartmann, K. R. Chan, B. Gary, M. Schoeberl, R. Newman, R. Martin, M. Loewenstein, J. Podlolske, and S. Strahan, "Potential vorticity and mixing in the south polar vortex during spring," *J. Geophys. Res.*, vol. 94, pp. 11625–11640, 1989.

[23] P. W. Terry, "Suppression of turbulence and transport by sheared flow," *Review of odern physics*, vol. 72, pp. 109–165, 2000.

[24] C. Trepte and M. Hitchman, "Tropical stratospheric circulation deduced from satellite aerosol data," *Nature*, vol. 355, pp. 626–628, 1992.

[25] L. Richardson, "Atmospheric diffusion shown on a distance-neighbour graph," *Proc. R. Soc. A*, vol. 110, pp. 709–737, 1926.

[26] G. I. Taylor, "Statistical theory of turbulence," *Proc. Roy. Soc. London*, vol. A151, pp. 421–454, 1935.

[27] G. I. Taylor, "The spectrum of turbulence," *Proc. Roy. Soc. London*, vol. A164, pp. 476–490, 1938.

[28] A. N. Kolmogorov, "The local structure of turbulence in incompressible viscous fluid for very large Reynolds numbers," *Dokl. Akad. Nauk. SSSR*, vol. 30, pp. 301–305, 1941.

[29] A. N. Kolmogorov, "Dissipation of energy in the locally isotropic turbulence," *Dokl. Akad. Nauk. SSSR*, vol. 32, pp. 15–17, 1941.

[30] A. M. Obukhov, "On the distribution of energy in the spectrum of turbulent flow," *Dokl. Akad. Nauk SSSR*, vol. 32, pp. 22–24, 1941.

[31] V. S. Zakharov, V. S. Lvov, and G. Falkovich, *Kolmogorov Spectra of Turbulence*. Berlin: Springer-Verlag, 1992.

[32] R. Peierls, "Zur kinetischen theorie der wärmeleitung in kristallen," *Annalen der Physik*, vol. 395, pp. 1055–1101, 1929.

[33] S. Nazarenko, *Wave Turbulence (Lecture notes in Physics)*. Springer, 2011.

[34] M. S. Longuet-Higgins and A. E. Gill, "Resonant interactions between planetary waves," in *Proceedings of the Royal Society of London, Mathematical and Physical Sciences*, vol. 299 of *A*, (London, UK), 1967.

[35] R. Z. Sagdeev and A. A. Galeev, *Nonlinear Plasma Theory*. New York: Benjamin, 1969.

[36] W. F. Vinen and J. J. Niemela, "Quantum turbulence," *J. Low Temp. Phys.*, vol. 128, pp. 167–231, 2002.

[37] A. Hasegawa and C. G. Maclennan, "Nonlinear behavior and turbulence spectra of drift waves and Rossby waves," *Phys. Fluids*, vol. 22, pp. 2122–2129, 1979.

[38] E. N. Lorentz, "Barotropic instability of Rossby wave motion," *J. Atmo. Sci.*, vol. 29, pp. 258–269, 1972.

[39] O. Onishchenko, O. Pokhotelov, R. Sagdeev, P. Shukla, and L. Stenflo, "Generation of zonal flows by Rossby waves in the atmosphere," *Nonlin. Proc. Geophys.*, vol. 11, pp. 241–244, Apr. 2004.

[40] K. Mima and Y. C. Lee, "Modulational instability of strongly dispersive drift waves and formation of convective cells," *Phys. Fluids*, vol. 23, p. 105, 1980.

[41] A. I. Smolyakov, P. H. Diamond, and V. I. Shevchenko, "Zonal flow generation by parametric instability in magnetized plasmas and geostrophic fluids," *Phys. Plasmas*, vol. 7, pp. 1349–1351, 2000.

[42] A. I. Smolyakov, P. H. Diamond, and M. Malkov, "Coherent structure phenomena in drift wave - zonal flow turbulence," *Phys. Rev. Lett.*, vol. 84, pp. 491–494, 2000.

[43] R. Fjørtoft, "On the changes in the spectral distribution of kinetic energy for two-dimensional non-divergent flow," *Tellus*, vol. 5, pp. 225–230, 1953.

[44] R. H. Kraichnan, "Inertial ranges in two-dimensional turbulence," *Phys. Fluids*, vol. 10, pp. 1417–1423, 1967.

[45] A. M. Balk, S. V. Nazarenko, and V. E. Zakharov, "New invariant for drift turbulence," *Phys. Lett. A*, vol. 152, pp. 276–280, 1991.

[46] A. M. Balk, "A new invariant for Rossby wave systems," *Phys. Lett. A.*, vol. 155, pp. 20–24, 1991.

[47] A. M. Balk, "New conservation laws for the interaction of nonlinear waves," *SIAM Review*, vol. 39, pp. 68–94, 1997.

[48] G. P. Williams, "Planetary circulations: Barotropic representation of Jovian and terrestrial turbulence," *J. Atmos. Sci.*, vol. 35, pp. 1399–1426, 1978.

[49] P. Rhines, "Waves and turbulence on a beta-plane," *J. Fluid Mech.*, vol. 69, pp. 417–443, 1975.

[50] P. Rhines, "Geostrophic turbulence," *Ann. Rev. Fluid Mech.*, vol. 11, pp. 401–441, 1979.

[51] T. Benjamin and J. Feir, "The disintegration of wave trains on deep water. Part 1. Theory," *J. Fluid Mech.*, vol. 27, pp. 417–430, 1967.

[52] P. A. E. M. Janssen, "Nonlinear four-wave interactions and freak waves," *J. Phys. Ocean.*, pp. 863–884, 2003.

[53] R. Dendy, ed., *Plasma Physics, An Introductory course*. Cambridge University Press, 1993.

[54] J. A. Wesson, *Tokamaks*. Oxford University Press, 1987.

[55] S. I. Krasheninnikov, L. E. Zakharov, and G. V. Pereverzev, "On lithium walls and the performance of magnetic fusion devices," *Phys. Plasmas*, pp. 1678–1682, 2003.

[56] L. J. D., "Some criteria for a power producing thermonuclear reactor," *Proc. Phys. Soc. B*, vol. 70, pp. 6–10, 1957.

[57] F. Wagner, G. Becker, K. Behringer, D. Campbell, A. Eberhagen, W. Engelhardt, G. Fussmann, O. Gehre, J. Gernhardt, G. v. Gierke, G. Haas, M. Huang, F. Karger, M. Keilhacker, O. Klüber, M. Kornherr, K. Lackner, G. Lisitano, G. G. Lister, H. M. Mayer, D. Meisel, E. R. Müller, H. Murmann, H. Niedermeyer, W. Poschenrieder, H. Rapp, and H. Röhr, "Regime of improved confinement and high beta in neutral-beam-heated divertor discharges of the ASDEX tokamak," *Phys. Rev. Lett.*, vol. 49, no. 19, pp. 1408–1412, 1982.

[58] W. Horton, "Anomalous transport due to drift wave turbulence," *Physica D*, vol. 2, pp. 107–116, 1981.

[59] R. L. I. and R. Z. Sagdeev, "On the instability of a nonuniform rarefied plasma in a strong magnetic field," *Dokl. Akad. Nauk SSSR*, vol. 138, p. 581, 1961.

[60] C. G. Rossby and Collaborators, "Relation between variations in the intensity of the zonal circulation of the atmosphere and the displacements of the semi-permanent centres of action," *J. Marine Res.*, vol. 2, pp. 38–55, 1939.

[61] C. G. Rossby, "Planetary flow patterns in the atmosphere," *Quart. J. Roy. Meteor. Soc. (suppl)*, vol. 66, pp. 68–87, 1940.

[62] L. Marié, "A study of the phase instability of quasi-geostrophic Rossby waves on the infinite β-plane to zonal flow perturbations," *Nonlin. Processes Geophys.*, vol. 17, pp. 49–63, 2010.

[63] D. Y. Manin and S. V. Nazarenko, "Nonlinear interaction of small–scale Rossby waves with an intense large-scale zonal flow," *Phys. Fluids*, vol. 6, no. 3, pp. 1158–1167, 1994.

[64] A. M. Balk, "Conservation style of the extra invariant for Rossby waves," *Physica D*, vol. 223, pp. 109–120, 2006.

[65] A. M. Balk and T. Yoshikawa, "The Rossby wave extra invariant in the physical space," *Physica D*, vol. 238, pp. 384–394, 2009.

[66] A. M. Balk, S. V. Nazarenko, and V. E. Zakharov, "On the structure of the rossby/drift turbulence and zonal flows," in *Proceedings of the international symposium: Generation of large-scale structures in continuous Media*, no. 34–35, (Perm, Moscow), 1990.

[67] V. E. Zakharov, "Slabaya turbulentnost v sredakh s raspadnym spektrom," *Zh. prikl. mekhaniki i tekhn. fiziki*, vol. 4, pp. 35–39, 1965.

[68] V. E. Zakharov, "Weak turbulence in media with a decay spectrum," *J. Appl. Mech. and Tech. Phys.*, vol. 6, no. 4, pp. 22–24, 1965.

[69] L. Onsager, "Statistical hydrodynamics," *Nuovo Cimento*, vol. 6, pp. 279–287, 1949.

[70] T. D. Lee, "Difference between turbulence in a two-dimensional fluid and in a three-dimensional fluid," *J. Appl. Phys*, vol. 22, p. 524, 1951.

[71] V. E. Zakharov and L. Piterbarg, "Canonical variables for Rossby waves and plasma drift waves," *Phys. Lett. A*, vol. 126, no. 8, 9, pp. 497–500, 1988.

[72] G. C. Wick, "The evaluation of the collision matrix," *Physical Review*, vol. 80, pp. 268–272, 1950.

[73] E. Kartashova and V. S. L'vov, "Model of intraseasonal oscillations in earth's atmosphere," *Phys. Rev. Lett.*, vol. 98, no. 19, p. 198501, 2007.

[74] M. D. Bustamante and E. Kartashova, "Effect of the dynamical phases on the nonlinear amplitudes' evolution," *Europhys. Lett.*, vol. 85, no. 3, p. 34002, 2009.

[75] V. I. Arnold and L. D. Meshalkin, "Seminar led by A. N. Kolmogorov on selected problems of analysis (1958-1959)," *Usp. Mat. Nauk*, vol. 15, p. 247, 1960.

[76] L. D. Meshalkin and Y. G. Sinai, "Investigation of the stability of a stationary soution of a system of equations for the plane movement of an incompressible viscous liquid," *J. Appl. Math. Mech.*, vol. 25, pp. 1700–1705, 1962.

[77] C. Connaughton, S. Nazarenko, and A. Pushkarev, "Discreteness and quasi–resonances in weak turbulence of capillary waves," *Phys. Rev. E*, vol. 63, no. 4, p. 046306, 2001.

[78] D. G. Dritschel and M. E. McIntyre, "Multiple jets as PV staircases: the Phillips effect and the resilience of eddy- transport barriers," *J. Atmos. Sci.*, vol. 65, pp. 855–874, 2008.

[79] A. C. Mahanti, "The oscillation between Rossby wave and zonal flow in a barotropic fluid," *Arch. Met. Geoph. Biokl., Ser. A*, vol. 30, pp. 211–225, 1981.

[80] J. L. Webster, P. J. and Keller, "Atmospheric variations: Vacillations and index cycles," *J. Atmos. Sci.*, vol. 32, pp. 1283–1300, 1975.

[81] J. C. McWilliams, *Fundamentals of Geophysical Fluid Dynamics*. Cambridge University Press, 2006.

[82] H. L. Kuo, "Dynamic instability of two-dimensional nondivergent flow in a barotropic atmosphere," *J. Meteor.*, vol. 6, pp. 105–122, 1949.

[83] U. Frisch, *Turbulence: the legacy of A. N. Kolmogorov*. Cambridge: Cambridge University Press, 1995.

[84] G. K. Vallis and M. E. Maltrud, "Generation of mean flows and jets on a beta plane and over topography," *J.Phys. Oceanography*, vol. 23, pp. 1346–1362, 1993.

[85] P. Goldreich and S. Sridhar, "Toward a theory of interstellar turbulence. ii: Strong Alfvénic turbulence," *Astrophys. J., Part 1*, vol. 438, pp. 763–775, 1995.

[86] M. G. Shats, H. Xia, and H. Punzmann, "Spectral condensation of turbulence in plasmas and fluids and its role in low-to-high phase transitions in toroidal plasma," *Phys. Rev. E*, vol. 71, p. 046409, 2005.

[87] O. G. Onishchenko, O. A. Pokhotelov, and N. M. Astafieva, "Generation of large-scale eddies and zonal winds in planetary atmospheres," *Physics-Uspekhi*, vol. 51, pp. 577–589, 2008.

[88] M. C. Labelle, J. and Kelley and C. E. Seyler, "An analysis of the role of drift waves in equatorial spread F," *J. Geophys. Res.*, vol. 91, p. 5513, 1986.

[89] R. Numata, R. Ball, and R. L. Dewar, "Bifurcation in electrostatic resistive drift wave turbulence," *Phys. Plasmas*, vol. 14, p. 102312, 2007.

[90] L. Villard, A. Allfrey, S. J. and Bottino, M. Brunetti, G. L. Falchetto, V. Grandgirad, R. Hatzky, A. G. Nührenberg, J. and Peeters, O. Sauter, S. Sorge, and J. Vaclavik, "Full radius linear and nonlinear gyrokinetic simulations for tokamaks and stellarators: zonal flows, applied $E \times B$ flows, trapped electrons and finite beta," *Nucl. Fusion*, vol. 44, pp. 172–180, 2004.

[91] E. A. Kuznetsov, "Turbulence of ion sound in a plasma located in a magnetic field," *Sov. Phys. JETP*, vol. 35, pp. 310–314, 1972.

[92] A. S. Monin and L. I. Piterbarg, "A kinetic equation for Rossby waves," *Sov. Phys. Dokl.*, vol. 32, pp. 622–624, 1987.

[93] A. B. Mikhailovskii, S. V. Novakovskii, V. P. Lakhin, S. V. Makurin, E. A. Novakovskaya, and O. G. Onishchenko, "Kolmogorov weak turbulence spectra of an inhomogeneous magnetized plasma," *Zh. Eksp. Teor. Fiz.*, vol. 94, pp. 159–171, 1988.

[94] A. B. Mikhailovskii, S. V. Novakovskii, V. P. Lakhin, S. V. Makurin, E. A. Novakovskaya, and O. G. Onishchenko, "Kolmogorov weak turbulence spectra of an inhomogeneous magnetized plasma," *Sov. Phys. JETP*, vol. 68, pp. 1386–1392, 1988.

[95] A. M. Balk and S. V. Nazarenko, "Physical realizability of anisotropic weak-turbulence kolmogorov spectra," *Zh. Eksp. Teor. Fiz.*, vol. 97, pp. 1827–1846, 1990.

[96] A. M. Balk and S. V. Nazarenko, "Physical realizability of anisotropic weak-turbulence kolmogorov spectra," *Sov.Phys.JETP*, vol. 70, pp. 1031–1041, 1990.

[97] A. I. Dyachenko, S. V. Nazarenko, and V. Zakharov, "Wave-vortex dynamics in drift and beta-plane turbulence," *Phys. Lett. A*, vol. 165, pp. 330–334, 1992.

[98] S. V. Nazarenko, A. C. Newell, and S. Galtier, "Non-local MHD turbulence," *Physica D*, vol. 152–153, pp. 646–652, 2001.

[99] W. Horton, "Statistical properties and correlation functions for drift waves," *Phys. Fluids*, vol. 29, pp. 1491–1503, 1986.

[100] J. F. Drake, P. N. Guzdar, A. B. Hassam, and J. D. Huba, "Nonlinear mode coupling theory of the lower-hybrid-drift instability," *Phys. Fluids*, vol. 27, pp. 1148–1159, 1984.

[101] G. Hammett, "The ion temperature gradient (itg) instability." From a lecture at CMPD/CMSO Winter School, UCLA, sept 2007.

[102] B. Galperin, S. Sukoriansky, and H.-P. Huang, "Universal n^{-5} spectrum of zonal flows on giant planets," *Phys. Fluids*, vol. 13, pp. 1545–1548, 2001.

[103] O. T. Kingsbury and R. E. Waltz, "Numerical simulation of drift waves and trapped ion modes," *Phys. Plasmas*, vol. 1, pp. 2319–2328, 1994.

[104] K. H. Burrell, P. Gohil, D. H. Groebner, R. J. and Kaplan, J. I. Robinson, and W. M. Solomon, "Improved charge-coupled device detectors for high-speed, charge exchange spectroscopy studies on the DIII-D tokamak," *Rev. Sci. Instrum*, vol. 75, pp. 3455–3458, 2004.

[105] Crombé, "Poloidal rotation velocity in JET advanced mode plasmas using charge exchange recombination spectroscopy," in *33rd EPS Conference on Plasma Phys.*, (Rome), 2006.

[106] P. Berloff, I. Kamenkovich, and J. Pedlosky, "A mechanism of formation of multiple zonal jets in the oceans," *J. Fluid Mech.*, vol. 628, pp. 395–425, 2009.

[107] R. L. Dewar and R. F. Abdullatif, "Zonal flow generation by modulational instability," in *Frontiers in Turbulence and Coherent Structures: Proceedings of*

the CSIRO/COSNet Workshop on Turbulence and Coherent Structures, Canberra, Australia, 10-13 January 2006 (J. Denier and J. S. Frederiksen, eds.), vol. 6 of *World Scientific Lecture Notes in Complex Systems*, (Singapore), pp. 415–430, World Scientific, 2007.

[108] V. E. Zakharov and E. A. Kuznetsov, "Hamiltonian formalism for systems of hydrodynamic type," *Sov. Sci. Rev. C*, vol. 4, pp. 167–220, 1984.

[109] A. Weinstein, "The evaluation of the collision matrix," *Phys. Fluids*, vol. 26, pp. 388–390, 1983.

[110] S. M. Cox and P. C. Matthews, "Exponential time differencing for stiff systems," *J. Comp. Phys.*, vol. 176, pp. 430–455, 2002.

[111] A. Ralston, *A First Course in Numerical Analysis*. McGraw-Hill, 1965.

[112] V. D. Larichev and G. M. Reznik, "Strongly nonlinear two-dimensional isolated Rossby waves," *Oceanologia*, vol. 16, pp. 547–550, 1976.

[113] L. Rayleigh, "On the stability of the laminar motion of an inviscid fluid," *Phil. Mag.*, vol. 26, pp. 1001–1010, 1913.